# Structural properties of nanoclusters: energetic, thermodynamic, and kinetic effects

Francesca Baletto* and Riccardo Ferrando†

*INFM and Dipartimento di Fisica, via Dodecaneso 33, 16146 Genova, Italy*

The structural properties of free nanoclusters are reviewed. Special attention is paid to the interplay of energetic, thermodynamic and kinetic factors in the explanation of the clusters structures which are actually observed in the experiments. The review starts with a brief summary of the experimental methods for the production of free nanoclusters, and then proceeds with a guideline given by theoretical and simulation issues, always discussed in close connection with the experimental results. The energetic properties are treated first, evidencing general trends, describing the methods for modelling the interactions between the elementary cluster constituents, and for the global optimization on the cluster potential energy surface. After that, a chapter on cluster thermodynamics follows. The discussion includes the analysis of solid-solid structural transitions, and of melting with its size dependence. The last part is devoted to the growth kinetics of free nanoclusters, and treats the growth of isolated clusters and their coalescence. Several specific systems are analyzed.

## Contents



## I. INTRODUCTION

In the last decade, there has been an explosive development of a new field in science, which is now commonly known as nanoscience (Nalwa, 2004). This field extends through physics, chemistry and engineering, and contains a huge number of important issues, ranging from basic science to a variety of technological applications (in the latter case, the word nanotechnology is often employed). The purpose of nanoscience and nanotechnology is to understand, control and manipulate objects of a few nanometer size (say 1-100 nm), the nanoobjects, which are thus intermediate between single atoms and molecules and bulk matter. These objects can present peculiar properties, which are qualitatively different from those of their constituent parts (being either atoms or

*Present address: The Abdus Salam ICTP, Strada Costiera 11, I34014 Trieste, Italy; Electronic address: baletto@ictp.trieste.it

†Electronic address: ferrando@fisica.unige.it

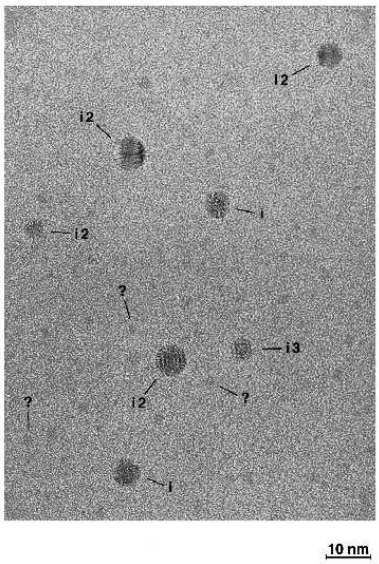


FIG. 1 High-resolution electron microscopy image of Ag clusters deposited on an inert substrate, after being produced in a inert gas aggregation experiment (after Reinhard *et al.* (1997b)). The clusters indicated by arrows are identified as being icosahedra.

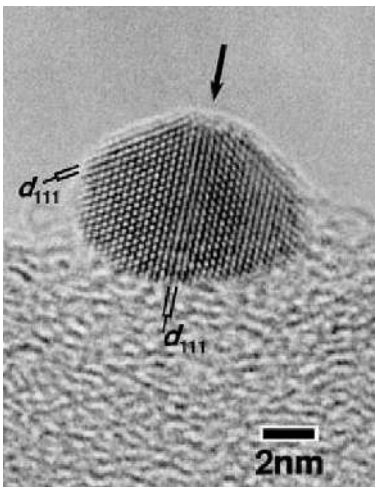


FIG. 2 High-resolution electron microscopy image of a 8.6 × 6.3 nm truncated decahedral gold particle deposited on amorphous carbon. The particle was produced in a inert gas aggregation experiment and then deposited and observed (after Koga and Sugawara (2003)).

molecules) and of macroscopic pieces of matter. In particular, nanoobjects can present properties which vary dramatically with size. This opens the possibility of a fine tuning of these properties, which can however be reached only by controlling precisely the formation process of the nanoobjects.

Among nanoobjects, *nanoclusters* occupy a very important place, since they are the building blocks of nanoscience. Nanoclusters are aggregates of atoms or molecules of nanometric size, containing thus a number of constituent particles ranging from $\sim 10$ to $10^6$ (Castleman and Bowen, 1996; Johnston, 2002; Wales, 2003).

Contrary to molecules, nanoclusters do not have a fixed size or composition. For example, the water molecule contains one oxygen and two hydrogen atoms, that are placed with a well defined angle between them. On the other hand, silver, gold (see Figs. 1, 2) or even water clusters, may contain any number of constituent particles, and, for a given size, present a variety of morphologies. There are borderline cases which are not easy to be classified unambiguously either as clusters or molecules, the fullerene buckyball ($C_{60}$) being an example. In the following, we shall classify $C_{60}$ as a molecule, since clusters and solids of buckyballs have been produced where each $C_{60}$ constituent preserves its individuality. Clusters can be homogeneous, that is composed by only one type of atoms or molecules, or heterogeneous. Clusters may be neutral or charged. Clusters may held together by very different kinds of forces: strong attraction between oppositely charged ions (as in NaCl clusters), van der Waals attraction (as in He and Ar clusters), covalent chemical bonds (as in Si clusters), metallic bond (as Na and Cu clusters). Small clusters of metal atoms are held together by forces more like those of covalent bonds than the forces exerted by the nearly-free electrons of bulk metals.

Clusters containing no more than a few hundreds of particles (diameters of 1-3 nm) are expected to present strongly size-dependent properties (for example, their geometric and electronic structure, binding energy, melting temperature). Larger clusters, with many thousands of atoms and diameters in the range of ten nm and more have a smoothly varying behavior which tends to the bulk limit as size increases.

Nanoclusters have peculiar properties because they are finite small objects. To finite objects, the constraint of translational invariance on a lattice does not apply. For this reason, clusters can present non-crystalline structures, icosahedra and decahedra being the most well known. Of course, it is possible also to build up crystalline clusters which are simply pieces of bulk matter. An important issue in cluster science is to understand whether crystalline or non-crystalline structures prevail for given size and composition. Being small objects, nanoclusters have a very high surface/volume ratio. Thus the surface energy contribution (including terms from facets, edges and vertices) is not negligible, and usually strongly size dependent.

Nanoclusters are well suited for several applications, whose number is increasing fast in last years. For example, there has been a traditional interest in connection with applications to catalysis (see for example Henry (1998)), because of the very favorable surface/volume ratio of nanoclusters. More recently, there have been developments towards applications in biology. For example, gold nanoparticles studded with short segments of DNA (Alivisatos *et al.*, 1996; Mirkin *et al.*, 1996) could form the basis of an easy-to-read test to single out genetic sequences (Alivisatos, 2001). However, applications of nan-

oclusters have a much older history, and here we would like only to mention a striking example which dates to several centuries ago. In fact, it has been recently discovered (Borgia *et al.*, 2002; Padeletti and Fermo, 2003) that the Renaissance masters in Umbria, Italy, used nanoparticles in the decoration of majolicas with lustre. Lustre consists of a thin film containing silver and copper clusters with diameters up to a few tens of nanometers, and often of non-crystalline structure. Due to the inclusion of these nanoparticles, lustre gives beautiful iridescent reflections of different colours.

The starting point to understand the peculiar cluster properties is the study of their structure. With this respect, the first question to answer to is the following: Given size and composition, what is the most stable cluster structure from the energetic point of view? To answer to this question we need to *find the global minimum* on the Potential Energy Surface (PES) of the cluster (Wales, 2003). The PES is the product of the elementary interactions among the cluster constituents.

Once the answer to this first question is given, a second one arises: What is the effect of raising the temperature on the structural properties of a cluster? The answer to this second question implies the study of a very fascinating field, the *thermodynamics of finite systems*.

Finally, the experimental time scales of clusters production are often short with respect to the time scales of morphology transitions. This leads to a third important question: What are the kinetic effects in the formation of nanoclusters? To answer to this question, the *cluster growth process* must be analyzed.

In this review, we try to summarize and discuss the present knowledge about these three points, and to give, as much as we can, some answers to the above questions for what concerns the behavior of free clusters. Two general results can however be anticipated.

First, what clearly emerges from the comparison of experimental and theoretical results is that all three factors, energetics, thermodynamics and growth kinetics of nanoclusters must be taken into account when dealing with the analysis of realistic situations. Second, basic concepts which allow the qualitative understanding of the energetic, thermodynamic and kinetic behavior of nanoclusters are the *range* and the *type* of the interactions among the constituent particles. The interaction range rules the behavior of systems with pair potentials (see for example Wales (2003)). In systems characterized by interactions with strong many-body character, metals for example, other factors come into play together with the interaction range, namely the bond order - bond length correlation and the directionality of the interactions.

The guideline of this review article is given by theoretical and simulation issues on free cluster science. We remark that cluster science is one of the fields where the interplay among experiments, theory and simulations is stronger: in fact, the analysis of the experiments is very often carried out by some kind of simulation. To quote the words by Marks (1994) *small particle structures cannot be understood purely from experimental data, and it is necessary to simultaneously use theoretical or other modelling*. The discussion of theoretical and simulation results will be made in close contact with the experiments.

We cannot pretend to be exhaustive on the subjects of our review, since thousands of articles about nanoclusters have been produced in the last decade. Some very fascinating fields, for example the field of binary clusters and nanoalloys, whose properties depends crucially not only on size but also on composition, are completely left out for space reasons. But we cannot pretend to be exhaustive even on the topics that we explicitly treat. If some contributions have been left out, we apologize in advance.

The review is structured as follows. In Section II we give a brief description of the methods for free cluster production. In Section III we deal with the energetics of free nanoclusters, from the point of view of describing general trends, modelling the elementary interactions, and finding the global minima of the PES. In Section IV we consider the thermodynamics of nanoclusters, focusing on the possibility of solid-solid transitions at finite temperature and on the melting transition. Finally Section V treats the growth kinetics of nanoclusters, which may take place either at the liquid or at the solid state, and the coalescence of nanoclusters. In each part, specific systems are treated in details.

## II. EXPERIMENTAL METHODS FOR FREE NANOCLUSTER PRODUCTION

The experimental methods for producing free nanoclusters have been reviewed by de Heer (1993) and more recently by Milani and Iannotta (1999) and Binns (2001). Here we present a brief summary, focusing on the aspects (such as the time scale of free nanocluster growth) which are more closely related to the subjects treated in the following.

Sources producing free beams of nanoscale clusters were made available about 30 years ago for the production of noble-gas clusters (Raoult and Farges, 1973) and more than 20 years ago for producing metallic clusters (Dietz *et al.*, 1981; Sattler *et al.*, 1980) ; more recent developments have made available sources that are ultra high vacuum compatible, can produce binary clusters (Cottancin *et al.*, 2000; Rousset *et al.*, 1996), and incorporate extremely efficient mass-selection techniques (see Binns (2001) and references therein).

In most cases, the heart of a cluster source is a region where a supersaturated vapor of the material forming the clusters is produced. The first step in cluster production is the heating up of the material to obtain a hot vapor. This can be done in different ways, for example by heating up a piece of bulk material in a crucible (as in seeded supersonic nozzle and inert gas aggregation sources), by hitting a target either with a laser pulse or with an ion beam (laser evaporation and ion sputtering sources). To

obtain supersaturation, the hot vapor must be cooled down. There are essentially two ways to achieve this. The first is by means of a supersonic expansion (as in seeded supersonic nozzle sources, where the material is mixed with a high-pressure inert gas and then expanded), which causes an adiabatic cooling (Anderson and Fenn, 1985). Hot clusters are usually produced, at temperatures close to the evaporation limit (Bjørnholm *et al.*, 1991). In the second way, the hot vapor is mixed with a cold inert-gas flow which acts as a collisional thermostat. This method is used in inert gas aggregation sources to produce even very cold metallic clusters. Here, due to the low temperature of the inert gas, cluster production proceeds mainly by the addition of single atoms, and reevaporation is negligible (de Heer, 1993). After the end of the growth, the clusters can be further reheated or cooled down by subsequent stages of contact with gas at different temperatures.

What are the typical time scales of nanocluster production? This question is extremely important, because, as we see in the following, the finite lifetime of free clusters in flight may cause their trapping into metastable structures. Let us consider an inert gas aggregation source for noble-metal clusters (Koga and Sugawara, 2003; Reinhard *et al.*, 1998, 1997b). There, the typical metal vapor temperature $T_v$ and pressure $p_v$ are of the order of $1000 - 1500$ K and $1 - 10$ mbar respectively. Consider now a growing nanocluster, say with a radius $R$ of 1 nm, which can correspond to 100 - 200 atoms. If we assume a spherical cluster, the kinetic theory of gases gives for the atomic flux $\Phi_v$ (i.e. the number of metal atoms per second hitting the cluster surface)

$$\Phi_v = \frac{p_v A_{eff}}{\sqrt{2\pi m_v k_B T_v}}, \tag{1}$$

where $A_{eff} = 4\pi R^2$, and $m_v$ is the mass of the atoms. This gives $\Phi_v \sim 10^7$ s$^{-1}$, corresponding to an interval between depositions $\tau_{dep} = \Phi_v^{-1} \sim 10^2$ ns. Thus, a cluster of $10^3$ atoms is grown on a time scale which is a fraction of a millisecond.

Once clusters are produced, they have to be detected in some way, possibly while they are still in their beam. Indeed, the detection of slow neutral clusters is a difficult task; however the cluster structures can be investigated by diffraction methods. Then clusters can be ionized for an efficient mass selective detection, and finally deposited and observed by several microscopy techniques (Henry, 1998; José-Yacamán *et al.*, 2001a).

In a diffraction experiment, a well collimated electron beam with an energy of 30 to 50 keV crosses a cluster beam. The fast electrons are scattered from the cluster atoms, and the diffraction pattern is recorded. A series of diffraction rings around the position of the primary electron beam is recorded. The interpretation of diffraction profiles is not straightforward (Hall *et al.*, 1991; Reinhard *et al.*, 1997a, 1998, 1997b), being based on a fit to a theoretical profile whose construction assumes the presence of some selected cluster structures. However, information on the geometry, the average size and the temperature of the clusters in the beam can be extracted as follows. Remembering that the scattered intensity is the squared modulus of the Fourier Transform (FT) of the scatterers with respect to the momentum transfer $\mathbf{q}$, a theoretical diffraction pattern is built up by weighting contributions from clusters of different structures. In fact, one can expect that for example an icosahedron (Ih) has a different FT than a part of an fcc lattice. The geometry is obtained directly by fitting the weights of the different structures to the experimental data. On the other hand, information on the size can be obtained from the width of the diffraction rings, because the larger the cluster, the narrower are the diffraction rings: the more scatterers add their contributions coherently, the sharper is the resulting pattern. Finally, information about the cluster temperature is contained in the temperature dependence of the scattered intensity

$$I(T) \;=\; I_{(T=0)} e^{-2W}. \tag{2}$$

$W$ is the Debye-Waller factor

$$W \;=\; \frac{1}{3}\langle u^2 \rangle q^2 \tag{3}$$

where $\langle u^2 \rangle$ is the mean square vibrational amplitude of the cluster atoms. For harmonic vibrations, $\langle u^2 \rangle \propto T$.

## III. ENERGETICS OF FREE NANOCLUSTERS

At low temperatures, the most favorable structure of a cluster of $N$ particles is the one which minimizes its total energy. For example, in atomic clusters, the most favorable structures is the global minimum of the potential energy as a function of the coordinates of the atomic cores (the potential energy surface or PES). Traditionally, a great effort has been devoted to find reliable methods to calculate the total energy, and to search for local and global minima. This task implies the following two steps:

(a) Construction of a model for the interactions between the elementary constituents of the cluster; this can be accomplished either by trying to solve directly the Schrödinger equation (*ab initio* methods) or by constructing semiempirical interparticle potentials (see Section III.C).

(b) Search for the the most favorable isomers by some global optimization algorithm (see Section III.D).

Depending on material and size, both (a) and (b) may present enormous difficulties. Therefore, as a preliminary step, it is extremely important to find general trends which help to single out sequences of favorable structures in different size ranges. This can be done either on the basis of geometric considerations, as in Section III.A (where the construction of families of highly symmetric structures, the *structural motifs*, is treated), or of electronic

shell effects, as in Section III.B. The sizes of the most energetically stable structures are often called *magic sizes*. Magic sizes may (tentatively) correspond either to the completion of a geometrically perfect structure (geometric magic sizes) or to the closing of an electronic shell (electronic magic sizes).

Section III.E is devoted to the study of selected systems of special interest.

### A. Geometric shells: structural motifs and general trends about their energetics

In general, the binding energy $E_b$ of a cluster of size $N$ with a given structure can be written in the following form [1]

$$E_b = aN + bN^{2/3} + cN^{1/3} + d; \quad (4)$$

the first term corresponds to a volume contribution, while the others represent surface contributions from facets, edges and vertices. Volume and surface contributions are in competition. Clusters with low surface energy must have quasi-spherical shapes (thus optimizing the surface/volume ratio), and close-packed facets. On the other hand, it is not possible to build up clusters with spherical shape without internal strain, which gives a volume contribution.

A useful parameter to compare the stability of clusters in different size ranges is $\Delta(N)$

$$\Delta(N) = \frac{E_b(N) - N\varepsilon_{coh}}{N^{2/3}}, \quad (5)$$

where $\varepsilon_{coh}$ is the cohesive energy per particle in the bulk solid. $\Delta$ is the excess energy (namely the energy in excess with respect to $N$ atoms in a perfect bulk crystal) divided approximately by the number of surface atoms. Other indicators of structural stability are the binding energy per atom $E_b(N)/N$, and the first and second differences $\Delta_1(N)$ and $\Delta_2(N)$ in the binding energy

$$\begin{aligned} \Delta_1(N) &= E_b(N-1) - E_b(N) \\ \Delta_2(N) &= E_b(N-1) + E_b(N+1) - 2E_b(N). \end{aligned} \quad (6)$$

$\Delta_1$ and $\Delta_2$ measure the relative stability of clusters of nearby sizes. Peaks in $\Delta_2(N)$ were found to be well correlated to peaks in the mass spectra (Clemenger, 1985).

Let us now build up structural motifs by trying to optimize either volume or surface energy contributions. The easiest way to minimize volume contributions is to cut a piece of bulk matter, so that interparticle distances inside the cluster are automatically optimized. For such clusters of *crystalline* structure the parameter $a$ in Eq. (4) is simply $\varepsilon_{coh}$, so that $\lim_{N\to\infty} \Delta = b$. As we shall see in the following, nanoclusters can be also of *non-crystalline* structures; for these clusters $a$ is larger than $\varepsilon_{coh}$, and $\Delta$ diverges at large sizes (see Fig. 3).

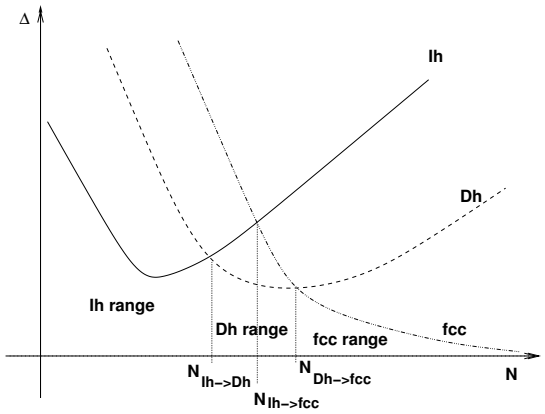


FIG. 3 Qualitative behavior of $\Delta$ (Eq. (5)) for crystalline, Ih and Dh clusters.

Consider now fcc crystalline structures. Try to cut a cluster from a bulk fcc crystal in such a way that its surface has only close-packed facets. A possible resulting shape is the *octahedron* (Oh) (see Fig. 4), namely two square pyramids sharing their basis. Even if the whole surface of the Oh is close-packed, its shape does not optimize the surface energy because of its high surface/volume ratio. Clusters with more spherical shapes are obtained by cutting the vertices, thus producing the *truncated octahedron* (TO). Its surface has eight close-packed (111) and six square (100) facets; the latter have a higher surface energy in most materials. A deeper cut gives a more compact shape having however larger square facets. If size is sufficiently large, the optimal cut is given by the Wulff construction. This was developed to find the equilibrium shape of macroscopic crystals by minimizing the surface energy at fixed volume (see for example Pimpinelli and Villain (1998)). From the Wulff construction, the best TO structure should fulfill the condition

$$\frac{\gamma_{(100)}}{\gamma_{(111)}} = \frac{d_{(100)}}{d_{(111)}}, \quad (7)$$

where $\gamma_{(100)}$ and $\gamma_{(111)}$ are the (100) and (111) surface energies respectively, whereas $d_{(100)}$ and $d_{(111)}$ are the distances of the facets from the center of the cluster. At large size, the introduction of higher-order facets can make fcc clusters more spherical (see for example Raoult *et al.* (1989a)). Different groups (Baletto *et al.*, 2002b; Cleveland and Landman, 1991; Valkealahti and Manninen, 1998) have shown that the Wulff construction is a reliable tool for identifying the best crystalline clusters already for nanometric sizes. In any case, even the optimal Wulff shapes are quite far from being spherical, and are expected to be the most favorable clusters at large sizes.

A better solution to the problem of building up

[1] See for example Hill (1964), Northby *et al.* (1989), Xie *et al.* (1989a), Cleveland and Landman (1991), Jortner (1992), Uppenbrink and Wales (1992), Baletto *et al.* (2002b).

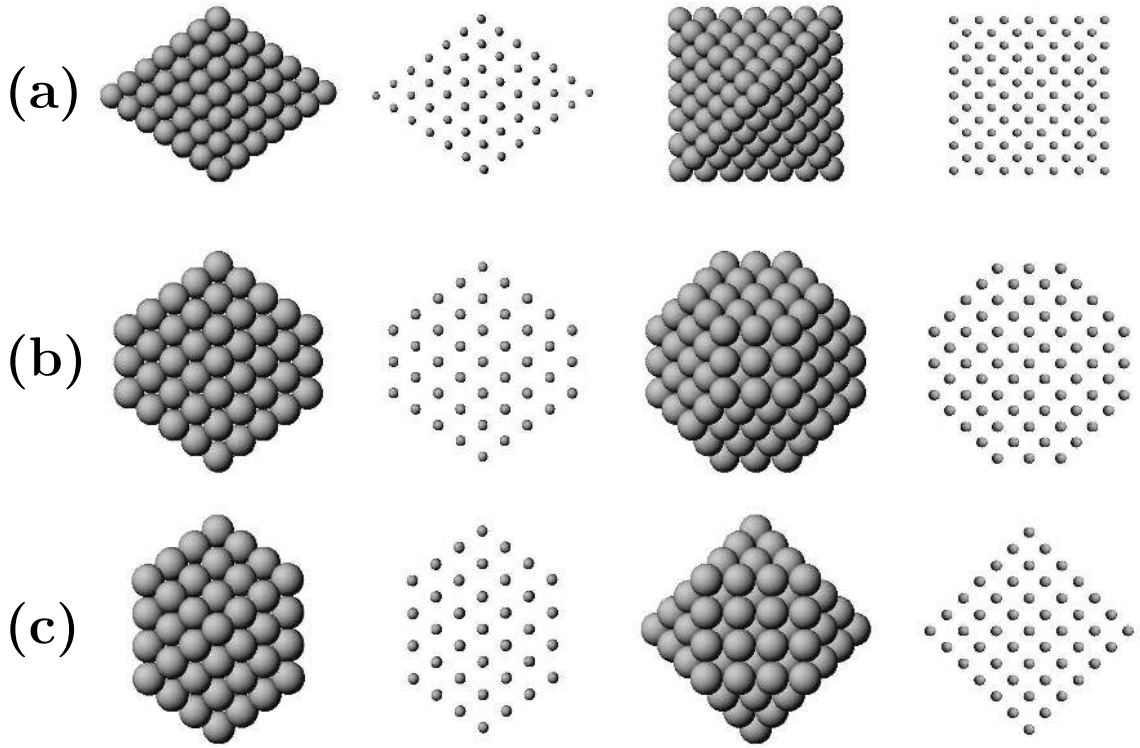


FIG. 4 Face centered cubic clusters: (a) octahedron (Oh); (b) truncated octadedron (TO); (c) cuboctahedron (CO). Each cluster is shown in four views. (a) An octahedron is made up of two square pyramids sharing a common basis. Its surface consists of eight triangular close-packed (111) facets, but the structure has a high surface/volume ratio. Polyhedra with a lower surface/volume ratio, are obtained truncating symmetrically the six vertices of an Oh, thus obtaining square and hexagonal (or triangular, see below) facets. A truncated octahedron can be characterized by two indexes: $n_l$ is the length of the edges of the complete Oh; $n_{cut}$ is the number of layers cut at each vertex. In the figure, for the Oh in (a) $(n_l, N_{cut}) = (7, 0)$, the TO in (b) $(n_l, N_{cut}) = (7, 2)$, and the CO in (c) $(n_l, N_{cut}) = (7, 3)$. A perfect TO has thus a number of atoms

$$N_{TO}(n_l, n_{cut}) = \frac{1}{3}(2n_l^3 + n_l) - 2n_{cut}^3 - 3n_{cut}^2 - n_{cut}.$$

This equation defines the series of the magic numbers for TO structures. The square facets have a (100) symmetry and edges of $n_{cut} + 1$ atoms. The (111) facets are not in general regular hexagons. In fact, three edges of the hexagons are in common with square facets, having thus $n_{cut} + 1$ atoms, while the remaining three edges have $n_l - 2n_{cut}$ atoms. Regular hexagons are thus possible if $n_l = 3n_{cut} + 1$; TO with regular hexagonal facets are referred to as regular TO. When $n_l = 2n_{cut} + 1$ the hexagonal facets degenerate to triangles and the cuboctahedron is obtained, which is usually energetically unfavorable because of its large (100) facets.

compact quasi-spherical shapes was found by Mackay (1962)(see also Martin (1996)) who constructed the *Mackay icosahedron* (Ih, see Fig. 5). This is a non-crystalline structure, with fivefold rotational axes. Icosahedral clusters are limited by (111)-like close-packed facets only, thus optimizing the surface energy well. However, this is obtained at the expense of a volume contribution, since interatomic distances are not the ideal ones: radial (intershell) bonds are compressed, while intrashell bonds are expanded. Therefore, Mackay icosahedra are highly strained structures, and their $\Delta$ is proportional to $N^{1/3}$ as $N \to \infty$. This indicates that icosahedra could be expected to be the most favorable structures only at small sizes.

Icosahedra are not the only possible non-crystalline structures. Another non-crystalline motif is represented by the *decahedra* (see Fig. 6). A decahedron (Dh) is formed by two pentagonal pyramids sharing their basis; its surface has only close-packed facets, but its shape is very far from being spherical, so that truncations are advantageous also in this case. Ino (1969) proposed a truncation where the five edges limiting the common basis of the pyramids are cut to expose (100)-like facets. This improves the surface/volume ratio, but usually does not produce the best possible decahedra in a given size range (see for example Baletto *et al.* (2002b)) because it creates large (100)-like facets. Marks (1984, 1994) proposed a more efficient truncation scheme, with reentrances ex-

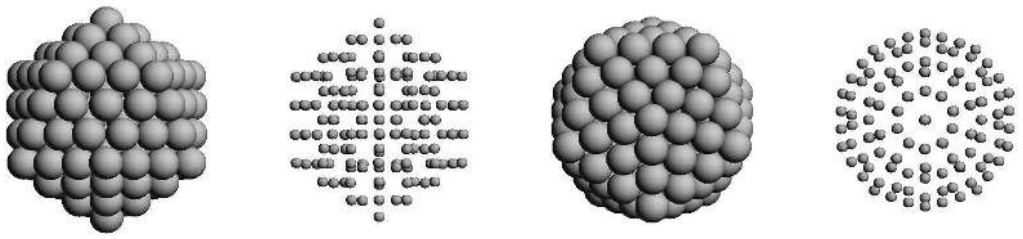

FIG. 5 Icosahedral clusters. The Mackay icosahedron (Ih) is a non-crystalline structure organized in shells. An Ih with $k$ shells has

$$N_{Ih}(k) = \frac{10}{3}k^3 - 5k^2 + \frac{11}{3}k - 1$$

atoms (so that the series of magic numbers is 1, 13, 55, 147...). The Ih in the figure has $k = 4$ shells. An Ih with $k$ shells has the same number of particles as a CO with $n_{cut} = k - 1$. An Ih has 20 triangular facets of side $k$ and twelve vertices. Each pair of opposite vertices lie along a fivefold symmetry axis. An Ih can be thought as composed of twenty fcc tetrahedra sharing a common vertex (in the central site). When twenty regular tetrahedra are packed around a common vertex, large interstices remain. To fill these spaces the tetrahedra must be distorted, thus generating a huge strain in the structure. Intershell distances are compressed, while intrashell distances are expanded. The facets of an Ih are of distorted (111) symmetry. Adatoms deposited on the facets of a Mackay Ih can be placed either on sites of fcc or hcp stacking. Islands of fcc stacking are part of the next Mackay shell, while islands of hcp stacking form a so-called anti-Mackay overlayer.

posing further close-packed facets which separate neighboring (100)-like facets. Marks decahedra can achieve a better optimization of the surface energy than TO structures. On the other hand, also decahedra are strained structures, with a volume contribution to the excess energy giving $\Delta \propto N^{1/3}$ at large $N$. The strain is however much smaller than for icosahedra.

In summary, the Ih motif should be the most favorable at small sizes, while TO clusters are expected for large sizes; truncated decahedra could be favorable in intermediate ranges. This trend has been verified in experiments. Farges *et al.* (1986) found a transition from Ih to close-packed (not necessarily fcc, see van de Waal *et al.* (2000)) structures at $N \sim 750$ in Ar clusters obtained in a free-jet expansion; Reinhard *et al.* (1997a, 1998) were able to identify small Ih, intermediate-size Dh and large fcc clusters in inert-gas aggregation experiments on Cu. Several systems have been investigated theoretically, showing that the Ih $\rightarrow$ Dh and Dh $\rightarrow$ fcc crossover sizes are strongly material-dependent [2].

Doye *et al.* (1995) proposed a quite simple criterion to understand the qualitative trends about crossover sizes. This criterion states that *soft interactions*, with wide potential wells, stabilize strained structures, while *sticky interactions*, with narrow potential wells, cannot easily accommodate the strain thus favoring crystalline structures. Doye *et al.* (1995) considered a pair potential and decomposed the cluster energy into three parts

$$E_b = -n_{NN}\varepsilon_{NN} + E_{strain} + E_{NNN} \qquad (8)$$

where $n_{NN}$ is the number of nearest-neighbor pairs, $\varepsilon_{NN}$ is their bond strength at the optimal distance, $E_{strain}$ is the strain contribution due to the fact that some nearest-neighbor pairs can be at non-optimal distances and $E_{NNN}$ is the contribution from further neighbors, which is, to a first approximation, negligible. The usual competition is between the first and the second term in Eq. (8); Ih structures, which have the largest number of nearest-neighbor bonds, optimize the first term at the expense of the second, while the opposite holds for fcc clusters. The relative weights of these two terms depend on the range of the potential. Decreasing the range has the effect of destabilizing strained structures, because the potential wells narrow so that the distortion of the nearest-neighbor distance with respect to its ideal value becomes more costly. In the case of a Morse (1929) interaction potential, Doye *et al.* (1995) were able to construct a structural phase diagram. The Morse potential $U_M$ can be written as

$$U_M = \epsilon \sum_{i<j} \mathrm{e}^{\rho_0(1-r_{ij}/r_0)} \left[\mathrm{e}^{\rho_0(1-r_{ij}/r_0)} - 2\right] \qquad (9)$$

where the $r_{ij}$ are the interatomic distances, $r_0$ is the equilibrium separation and $\epsilon$ is the well depth. Thus varying the parameter $\rho_0$, one can adjust the width of the potential well without changing the position and the depth of the minimum. Large values of $\rho_0$ give short-ranged attractions with a steep repulsive part, namely a narrow well and a sticky interaction (see Fig. 7). Small $\rho_0$ correspond to soft potentials. As can be seen in Fig. 8, the most favorable structure changes from Ih at small $\rho_0$, to Dh in the intermediate range, and finally close-packed clusters at high values of $\rho_0$. A qualitative idea of the trends among different materials can be obtained by fitting the parameters of the Morse potential. This fit gives large values of $\rho_0$ for the interaction potentials between

[2] See Raoult *et al.* (1989b), Cleveland and Landman (1991), Uppenbrink and Wales (1992), Turner *et al.* (2000), Doye *et al.* (2001), Baletto *et al.* (2002b), Doye and Hendy (2003) and Section III.E for details on some specific systems.

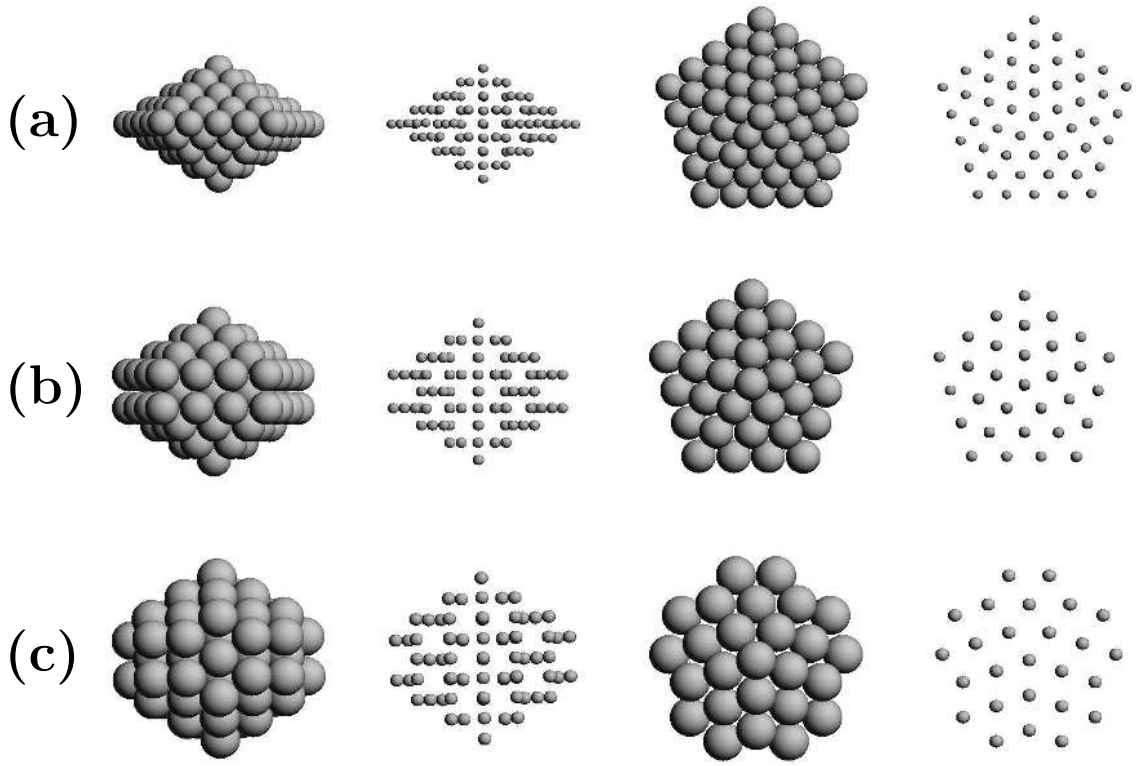


FIG. 6 Decahedral clusters: (a) regular decahedra; (b) Ino truncated decahedra; (c) Marks truncated decahedra. A decahedron (Dh) is made up of two pentagonal pyramids sharing a common basis. It has a single fivefold axis and is formed by five tetrahedra sharing a common edge along the fivefold axis. By packing five regular tetrahedra gaps remain, but smaller than in the case of the Ih. These gaps are filled by distorting the tetrahedra, thus introducing some strain. Regular Dh (first row) are limited by ten close-packed (111)-like facets, but have a large surface/volume ratio which can be lowered truncating the edges around the common basis, thus obtaining the Ino Dh with five (100)-like facets. An even better structure is the Marks Dh, obtained introducing reentrances which separate the (100)-like facets (see the third row). A Dh is characterized by three integer indices $(m, n, p)$. $m$ and $n$ are the lengths of the sides of the (100) facets, perpendicular and parallel to the axis respectively; $p$ is the depth of the Marks reentrance. A regular Dh has indices of the form $(m, 1, 1)$ (the (5,1,1) Dh is shown in the top row), Ino Dh have indices $(m, n, 1)$, with $n > 1$ (the (4,2,1) Ino Dh is shown in the second row), and Marks Dh have $(m, n, p)$ with $n, p > 1$ (the (2,2,2) Marks Dh is shown in the third row). A Marks Dh has $h = m + n + 2p - 3$ atoms along its symmetry axis, and a total number of atoms given by

$$N_{M-Dh} = (30p^3 - 135p^2 + 207p - 102)/6 + \left\{5m^3 + (30p - 45)m^2 + \left[60(p^2 - 3p) + 136\right] m\right\}/6 +$$

$$+ \left\{n\left[15m^2 + (60p - 75)m + 3(10p^2 - 30p) + 66\right]\right\}/6 - 1.$$

From this formula follows that a Ino Dh has

$$N_{Ino} = \left[5m^3 - 15m^2 + 16m + n(15m^2 - 15m + 6)\right]/6 - 1$$

atoms. For $n = m$ and $p = 1$ (square (100)-like facets) a Dh has thus the same number of atoms as an Ih of $m$ shells and as a CO with $n_{cut} = m - 1$. Finally, a regular Dh has $N_{Dh} = (5m^3 + m)/6$ atoms.

fullerene molecules ($\rho_0 = 13.62$ and 11.92 for Girifalco (1992) and Pacheco and Prates-Ramalho (1997) potentials respectively), $\rho_0 = 6$ for a Lennard-Jones crystal, $\rho_0 = 3.96$ for Ni (Stave and DePristo, 1992) and even smaller values for alkali metals ($\rho_0 = 3.15$ and 3.17 for sodium and potassium (Girifalco and Weizer, 1959)).

Baletto *et al.* (2002b) applied a similar criterion, based on the stickiness of the interactions, to discuss crossover sizes in noble and quasi-noble metal clusters modelled by many-body semiempirical potentials. This point is discussed in detail in Section III.E.3, where it is shown that there are other factors, besides the interaction range, that determine the structure of metallic clusters (Soler *et al.*, 2000). These factors arise from the many-body character of the metallic interactions, which causes a strong bond order - bond length correlation whose effects tend to make Ih structures less stable than what follows from the analysis of the interaction range. Moreover, bond

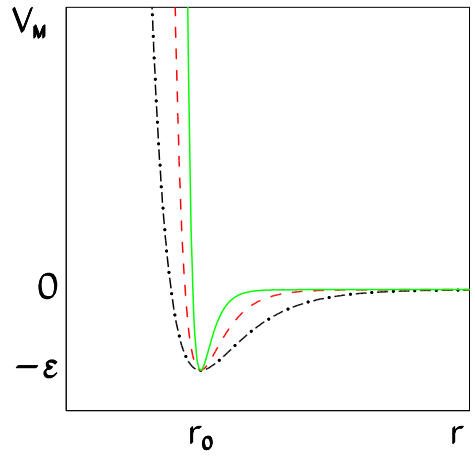


FIG. 7 Morse potential for $\rho_0$ values corresponding to sodium (dash-dotted line), Lennard-Jones (dashed line) and $C_{60}$ molecules (full line). The latter is a very sticky interaction.

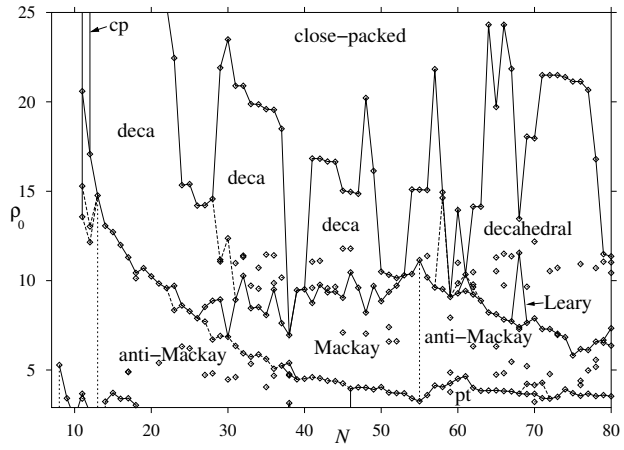


FIG. 8 Phase diagram for Morse clusters (courtesy of Jonathan Doye). The lines separate domains pertaining to different structural motifs.

directionality effects can be important. Finally, the presence of multiple minima or of secondary maxima in the two-body part of the interaction (Doye and Wales, 2001; Doye, 2003) can have strong effects on the preferred cluster structures.

### B. Electronic shells

Electronic shell closing has been extremely successful in explaining the observed experimental abundances of alkali-metal clusters as those found in the seminal experiments by Knight *et al.* (1984) on sodium clusters. In this framework, a cluster is modelled as a superatom; valence electrons are delocalized in the cluster volume and fill discrete energy levels. There are several degrees of sophistication of this model. Detailed accounts can be found in the reviews by de Heer (1993) and Brack (1993); a simple and very clear discussion is found in Johnston (2002). Here we briefly sketch only the spherical jellium model.

The spherical jellium model assumes an uniform background of positive charge, where electrons move and are subjected to an external potential. The simplest forms of the potential are the infinitely deep spherical well and the harmonic well. The solution of the single-electron Schrödinger equation for the spherical well gives the following series of magic numbers: 2, 8, 18, 20, 34, 40, 58... etc. On the other hand, the harmonic well gives the series: 2, 8, 20, 40, 70... etc. The experimental spectra in Knight *et al.* (1984) reveal high peaks at 8, 20, 40 in agreement with both models. There are however less evident peaks at 18 and 58, which appear only in the spherical well. Experiments on larger sodium clusters have revealed electronic shells in larger sodium clusters, up to about 2000 atoms (Martin *et al.*, 1991a; Martin, 1996, 2000), and in other metals, see for example Johnston (2002).

Candidates for observing electronic shell effects are the metals with weakly bound valence electrons, primarily the alkali and then the noble metals. It seems that also the temperature $T$, which determines whether the cluster is solid or liquid depending on $N$ (see Section IV.B.3), plays a crucial role. The major evidence for electronic shell closing is for small alkali metal clusters (Bjørnholm *et al.*, 1990; Knight *et al.*, 1984; Nishioka *et al.*, 1990). For these systems, several calculations (Röthlisberger and Andreoni, 1991; Solov'yov *et al.*, 2002; Spiegelman *et al.*, 1998) indicate that electronic shell closing is a better criterion than atomic packing to determine the most stable clusters. For larger alkali clusters the situation is more complicated. In fact, Martin *et al.* (1991a), Martin (1996, 2000) have shown that Na clusters, after presenting electronic magic numbers up to 2000 atoms, reveal a series of geometric magic numbers at larger sizes (see Fig 9). This would correspond to a transition from liquid to solid clusters at increasing size. Moreover, when heating and melting solid Na clusters, geometric magic numbers disappear to the advantage of electronic magic numbers. The same kind of behavior was found also for aluminum clusters (Baguenard *et al.*, 1994; Martin *et al.*, 1992). Therefore, the indication is that electronic shells are seen when hot liquid clusters are produced, while geometric shells are exhibited by cold, solid clusters (Johnston, 2002). In small clusters, both electronic and geometric effects can play important roles, as Zhao *et al.* (2001) have shown in their tight-binding global optimization study of Ag clusters at $N \leq 20$. In conclusion, the interplay of electronic and geometric shell effects, depending on material and size, is still to be understood to a large extent.

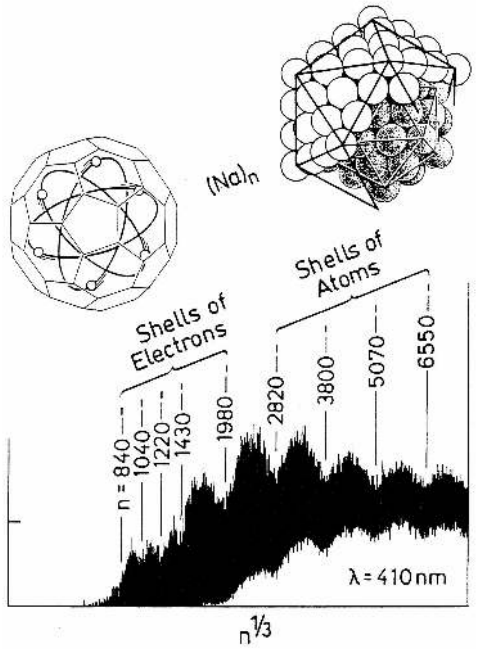


FIG. 9 Mass spectrum of $Na_n$ clusters ($n$ is the size) photoionized with with 3.02 eV photons. Closed-shell clusters are more difficult to ionize, so that they correspond to minima in the spectrum. Two sequences of minima appear in the spectrum. These sequences are at equally spaced $n^{1/3}$ intervals on the size scale and correspond to an electronic shell sequence and a structural shell sequence (after Martin (2000)).

### C. Calculation of the total energy of nanoclusters

A key point in the theoretical study of clusters is the choice of an appropriate energetic model. This depends on the material and the size of the cluster, and on the physical and chemical properties which one wishes to investigate. To cover and illustrate in detail all methods used in theoretical cluster science would require an entire book, and it is well beyond the scope of our review. Here we mention only the main methods, trying give an idea of their underlying philosophy and range of applicability.

As pointed out in the review by Bonacić-Koutecký *et al.* (1991), even clusters of a few atoms are very complicated systems. Indeed, the complexity of quantum mechanics forces one to employ approximate methods.

The *ab initio* methods of quantum chemistry (Hartree-Fock and post Hartree-Fock, see Bonacić-Koutecký *et al.* (1991) and references therein) have been extensively applied to the study of small clusters already about 20 years ago. For example, small-size ($2 \leq N \leq 9$) Li and Na clusters contains relatively few electrons, so that all-electron calculations have been possible (Boustani *et al.*, 1987). When either the size of the cluster, or the nuclearity of the atoms increase, these methods become cumbersome, and presently they are less commonly employed than in the past.

Methods based on density-functional theory (Hohenberg and Kohn, 1964; Kohn and Sham, 1965), when adequately tested, can be of very high accuracy, and less cumbersome from the computational point of view, giving the possibility to treat a wide variety of systems and somewhat larger sizes. Calculations concerning metals up to a few hundred atoms are present in the literature also for difficult systems such as the transition and noble metals (see for example Häberlen *et al.* (1996), Jennison *et al.* (1997), Garzón *et al.* (1998b), Fortunelli and Aprà (2003), Nava *et al.* (2003)). The weak point in density-functional calculations is often the exchange and correlation term, which is treated in an approximate way, whose validity depends on the systems and has to be checked each time. The simplest approximation is the local density approximation; more sophisticated approaches include the gradient corrections (being very important in transition and noble metals), and are called often Generalized Gradient Approximation. At this level, different exchange and correlation functionals are available (see Perdew and Wang (1986), Perdew *et al.* (1996, 1992) and Becke (1988, 1996)). In order to check the validity of the gradient-corrected density-functional calculations, Mitás *et al.* (2000) have performed quantum Monte Carlo (MC) simulations (Ceperley, 1994) on small-size silicon clusters. In quantum MC, which is computationally very demanding, many-body correlations are directly taken into account by an explicit correlation in the trial wave function. It turned out that there can be significant discrepancies between the density-functional (with different types of exchange and correlation functionals) and the quantum MC results. Mitás *et al.* (2000) confirmed the already known bias of density-functional calculations towards compact structures; this bias is very strong at the level of the local-density approximation, and considerably reduced if gradient corrections are included. There are some functionals which give the same qualitative results as the quantum MC calculations about the ordering of the different isomers of the $Si_{20}$ cluster, even though there are still some quantitative differences.

Density-functional calculations can be inserted in a molecular dynamics (MD) procedure to give the *ab initio* MD, whose best known example is the Car-Parrinello method (Car and Parrinello, 1985), which is well suited to investigate thermodynamic and kinetic properties at $T > 0$ K.

Even though density-functional methods are nowadays reliable and efficient for a large variety of systems, there is still a great interest to develop methods requiring a smaller computational effort. In fact, global optimization (see Section III.D) of clusters in the framework of *ab initio* calculations is not feasible at present except for a few systems and at very small sizes. Moreover, *ab initio* MD is limited to small systems on short time scales, so that either the accurate sampling of thermodynamic properties or the simulation of kinetic processes (diffusion, structural transformations, growth) is far beyond the present possibilities.

Therefore, several approximate energetic models for

clusters have been developed, often on semiempirical grounds. At an intermediate degree of computational effort, there is the tight-binding model for semiconductors (Ho *et al.*, 1998) and metals (Barreteau *et al.*, 2000b; Bobadova-Parvanova *et al.*, 2002). This allows global optimization searches for clusters of a few tens of atoms, and MD simulations even for clusters of $10^2$ atoms (Yu *et al.*, 2002), even though on rather short time scales.

Larger sizes and longer time scales can be now treated by classical atom-atom (or even molecule-molecule) potentials, which are built up on the basis of approximate quantum models. These potentials contain parameters fitted on experimental material properties (semiempirical potentials) or on density-functional calculations (*ab initio* based potentials (Garzón *et al.*, 1998a; Kallinteris *et al.*, 1997)). For metallic systems, several atom-atom potentials have been developed, such as embedded-atom (Daw and Baskes, 1984; Voter, 1993), glue (Ercolessi *et al.*, 1988), second-moment tight-binding (Gupta, 1981; Rosato *et al.*, 1989), Sutton-Chen (Sutton and Chen, 1990), and effective-medium (Jacobsen *et al.*, 1987) potentials. A discussion on the criteria for fitting the parameters in Gupta (1981) potentials is found in López and Jellinek (1999). For metals, these potentials must contain a many-body term, which is responsible for the correct surface relaxations (Desjonqueres and Spanjaard, 1998). The advantage of this approach is that it allows full global optimization to sizes of the order of $\sim 200$ atoms, local relaxation of clusters of $\sim 10^5$ atoms, and MD simulations on time scales of 10 $\mu$s and more for clusters of $10^2$ atoms, which are quite close to the growth time scales of free clusters in inert-gas aggregation sources. The disadvantage is that the (even qualitative) accuracy of these potentials is often questionable, and they must be tested carefully before being used (see for example Ala-Nissila *et al.* (2002)). As we shall see in the following, there are several systems where reliable potentials have been developed. In any case, the use of semiempirical potentials is in practice a necessary tool for the study of medium- or large size clusters. Contrary to bulk materials and crystal surfaces, where one usually knows where to place the atoms, the best structures of clusters are not known in principle, so that a semiempirical modelling is the starting point for more sophisticated approaches. For example in the work of Garzón *et al.* (1998b), the global optimization by a semiempirical potential selects the most promising candidates for a further relaxation study by *ab initio* methods.

Semiempirical interaction potentials for molecular clusters have been built up too. Here we note the Girifalco (1992) and Pacheco and Prates-Ramalho (1997) potentials for fullerene molecules. Finally we mention the oldest semiempirical potentials, Lennard-Jones (LJ) and Morse, which are the usual benchmarks to test new theoretical tools. The Lennard-Jones potential is also a popular model for noble gases.

### D. Global optimization methods

Given the potential energy surface (PES) of the cluster, namely the potential energy $U(\{\mathbf{r}\})$ [where $\{\mathbf{r}\} = (\mathbf{r_1}, \mathbf{r_2}, ...., \mathbf{r_N})$] as obtained by methods such as those of the previous Section, one is confronted with the formidable task of finding its deepest minimum. Indeed, Wille and Vennik (1985) demonstrated that this problem is NP-hard by a mapping to the travelling salesman problem. The number of minima increases more than polynomially with the size (there are indications of a proportionality to $\exp(N)$ ): a Lj cluster of 13 atoms has about $10^3$ local minima (Hoare and McInnes, 1976; Tsai and Jordan, 1993), but this number is at least $10^{12}$ for a 55-atom cluster (Doye and Wales, 1995). Clearly, a complete sampling of all these minima would be simply impossible, and the ability of a given system in reaching its energy global minimum (or at least one of the usually few good local minima) should reside in some special features of its PES. This point has been extensively debated also in the field of protein folding (Wales, 2003), since proteins efficiently fold to their native state (which may not coincide with the lowest minimum in the PES) even if their PES presents an incredibly huge number of local minima. A good search algorithm should exploit the features of the PES to ensure a fast convergence to low-lying minima. However, as we show below, depending on the interaction potential, on the size and composition of the cluster, there are easy PES where most algorithms converge fast to some good *putative* global minima, and others where there are low-lying minima (often of very high symmetry) which are extremely difficult to reach, so that most algorithms get stuck in some other less favorable configuration. A remark is necessary at this stage: no global optimization technique can warrant that the lowest minimum is really reached; the only way to reach the global minimum with probability one is to sample all minima, compare them and choose the lowest one. This can be done only in essentially infinite time in cases of practical interest. For example, while good putative global minima for Lj clusters have been obtained at sizes well above 100 atoms, only for much smaller sizes have these minima proven to be global (Maranas and Floudas, 1992).

Let us now analyze the good features of a PES which allows fast convergence to its global minimum and correspondingly how an efficient global-optimization algorithm must be constructed to exploit these features (Doye, 2004). To this end, a few definitions are needed in the framework of what was proposed by Stillinger and Weber (1982) introducing the inherent structure of liquids. Here below we follow the very clear exposition by Becker and Karplus (1997). A thorough account is given in the excellent book by Wales (2003).

We introduce a mapping from the continuum configurational space of the cluster into the discrete set of its local minima. The mapping associates to each point $\{\mathbf{r}\}$ its closest minimum, i.e. the one which is reached by a

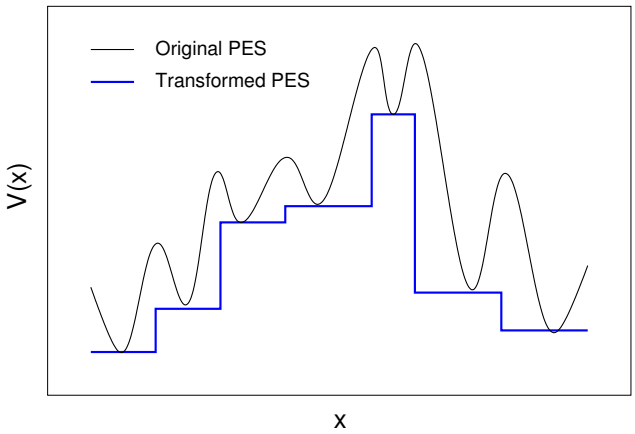


FIG. 10 Transformation of the PES to a staircase (courtesy of Giulia Rossi).

steepest-descent (or a quenching) minimization starting at $\{\mathbf{r}\}$. This amounts effectively to the following transformation of the PES (see Fig. 10)

$$\tilde{U}(\{\mathbf{r}\}) = \min[U(\{\mathbf{r}\})], \tag{10}$$

where min means that the minimization is started from $\{\mathbf{r}\}$. $\tilde{U}(\{\mathbf{r}\})$ is a multidimensional staircase potential (Doye and Wales, 1998a; Li and Scheraga, 1987).

The set of all points which are associated to a minimum $s$ constitutes its *basin*. All points of a given basin are connected by definition. This mapping is a partition of the $3N-6$ dimensional space of the internal coordinates of the cluster into disjoint sets, which are indeed the attraction basins of the different minima. The boundaries between the basins constitute a network of $3N-7$ dimensions, where the mapping is not defined. Nearby basins (usually pertaining to the same structural family) can be grouped into *metabasins*, at different level of complexity. A very convenient representation of the connections between basins, metabasins etc. is given by the *disconnectivity diagrams* (see Fig. 11), which allow one to understand pictorially which basins are connected at different values of the total energy of the cluster (two basins are connected when the highest point on the minimum-energy path between them lies below that total energy).

Portions of the PES can be classified into three different types according to the features of the connections among the basins that they contain: rough PES, single-minimum PES with weak noise, and funnel-like PES (see Fig. 11). It can be easily understood that the absolute minimum is reached quickly in both a single-minimum or a steep funnel-like portion of the PES, while a rough PES will resist against global minimization. Therefore, we expect that the systems whose entire PES is given by a single minimum with weak noise or by a single funnel find their global minimum fast. Correspondingly, such systems are much easier to attack by good global optimization algorithms than the ones with rough PES or with multiple-funnel PES. As an example, for a cluster of given size, Ih structures are usually grouped in a wide metabasin with a funnel structure, which is easily accessible from liquid-like configurations (Doye and Wales, 1998a), because the latter have in common with the icosahedra a pronounced polytetrahedral character (Doye and Wales, 1996a; Nelson and Spaepen, 1989), being formed by tetrahedral units packed together. On the contrary, Dh and TO funnels are much narrower, so that global minima pertaining to these motifs are not easily reached from liquid-like configurations. The best-known example of this kind is the Lj cluster of 38 atoms, which presents a double-funnel PES (see Fig. 11), with a wide Ih funnel and a narrower but deeper close-packed funnel, so that the trapping of search algorithms in the former is very likely. Moreover, one can expect that systems with short-range (sticky) potentials present a larger number of minima and a rougher PES than systems with soft potentials (Doye, 2004; Wales *et al.*, 2000). Multicomponent systems will be harder to optimize because of their much smaller number of equivalent permutational isomers with respect to pure systems (Darby *et al.*, 2002).

From the above considerations, one can understand that an efficient search algorithm must be able to perform and integrate the following tasks:

(a) From any given point on the PES, to find the local minimum at which it is associated; this is simply what is needed to construct the above described mapping, or equivalently to transform the PES into a multidimensional staircase.

(b) To make transitions possible from a given basin to another, and more important, from a metabasin to another. In this way, the algorithm would be able to explore also multiple-funnel PES.

The search by global optimization algorithms can be *unbiased* when the starting configuration is randomly chosen, or *seeded* when a set of (supposedly) good structures is used to begin the optimization procedure. Seeded searches are often faster, since they use the prior knowledge about the system under study, but have the disadvantage of making difficult the finding of unexpected low-lying minima. Almost each algorithm mentioned below can be used either for unbiased or seeded searches; obviously, when comparing different algorithms, the unbiased search is more significant.

Genetic algorithms have applications in a large variety of fields; they are based on the analogy of evolution through natural (fitness based) selection. The fitness is the parameter to be optimized, here the potential energy. The coordinates of each cluster are encoded in a string of bits, called the chromosome. At each step, from the present generation of clusters, a new generation is built up. Sons are built up by mixing the chromosomes of parent clusters, or simply by inserting some mutation in the present chromosomes. The individuals of the old generation are compared to the sons via their fitness, and a new generation is formed from the old individuals and

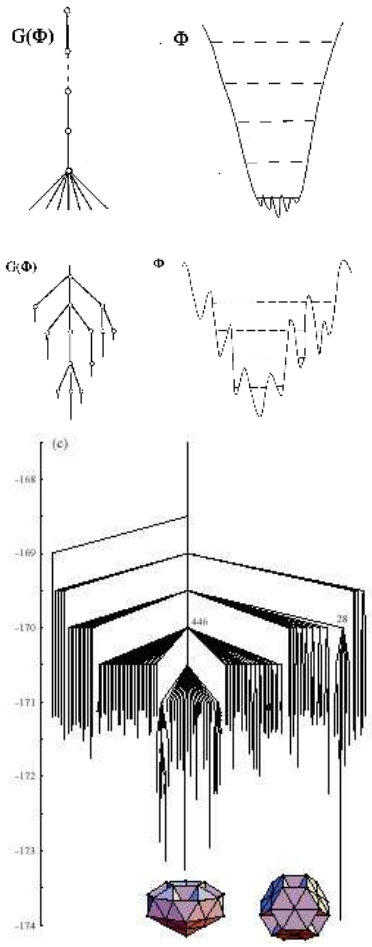


FIG. 11 Disconnectivity diagrams. In the first two panels from top to bottom, schematic of a single-minimum PES with weak noise and of a single funnel PES (after Becker and Karplus (1997)), with their disconnectivity diagrams which show at which energetic level the different local minima of a PES can be considered connected. The lowest panel gives the disconnectivity diagram for the complete double-funnel PES of $LJ_{38}$ (courtesy of Jonathan Doye).

the sons, by some rule that however includes always the best fit individual in the new generation. Very often, several populations are evolved in parallel, and individuals are exchanged between them from time to time. In a genetic algorithm, task (b) is accomplished by chromosome mixing and mutations, and by exchanges of individuals between subpopulations, while task (a) corresponds to compare the fitness of the individuals after a local minimization on them, i.e. comparing $\tilde{U}(sons)$ to $\tilde{U}(parents)$. Recent developments include similarity checking among cluster structure to keep the diversity of the population as the genetic optimization goes on, as in Cheng *et al.* (2004). The use of genetic algorithms in cluster optimization was pioneered by Hartke (1993) and by Xiao and Williams (1993), who made applications to $Si_4$ and various molecular clusters respectively. Then there have been applications to a wide variety of systems. Michaelian *et al.* (1999) optimized transition and noble metal clusters by a symbiotic variant of a genetic algorithm (Michaelian, 1998); Hartke (2000, 2003) treated also water clusters; Deaven and Ho (1995), Deaven *et al.* (1996) and Ho *et al.* (1998) optimized LJ and silicon clusters; Rata *et al.* (2000) and Bobadova-Parvanova *et al.* (2002) considered silicon and iron clusters; Darby *et al.* (2002), Massen *et al.* (2002), Bailey *et al.* (2003), and Lloyd *et al.* (2004) optimized Pd-Pt, Au-Cu and Al-Ni nanoalloy clusters; finally Rossi *et al.* (2004) searched for the global minima of Ag-Cu, Ag-Ni and Ag-Pd clusters. Recent reviews are found in Hartke (2002) and Johnston (2003).

The basin-hopping algorithm (Doye and Wales, 1998a; Doye, 2004; Li and Scheraga, 1987) differs from genetic algorithms because it accomplishes task (b) simply by a canonical MC simulation at constant $T$ on the transformed PES. In this framework, the transformation of the PES amounts to lowering the barriers between basins to the maximum possible extent, while keeping the levels of the minima unchanged. Starting from a given basin, a move with random displacements is tried and the energy difference between the old and the new position $\Delta\tilde{U}$ is calculated. If $\Delta\tilde{U} < 0$ the move is accepted with probability 1, otherwise with probability $\exp[-\Delta\tilde{U}/(k_B T)]$. On $\tilde{U}$, transitions can occur in any direction, not only through saddle points, and transition to lower-lying minima are always accepted. Basin hopping has been applied successfully to the optimization of a large variety of systems, from LJ clusters (Wales and Doye, 1997), to clusters of fullerene molecules (Doye *et al.*, 2001), of transition and noble metals (Doye and Wales, 1998b) and of aluminum (Doye, 2003). Basin hopping was able to find the difficult putative global minima in LJ clusters at sizes 38, 75, 76, 77 and 98, starting from random initial conditions. Recently, Lai *et al.* (2002) optimized sodium clusters by both genetic and basin-hopping algorithms, finding the same set of minima. This could indicate both algorithms have comparable efficiency.

Another popular algorithm is simulated annealing (Biswas and Hamann, 1986; Freeman and Doll, 1996; Kirkpatrick *et al.*, 1983). In thermal simulated annealing, the system is evolved at constant high $T$ on the untransformed PES by either MC or molecular dynamics (MD), and it is slowly cooled down. Simulated annealing has the advantage of being pretty much physical: one tries to mimic the procedure of cooling a sample which hopefully will reach its most stable configuration if cooling is sufficiently slow. This algorithm is easily implemented into standard MC and MD codes (including *ab initio* MD), and the analysis of its output is easy and intuitive. For these reasons, this algorithm has been used for a large variety of systems [3]. There is however a major draw-

[3] To cite but a few, Röthlisberger and Andreoni (1991), Jones (1991), Kumar and Car (1991), Vlachos *et al.* (1992), Jones and

back in simulated annealing: there is effectively a single local optimization, and if the system fails to be confined to the basin of attraction of the global minimum as the temperature is decreased, the algorithm may fail, even if it passed through the basin of the global minimum when $T$ was high. As a result, simulated annealing is less efficient than genetic and basin-hopping algorithms (Hartke, 1993; Zeiri, 1995). To avoid trapping in a single basin, one can make long high-$T$ MC or MD runs, collecting a large quantity of different snapshots and quenching them down (Baletto *et al.*, 2004; Sebetci and Güvenc, 2003), monitoring the short-term average of kinetic energy (Garzón and Posada-Amarillas, 1996; Jellinek and Garzón, 1991). $T$ must be chosen carefully. If it is too high, the probability of catching the global minimum is very small; if $T$ is too low, the cluster is likely to remain trapped in the basin where it started from.

Another family of annealing algorithms is known under the name of quantum annealing (Amara *et al.*, 1993; Finnila *et al.*, 1994; Freeman and Doll, 1996). In quantum annealing, the system is first collapsed into its quantum ground state by using diffusion or Green function MC techniques (Ceperley, 1994) and then quantum mechanics is slowly turned off. This algorithm utilizes delocalization and tunnelling as the primary means for avoiding trapping in metastable states. Amara *et al.* (1993) and Finnila *et al.* (1994) applied quantum annealing to LJ clusters up to $N = 19$. Lee and Berne (2000) coupled quantum and thermal annealing being thus able to find the difficult $LJ_{38}$ close-packed global minimum, but failing for other difficult cases at larger size, such as the Marks Dh at $N = 75$. Recently, Liu and Berne (2003) have developed a new quantum annealing procedure. This is based on quantum staging path integral MC sampling and local minimization of individual imaginary time slices, and it is able to locate all LJ minima for $N \leq 100$ except at $N = 76, 77, 98$, being thus comparable to basin-hopping and genetic algorithms. This form of quantum annealing uses local minimization to accomplish task (a), and mutations (in which coordinates of randomly selected atoms are reset) to facilitate task (b).

An algorithm which tries to combine the advantages of simulated-annealing, genetic and basin-hopping approaches has been recently developed by Lee *et al.* (2003). Their algorithm was able to optimize LJ clusters up to size 201.

Finally, a very recent proposal is to search for global minima by means of a growth procedure. Solov'yov *et al.* (2003a,b) applied this method to LJ clusters, starting from a tetrahedron, and adding one atom at a time according to different procedures (adding an atom on the surface, inside the surface, or at the center of mass of the cluster). After adding a new atom, the cluster is quenched down to search for the closest local minimum, and the results of the different addition procedures are compared to select the best minimum. This procedure exploits the fact that clusters of nearby sizes are likely to have global minima with some resemblance, and with this respect it is a seeded algorithm. Solov'yov *et al.* (2003b) were able to find all global minima up to $N = 150$. Again, their procedure works on $\tilde{U}$, since clusters are compared for selection after local minimization.

This last observation lead us to a summarizing comment. The most successful algorithms make extensive use of local minimization, comparing the structures for selection *after* having performed that minimization. This amounts to effectively working on $\tilde{U}$. To use the words of Doye (2004), *the method for searching $\tilde{U}$ is of secondary importance to the use of the transformation itself.* The searching method may be based on thermal MC, quantum tunnelling or genetic operations, but at the end the efficiencies are comparable, given that the algorithms are well constructed.

Doye and Wales (1998a) have shown that the transformation to $\tilde{U}$ modifies the system thermodynamics in such a way that the temperature range in which transitions among different funnels are possible is enlarged, and the probability of occupying the basin of the global minimum is increased. This can be understood by analyzing the occupation probability of a minimum $s$. For the untransformed PES within the harmonic approximation (see Section IV) $p_s \propto \exp(-\beta E_s)/\Omega_s^{3N-6}$, where $E_s$ is the potential energy of minimum $s$, $\Omega_s$ is the geometric mean vibrational frequency, and $\beta = (k_B T)^{-1}$, with $k_B$ the Boltzmann constant. For the transformed PES, $p_s \propto A_s \exp(-\beta E_s)$, where $A_s$ is the hyperarea of the basin of attraction of minimum $s$. The differences between these expressions, the vibrational frequency and hyperarea terms, have opposite effects on the thermodynamics. The higher energy minima are generally less rigid and with a favorable vibrational entropy, so that the transitions are pushed down to lower temperature and sharpened. By contrast, the hyperarea of the minima decreases with increasing potential energy, thus stabilizing the lower energy states and broadening the thermodynamics. The transformation to a staircase PES is not the only useful transformation. Other possibilities are found for example in Pillardy and Piela (1995), Locatelli and Schoen (2003), and Shao *et al.* (2004).

What are the maximum sizes presently tractable by global optimization? This answer depends on the system under study, and on the degree of sophistication of the interaction potential. In the Cambridge Cluster Database (see www-wales.ch.cam.ac.uk/CCD.html), putative global minima for several systems are reported, ranging from LJ to Morse, metallic, and water clusters. Even for the simplest potentials, the largest sizes are up to $N = 190$ (Al (Doye, 2003) and Pb clusters (Doye and Hendy, 2003) modelled by the glue potential (Lim *et al.*, 1992)), and decrease for more complex interactions. Very

Seifert (1992), Stave and DePristo (1992), Cheng *et al.* (1993), Jones (1993), Christensen and Cohen (1993), Ma and Straub (1994), Bacelo *et al.* (1999), Ahlrichs and Elliott (1999).

recent seeded optimizations of LJ clusters (Shao *et al.*, 2004) arrived to $N = 330$. In order to treat large sizes, Krivov (2002) has proposed a hierarchical method for optimizing quasiseparable systems. In these systems, distant parts are independent, so that a perturbation to the coordinates of a given part has very little influence on distant atoms. According to Krivov (2002), one can exploit this property to build up a hierarchical procedure allowing to treat LJ clusters of several hundreds of atoms. More complex systems such as water clusters have been optimized up to $N \simeq 30$ (Hartke, 2003; Wales and Hodges, 1998). Ahlrichs and Elliott (1999) optimized aluminum clusters within a density-functional approach up to $N = 15$ by simulated annealing. Tekin and Hartke (2004) optimized Si clusters by a combination of empirical global search and density-functional local optimization up to $N = 16$. In the case of tight-binding modelling of the interactions the sizes amenable by global optimization approaches extend to a few tens of atoms, see for example Zhao *et al.* (2001) who optimized Ag clusters up to $N = 20$ by a genetic algorithm.

How do the best algorithms scale with cluster size? This might be an ill-posed question, since there is no demonstration that the minima found by the different algorithms are really global. However, Liu and Berne (2003) find that their quantum annealing algorithm scales as $N^{3.2}$ for LJ clusters in the size range $11 - 55$, and Hartke (1999) finds that his genetic algorithm scales approximately as $N^3$, again for LJ clusters up to $N = 150$.

### E. Studies of selected systems

In this Section we review the energetics of atomic clusters of some selected materials, chosen both for their importance from the point of view of basic science (see for example noble-gas and alkali-metal clusters, which have been the benchmark for testing theoretical models) and for their practical applications (silicon clusters, transition and noble-metal clusters). Finally, we treat a specific kind of molecular clusters, those of fullerene molecules, which present experimental structures whose interpretation in energetic terms has been a long-standing puzzle.

#### 1. Noble-gas clusters

Noble-gas clusters have been thoroughly studied in the past decades. Excellent accounts about their properties are in Haberland (1994) and Johnston (2002). Here we briefly review their energetics, focusing on the transition sizes among structural motifs, and comparing theory with experiments. A special place among noble-gas clusters is occupied by He clusters, which are the best known example of quantum clusters. Recently, there has been a noticeable experimental interest in He clusters, which can be formed by $^4$He, $^3$He or by a mixture of the two [4]. In the following, we treat "classical" clusters first, and then He clusters.

In a classical series of electron-diffraction experiments, Farges *et al.* (1983, 1986) investigated the structure of neutral Ar clusters produced in a free jet expansion. They compared the experimental diffraction patterns with those obtained by freezing LJ droplets of different sizes in MD simulations, being thus able to identify the experimental products up to $N \sim 10^3$ atoms. Harris *et al.* (1984) measured the mass spectra of charged Ar clusters at $N < 100$. At $20 < N < 50$, both experiments found polyicosahedral structures, composed by interpenetrating 13-atom icosahedra. From $N = 50$ to $N \sim 750$ multishell structures based on the Mackay Ih were found. Farges *et al.* (1986) were also able to single out features from diffraction by fcc planes in their spectra of clusters with $N > 600$ atoms . Thus they came to the conclusion that the Ih $\rightarrow$ fcc transition is placed at $N \sim 750$. However, in a more recent analysis, van de Waal *et al.* (2000) have shown that the transition is to a mixture of fcc, hcp, and random close-packed regions, with no significant preference for the fcc bulk structure.

Let us see how the energetics calculation compare with these experimental results. Most of the calculations are based on the use of the Lj potential, which is a very popular model for noble-gas systems even though not completely accurate. Several global-optimization studies showed that the Ih motif is by far dominant at small sizes [5], with few exceptions. Polyicosahedral clusters are formed at sizes 19, 23, 26 (Farges *et al.*, 1988; Ikeshoji *et al.*, 1996). Indeed, Wales and Doye (1997) found that there are only seven exceptions in the range $13 \leq N \leq 150$: at $N = 38$ the global minimum is a TO; at $N = 75, 76, 77$ and $N = 102, 103, 104$ the best structures are based on the (2,2,2) and (2,3,2) Marks Dh respectively. Later on, Leary and Doye (1999) discovered that the global minimum at $N = 98$ is tetrathedral. Romero *et al.* (1999) optimized clusters in the range $148 \leq N \leq 309$ on Ih and Dh lattices, finding again a prevalence of Ih putative global minima with only 11 Dh exceptions.

At larger sizes, Raoult *et al.* (1989b) compared perfect Ih and Dh structures and concluded that Marks decahedra finally prevail over icosahedra at $N > 1600$. Concerning the transition to fcc structures, Xie *et al.* (1989b) compared Ih and CO clusters finding a crossover at $N \sim 10^4$. However, cuboctahedra are not the most favorable fcc clusters. Therefore the crossover should be

[4] Recent accounts on He clusters are found in Whaley (1994), Toennies and Vilesov (1998), Scoles and Lehmann (2000), Northby (2001), Callegari *et al.* (2001), Johnston (2002), Jortner (2003).

[5] See Hoare and Pal (1975), Freeman and Doll (1985), Farges *et al.* (1985), Wille (1987), Northby (1987), Coleman and Shalloway (1994), Xue (1994), Pillardy and Piela (1995), Deaven *et al.* (1996), Wales and Doye (1997), Romero *et al.* (1999).

at much lower sizes (Raoult *et al.*, 1989a; van de Waal, 1989), comparable to the crossover size with Marks Dh.

The combination of these energy-minimization results gives a reasonable interpretation of the experiments, even though there are some points that cannot probably be explained in terms of the energetics alone. At small sizes, the agreement between the global optimization calculations and the experiments is good, even though the Dh global minima are not yet observed. This may indicate the presence of entropic effects, of the kind of those discussed in Section IV.A, or that even at small sizes some kind of kinetic trapping is taking place (see Section V.A). At larger sizes, the comparison of theory and experiments is much more difficult, and there has been a considerable debate in the interpretation of the diffraction data in terms of known structures (van de Waal, 1996). For example, fcc clusters with twin faults give electron diffraction patterns which are very similar to those of Marks Dh. In any case, a coarse grained picture is in agreement with the general trend of a transition from the Ih motif to other structures. A more detailed analysis reveals that several kinds of clusters can be present in the same size range, so that structural transitions are not really sharp. Quantitative agreement on the transition size between the LJ calculations and the experiments has not been reached, probably due to the limited accuracy of the LJ potential for Ar. At present, it is very difficult to ascertain whether the diffraction data from large clusters support the existence of either entropic or kinetic effects. Some interesting results about this point (Ikeshoji *et al.*, 2001) are discussed in Section V.A.

Let us now consider $^4$He clusters. While the dimer is stable but very weakly bound (Grisenti *et al.*, 2000; Luo *et al.*, 1993), the trimer (which should have a noticeable contribution from linear configurations according to the calculations by Lewerenz (1996)) and larger clusters are much more stable (Toennies and Vilesov, 1998). Chin and Krotscheck (1992) calculated the ground state properties of various $^4$He clusters modelled by the Aziz *et al.* (1987) potential, considering several sizes up to $N = 112$, by diffusion MC simulations. They found evidence of density oscillations indicating a possible shell structure. Chin and Krotscheck (1995) confirmed the existence of these oscillations also for larger clusters, and were also able to recover the bulk limit of the excitation spectrum. In a very recent experiments Brühl *et al.* (2004) observed magic sizes at $N = 10, 11, 14, 22, 26, 27$ and 44 atoms, in $^4$He clusters produced in a free-jet expansion. By comparing the experimental results with diffusion MC calculations, Brühl *et al.* (2004) showed that these magic sizes are not related to enhanced binding energies at specific values of $N$, but to the sizes at which excited levels cross the chemical potential curve and become stabilized.

Clusters of $^3$He are much less stable, because the constituent atoms are fermions, so that the minimum number of atoms $N_{min}$ needed to form a stable cluster is relatively large. A configuration interaction calculation based on a phenomenological density functional gave $N_{min} = 29$ (Barranco *et al.*, 1997), subsequent variational MC calculations with the Aziz potential gave 34-35 as an upper bound to $N_{min}$ (Guardiola and Navarro, 2000; Guardiola, 2000). The same kind of calculations (Guardiola and Navarro, 2002) have recently been applied to mixed $^4$He-$^3$He clusters, finding that their stability has a non-trivial dependence on size and composition.

### 2. Alkali-metal clusters

The structural properties of small Li and Na clusters have been the subject of a long-lasting theoretical activity which followed the seminal experiments by Knight *et al.* (1984). Bonacić-Koutecký *et al.* (1991) gave an excellent account of the earlier developments, which are very briefly summarized here. Systematic *ab initio* configuration-interaction studies on Li and Na clusters (Bonacić-Koutecký *et al.*, 1988; Boustani *et al.*, 1987) for $N \leq 9$ have shown the complete analogy between the two elements. The lowest isomers are planar up to the pentamer; at $N = 6$ a pentagonal pyramid and a triangular planar structure are in very close competition; larger clusters are 3D. In agreement with the experimental magic numbers and with the electronic shell closing arguments, the cluster of 8 atoms, of tetrahedral ($T_d$) symmetry (Jellinek *et al.*, 1994), is especially stable compared to neighboring sizes. At slightly larger sizes Röthlisberger and Andreoni (1991) and Röthlisberger *et al.* (1992) performed Car-Parrinello calculations on Na. At $N = 13$, they obtained that the most stable isomer is neither an Ih nor a CO but a capped pentagonal bipyramid. At $N = 18$ the most stable isomer was the double Ih minus one vertex, and at $N = 20$ the isomers based on pentagonal symmetries (which are closely related to the double Ih) were found to be more stable than structures with $T_d$ symmetry. On the other hand, Bonacić-Koutecký *et al.* (1991) found that two $T_d$ structures are the lowest in energy for $Li_{20}$ and $Na_{20}$ (Bonacić-Koutecký *et al.*, 1993b). Spiegelman *et al.* (1998) found results in reasonable agreement with the previous calculations by a tight-binding approach.

Recent developments are found in Ishikawa *et al.* (2001), Solov'yov *et al.* (2002) and Matveentsev *et al.* (2003). Ishikawa *et al.* (2001) reanalyzed the problem of $Li_6$, where planar and 3D structures were found to be in competition, by a global optimization procedure employing the Replica Exchange Method (Swendsen and Wang, 1986) applied to *ab initio* calculations. They found a 3D structure of $D_{4h}$ symmetry, which is slightly lower in energy than the planar triangle and the pentagonal pyramid. Poteau and Spiegelmann (1993) performed a search of the best Na isomers up to $N = 34$ by a growth MC algorithm in the framework of a distance-dependent tight-binding (Hückel) model. They found that at $N = 34$ the best isomer is the double Ih surrounded by a ring of 15 atoms. Sung *et al.* (1994) optimized Li clusters up to $N = 147$ by simulated annealing within the Lo-

cal Spin Density approximation to DFT, finding that for $55 \leq N \leq 147$ the structures based on the Mackay Ih are the lowest in energy. This has been recently confirmed by Reyes-Nava *et al.* (2002) who performed global genetic optimization of sodium modelled by Gupta (1981) potentials. A thorough global optimization study (both by genetic and basin-hopping algorithms) of Na, K, Rb and Cs clusters in the framework of the Gupta (1981) potential (as developed by Li *et al.* (1998)) has been performed by Lai *et al.* (2002) up to N=56. They found a sequence based on Ih clusters except for $N = 36$ and $N = 38$. At $N = 38$ the global minimum is a TO, with distorted facets in the cases of Na and Cs; at $N = 36$ the structure is a distorted incomplete TO.

The transition from electronic to geometric magic numbers in Na clusters has been already discussed in Section III.B. Here we simply recall that for $2000 < N < 20000$, there is experimental evidence (Martin *et al.*, 1991a; Martin, 1996, 2000) of peaks in the abundances of Na clusters at sizes corresponding to the completion of perfect Ih, Ino Dh or CO structures, which have exactly the same magic numbers. From these magic numbers, one cannot directly infer the actual cluster structures. However, there are is at least one indirect argument in favor of Ih structures: in fact, while complete icosahedra are surely more favorable than incomplete ones, neither Ino decahedra are usually the best Dh structures, nor cuboctahedra are the best among the possible TO clusters.

### 3. Noble and quasi-noble metal clusters

Here we treat the energetics of pure clusters of the elements of the last two columns of the transition series: Ni, Cu, Pd, Ag, Pt and Au. We restrict our treatment to neutral clusters unless otherwise specified.

*a. Gold clusters.* - Small Au clusters ($N \leq 10$) have been thoroughly treated by *ab initio* methods. Bravo-Pérez *et al.* (1999a) studied sizes $3 \leq N \leq 6$ finding that the best structures are planar (Bravo-Pérez *et al.*, 1999b) These results have been confirmed and extended in several works [6]. Au clusters are planar up to $N = 10$ at least according to Bonacić-Koutecký *et al.* (2002) (see Fig. 12), and only to $N = 6$ according to Wang *et al.* (2002), who however found that flat (but non planar) structures are the lowest in energy up to $N = 14$. In the experiments on Au cations by Gilb *et al.* (2002) there is evidence for planar clusters at least up to $N = 7$. The physical origin of the preference for planar structures is discussed in Section III.E.4. On the other hand, Li *et al.*

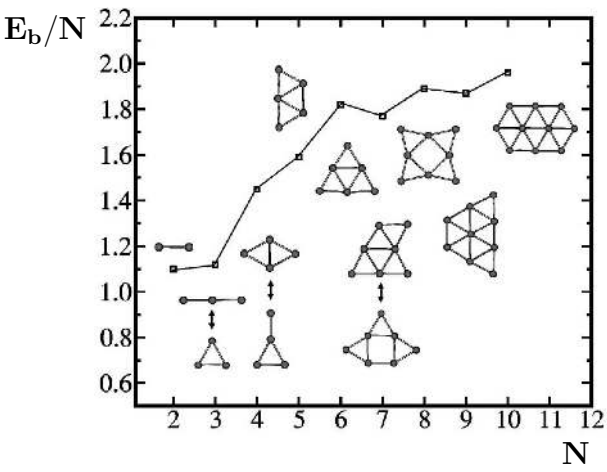


FIG. 12 Lowest energy isomers of Au clusters according to Bonacić-Koutecký *et al.* (2002). All clusters are planar up to $N = 10$ at least. The binding energy per atom $E_b/N$ (in eV) is also reported. For isomers with energy difference smaller than 0.1 eV, both competing structures are shown (see sizes 3, 4, and 7).

(2003) found experimental and computational evidence that $Au_{20}$ is a tetrahedron, well separated from higher isomers. This finding has been confirmed by the calculations by Wang *et al.* (2003a).

Global optimization methods (Wilson and Johnston, 2000) have been applied to larger clusters modelled by semiempirical potentials. Garzón *et al.* (2003, 1998b) and Michaelian *et al.* (1999) modelled Au by the Gupta (1981) potential and searched the best isomers by a genetic algorithm, to use them as the starting point of a local relaxation by the density-functional method. They found that Au presents low-symmetry structures at some geometric magic numbers, such as $N = 38$ and 55, that therefore are not true magic numbers for Au clusters. These structures are often called amorphous in the literature, even though the most appropriate terminology is low-symmetry structures. The low-symmetry cluster at $N = 55$ is a strongly rearranged and distorted Ih, which conserves some fivefold vertexes (see Fig. 13) . Low-symmetry structures are found in several semiempirical calculations [7], the only exception being the Murrell-Mottram potential (Cox *et al.*, 1999) which gives high-symmetry clusters. All these results indicate that high- and low-symmetry structures are in close competition, and the global minimum is sensitive to the fine details of the potential parametrization. An argument in favor of the low-symmetry structures follows from the density-functional relaxation at $N = 75$ by Michaelian *et al.* (1999), who found that a low-symmetry structure is lower in energy than the $(2, 2, 2)$ Marks Dh, in contrast with

[6] See Häkkinen and Landman (2000), Grönbeck and Andreoni (2000), Häkkinen *et al.* (2002), Gilb *et al.* (2002), Bonacić-Koutecký *et al.* (2002), Wang *et al.* (2002), Zhao *et al.* (2003).

[7] See for example Doye and Wales (1998b), Li *et al.* (2000a), Darby *et al.* (2002), Garzón *et al.* (2002).

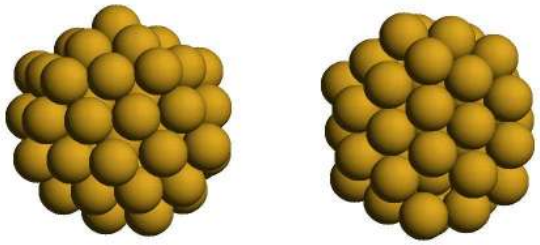

FIG. 13 Two views of the lowest energy isomer of Au at $N = 55$ as found by Garzón *et al.* (1998b). This cluster is a strongly rearranged and distorted $Ih_{55}$, similar to the double-rosette (Dr) structure discussed in the case of $Pt_{55}$ in Section V.A.4. Courtesy of Ignacio Garzón.

all semiempirical results. The physical origin of low-symmetry structures is discussed in Section III.E.4.

For larger sizes, Cleveland and Landman (1991) and Baletto *et al.* (2002b) performed semiempirical calculations to compare structures of the different motifs, finding that Marks Dh are the most favorable, the crossover with fcc structures being at $N \sim 500$.

The comparison of these theoretical predictions with the experiments is complicated by the fact that Au clusters are very often passivated during or after the formation process (Schaaff and Whetten, 2000; Whetten *et al.*, 1996), and it is difficult to determine to what extent the action of the passivating agents can modify the structures (Alvarez *et al.*, 1997). With this in mind, we try however to determine how the calculated crossover sizes compare with the experimental results. To this purpose, we must single out those experiments where the observed clusters are able to reach their equilibrium structure. This is very likely the case of the work by Patil *et al.* (1993), who produced free Au clusters in inert gas aggregation sources. The clusters were subsequently slowly heated up above their melting temperature and then slowly cooled down (for about one second). Finally, the clusters were deposited and observed. These clusters were identified as being fcc, even at the smallest sizes ($N \simeq 400$), in good agreement with the crossover sizes calculated in Baletto *et al.* (2002b) (see Table I and Fig. 14). On the other hand, there are several observations of large Ih structures [8], at $N \gg 400$. For example, Ascencio *et al.* (1998, 2000) have observed by high-resolution electron microscopy a variety of structures (Dh, TO, Ih and amorphous) for passivated particles of a few nanometer diameter, with a prevalence however of (possibly defected) Marks and Ino Dh. Defected clusters of diameter of 2 - 4 nm have been detected by X-ray diffraction (Zanchet *et al.*, 2000). Moreover, in a recent experiment, Koga and Sugawara (2003) have analyzed a large sample of free Au clusters obtained in an inert gas aggregation source, with diameters of 3-18 nm and found that icosahedra are firstly dominant and decahedra secondly dominant, fcc clusters being absent. These results are again an indication in favor of kinetic effects and are discussed in Section V.B.3.

[8] See Buffat *et al.* (1991), Marks (1994), Martin (1996), Ascencio *et al.* (1998), Ascencio *et al.* (2000), Koga and Sugawara (2003).

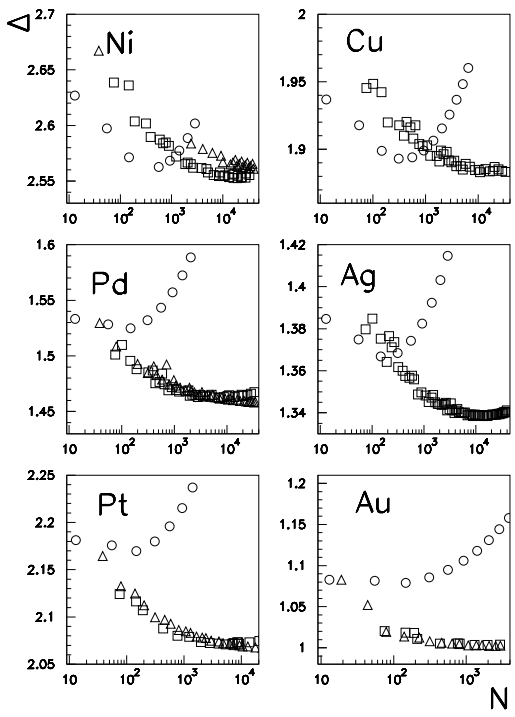


FIG. 14 $\Delta$ as a function of $N$ for Ih (circles), Dh (squares) and TO (triangles) clusters in the cases of Ni, Cu, Pd, Ag, Pt and Au. Data are taken from Baletto *et al.* (2002b), except for the data concerning Ni, which are original. For Dh and TO, only the most favorable clusters are shown in the different size ranges.

*b. Silver clusters.* As in the case of Au, the energetics of Ag clusters has been the subject of intensive study in all size ranges. For $N \leq 9$, Bonacić-Koutecký *et al.* (1993a, 1994) searched for the lowest energy clusters by a self-consistent Hartree-Fock procedure which was able to produce structures in good agreement with the experiments (Alameddin *et al.*, 1992; Ganteför *et al.*, 1990; Ho *et al.*, 1990; Jackschath *et al.*, 1992). They found that the best isomers are planar up to the pentamer, as confirmed by Matulis *et al.* (2003) by density-functional calculations. Santamaria *et al.* (1994) found a planar structure also at $N = 6$. Recent density-functional studies considered $N \leq 12$ (Fournier, 2001), and $N = 13$ (Oviedo and Palmer, 2002). The latter study suggested that the best isomer of 13 atoms is of low symmetry, and that even the CO is more favorable than the Ih. On the contrary, previous density-functional studies on larger Ag clusters

TABLE I Parameters $p, q$ of the Rosato *et al.* (1989) potential; parameters $\sigma_1 = pq/2$, $\sigma_2$, $\sigma_3$ and $\sigma_A$ (see Eqs. (16,17)); sizes where $\Delta$ is minimum ($N_\Delta^{Ih}$ for icosahedra and $N_\Delta^{Dh}$ for decahedra), and crossover sizes ($N_{Ih\to Dh}$, $N_{Dh\to fcc}$ and $N_{Ih\to fcc}$). in the case of the different noble and quasi-noble metals. The parameters of the potentials are taken from Baletto *et al.* (2002b) except for those of Ni, which are found in Meunier (2001) and Baletto *et al.* (2003b). The results on the crossover sizes are taken from Baletto *et al.* (2002b), except those for Ni which are published here for the first time. The results for $\sigma_A$ are taken from Soler *et al.* (2000).

| Metal | p | q | $\sigma_1$ | $\sigma_2$ | $\sigma_3$ | $\sigma_A$ | $N_\Delta^{Ih}$ | $N_\Delta^{Dh}$ | $N_{Ih\to Dh}$ | $N_{Dh\to fcc}$ | $N_{Ih\to fcc}$ |
|---|---|---|---|---|---|---|---|---|---|---|---|
| Cu | 10.55 | 2.43 | 13.1 | 0.062 | 0.35 | 0.24 | 309 | 20000 | 1000 | 53000 | 1500 |
| Ag | 10.85 | 3.18 | 17.2 | 0.065 | 0.29 | 0.54 | 147 | 14000 | <300 | 20000 | 400 |
| Au | 10.53 | 4.30 | 22.6 | 0.082 | 0.16 | 1.86 | 147 | 1300 | <100 | 500 | <100 |
| Ni | 11.34 | 2.27 | 12.9 | 0.055 | 0.37 | 0.05 | 561 | 17000 | 1200 | 60000 | 2000 |
| Pd | 11.00 | 3.79 | 20.9 | 0.062 | 0.21 | 0.78 | 147 | 5300 | <100 | 6500 | <100 |
| Pt | 10.71 | 3.85 | 20.6 | 0.073 | 0.22 | 1.40 | 147 | 5300 | <100 | 6500 | <100 |

(Jennison *et al.*, 1997) found that at $N = 55$ the Ih is lower in energy than the CO.

Larger clusters have been studied mainly by semiempirical interatomic potentials. This approach has allowed global minimum searches for $N$ up to 100 atoms (Doye and Wales, 1998b; Erkoç and Yilmaz, 1999), and the comparison of selected magic structures belonging to the Ih, Dh and TO motifs for $N$ up to 40000 atoms (Baletto *et al.*, 2002b). Doye and Wales (1998b) modelled Ag by the Sutton and Chen (1990) potential and optimized Ag clusters at $N \leq 80$, finding the same lowest energy structures as Bonacić-Koutecký *et al.* (1993a) at $N = 7, 8, 9$, and Ih global minima at $N = 13$ and 55. 30 of the global minima were Ih in character, but several Dh and fcc clusters were found, the most stable being at $N = 38$ (TO) and $N = 71, 75$ (Dh). Mottet *et al.* (1997) modelled Ag by the Rosato *et al.* (1989) semiempirical potential, reproducing essentially the same behavior as the Sutton and Chen (1990) potential at small sizes. They showed that clusters of high stability can be obtained by removing the central atom in perfect icosahedra. In fact, a central vacancy allows neighboring atoms to better relax expanding their intrashell distance. The same effect was found also in Cu and Au clusters. We note that, at variance with Au, there is no indication in Ag in favor of disordered structures at geometric magic numbers (38, 55, 75). Finally Baletto *et al.* (2002b) and Mottet *et al.* (2004) looked at the crossover sizes (see Table I) by an extensive comparison of clusters of the different motifs.

All the previous theoretical results agree in predicting that Ag follows the general trend outlined in Section III.A, with small icosahedra, intermediate-size decahedra and large TO clusters. This in clear contrast with the inert gas aggregation experiments by Reinhard *et al.* (1997b), in which small clusters ($\sim$ 2 nm of diameter) were mainly Dh (or fcc) while large clusters (above 5 nm) were mostly Ih. The explanation of this discrepancy can be achieved only by taking into account kinetic trapping effects leading to the growth of metastable structures, as discussed in Section V.B.3.

*c. Copper clusters* The energetics of small Cu clusters has been extensively treated in a recent review by Alonso (2000); here we give a brief summary of the results for small sizes and then focus on larger clusters.

Several *ab initio* calculations [9] have been performed for $N \leq 10$, again comparing a set of reasonably good structures. There is evidence of planar structures up to $N = 5$ or $N = 6$ maximum, as suggested by recent density-functional calculations (Jug *et al.*, 2002a). For $N = 13$, density-functional calculations (Fujima and Yamaguchi, 1989) indicate that the Ih is favored against the CO.

For larger size, up to $N \sim 100$, global optimization studies by semiempirical potentials have been performed. Doye and Wales (1998b) used the Sutton and Chen (1990) potential and Darby *et al.* (2002) the Gupta (1981) potential. In both cases, the best structure at $N = 13$ is the Ih, in agreement with density-functional calculations, and there is no indication in favor of disordered structures at geometric magic numbers. Cu thus behaves like Ag, and very differently from Au. Baletto *et al.* (2002b) compared the energies of Ih, Dh and TO clusters at larger sizes, finding that the crossover from Ih to Dh structures is around 1000 atoms and that Dh and TO structures are in close competition up to 30000 atoms at least (see Table I). Contrary to the Ag case, this behavior is in agreement with the inert gas aggregation experiments by Reinhard *et al.* (1997a, 1998), who were able to identify a prevalence of small Ih, intermediate-size Dh and large fcc clusters, with a wide size interval of coexistence of Dh and fcc clusters. The crossover size between Ih and Dh structures is in agreement with the calculations.

*d. Platinum clusters.* The energetic stability of small Pt clusters has been addressed by quite few studies, when

[9] See Bauschlicher *et al.* (1989, 1990, 1988); Bauschlicher (1989), Fujima and Yamaguchi (1989), Jug *et al.* (2002a), Jug *et al.* (2002b), Massobrio *et al.* (1995)

compared to the other metals treated here. Grönbeck and Andreoni (2000) performed a density-functional study in the size range $2 \leq N \leq 5$ finding that the lowest lying isomers are planar both for the tetramer and the pentamer. The preference for planar structures is in agreement with previous density-functional calculations by Yang *et al.* (1997) who found planar structures also for $N = 6$ by a dynamical quenching procedure. On the contrary, other *ab initio* calculations (Dai and Balasubramanian, 1995) on the tetramer gave preference to the tetrahedal structure, as in the density-functional results by Fortunelli (1999) who found that the lowest-lying isomer is indeed the tetrahedron, with a planar rhombic structure being slightly higher in energy.

At larger sizes, Sachdev *et al.* (1992) modelled Pt by an embedded atom potential and made simulated annealing calculations, finding that both at 13 and at 55 atoms low-symmetry isomers are the lowest in energy. On the other hand, further global optimization results based on semiempirical modelling (Baletto *et al.*, 2002b; Doye and Wales, 1998b; Massen *et al.*, 2002; Sebetci and Güvenc, 2003) gave preference to the Ih structure at $N = 13$. Doye and Wales (1998b); Massen *et al.* (2002) found a low-symmetry structure at $N = 55$, while Baletto *et al.* (2002b) found the Ih structure also at this size, however with small crossover sizes among Ih, Dh and TO structural motifs (see Table I). *Ab initio* results are even fewer. Yang *et al.* (1997) found that at $N = 13$ several low-symmetry structures are lower in energy than the Ih and the CO. Watari and Ohnishi (1998) found that the CO is more stable than the Ih at $N = 13$ by density-functional calculations. Recently, Fortunelli and Aprà (2003) extended their calculations to $N = 13$, 38 and 55. At $N = 13$, they found that the Ino Dh is lower in energy than the Ih and the CO, but a $D_{4h}$ structure originated from the symmetry breaking of the CO is even lower. At $N = 55$ the order of the structures is inverted, and the Ih becomes lower than the Ino Dh and the CO. Fortunelli and Aprà (2003) attributed the results at $N = 13$ to the small size of the molecule, while the behavior at $N = 55$ is intermediate between finite molecules and fully metallic systems. Very recent density-functional calculations by Aprà *et al.* (2004) show that rosette structures, originating from the disordering of one or two vertices in the $Ih_{55}$, are considerably lower in energy than the Ih itself. This result would support the preference of Pt for low-symmetry structures at icosahedral magic numbers.

*e. Palladium clusters.* The energetics of small Pd clusters has been investigated by several groups employing different methods [10]. Besides their catalytic properties, these clusters are very interesting because their lowest lying isomers could have nonzero spin (Reddy *et al.*, 1993; Watari and Ohnishi, 1998), being thus magnetic. Zhang *et al.* (2003) have recently performed an extensive study of the stability of Pd clusters within the density-functional approach at $N \leq 13$. In this size range they compared several 1D, 2D and 3D isomers; moreover, they considered a few selected structures at $N = 19$ and 55. Their results indicate that the lowest-lying isomers are 3D already starting for the tetramer (Moseler *et al.*, 2001; Zacarias *et al.*, 1999), and that Ih structures are favored over both Dh and CO structures for $N = 13$ and 55. These results are in good agreement with previous calculations by Kumar and Kawazoe (2002). On the other hand, Watari and Ohnishi (1998) found that the CO is more stable than the Ih at $N = 13$ by density-functional calculations. Moseler *et al.* (2001) were able to compare their results about vertical electron detachment energies for anionic clusters with the experimental data (Ervin *et al.*, 1988; Ganteför and Eberhardt, 1996; Ho *et al.*, 1991) obtaining a good agreement. At larger sizes, *ab initio* results are few, being restricted to the comparison of a small set of selected structures at some special sizes. Kumar and Kawazoe (2002) have compared Ih with CO and Ino Dh clusters at $N = 55$ and 147, obtaining that slightly distorted Ih structures are the lowest in energy in both cases. Also Nava *et al.* (2003) found that a Jahn-Teller distorted Ih is lower in energy than the perfect Ih at $N = 55$. Moreover, Nava *et al.* (2003) found that Ih and CO are very close in energy both at $N = 147$ and 309, with the Ih prevailing at 147 and the CO at 309. By tight-binding calculations, Barreteau *et al.* (2000a,b) found that the Ih is still lower in energy than the CO at $N = 309$, but not at $N = 561$. However, it must be kept in mind that the CO and the Ino Dh are not usually favorable fcc and Dh clusters. This observation is in agreement with previous density-functional calculations by Jennison *et al.* (1997), who showed that for $N = 140$, the TO is favored against the Ih structure obtained by removing seven vertex atom from the $Ih_{147}$, while in Ag the opposite happens.

Global optimization studies up to $N \simeq 100$ by the Sutton and Chen (1990) potential give for Pd the same results as for Ag, with Ih structure at $N = 55$, as confirmed also in the optimization of the Gupta (1981) potential (Massen *et al.*, 2002); at larger sizes, the comparison of the different structural motifs gives that Pd behaves in a similar way to Pt (with rather small crossover sizes, see Table I, and fcc clusters already in close competition with the other motifs already at $N \sim 100$) when modelled by the Rosato *et al.* (1989) potential, while it behaves closely to Ag when treated by means of embedded atom potentials (Baletto *et al.*, 2002b). The calculations by Jen-

[10] See Valerio and Toulhoat (1996, 1997), Jennison *et al.* (1997), Zacarias *et al.* (1999), Moseler *et al.* (2001), Krüger *et al.* (2001), Roques *et al.* (2001), Kumar and Kawazoe (2002), Zhang *et al.* (2003), Nava *et al.* (2003), Guirado-López *et al.* (2000), Barreteau *et al.* (2000b), Barreteau *et al.* (2000a), Efremenko and Sheintuck (2000), Efremenko (2001).

nison *et al.* (1997) better support the results from the Rosato *et al.* (1989) potential, giving that fcc structures are more favored in Pd than in Ag. However this point would need further investigation, and it is not resolved by the analysis of the available experimental data. José-Yacamán *et al.* (2001b) observed by transmission electron microscopy the thiol-passivated Pd nanoparticles in the range of $1-5$ nm of diameter, observing a variety of structures, ranging from fcc (simple and twinned), to Ih, to Dh, to amorphous structures. They were able to observe rather large Ih clusters, explaining their presence as being probably due to kinetic trapping effects.

*f. Nickel clusters.* As in the case of Cu, small Ni clusters have been recently reviewed in Alonso (2000). Reuse *et al.* (1995); Reuse and Khanna (1995) performed several density-functional studies of small Ni clusters, concluding that the lowest-lying isomers are non-planar already for $N \geq 4$. At $N = 7$, two isomers, the pentagonal bipyramid competes and the capped Oh, are in close competition (Nayak *et al.*, 1996). The former is favored by density-functional (Nygren *et al.*, 1992) and embedded-atom (Boyukata *et al.*, 2001) calculations, and the latter is most likely observed in the experiments (Parks *et al.*, 1994), even if the experimental data do not rule out completely the pentagonal bipyramid (Nayak *et al.*, 1996). Nayak *et al.* (1996) performed *ab initio* calculations, finding that these structures are almost degenerate in energy; then they performed MD simulations by the Finnis and Sinclair (1984) semiempirical potential, finding that the capped Oh has a wider catchment basin, becoming thus much more favorable at high temperatures. This is a clear evidence of an entropic effect (see Sect. IV.A). At size $N = 13$, Parks *et al.* (1994) experimentally identified the Ih as the most stable structure. *Ab initio* calculations at the same size (Reuse *et al.*, 1995; Reuse and Khanna, 1995) have shown that the Ih is favored against the CO, but the most stable isomer is obtained by distorting slightly the Ih to obtain a cluster with $D_{3d}$ symmetry. The experimental observations (Parks *et al.*, 1998, 1997, 1995) indicate a TO structure at $N = 38$, a capped Dh structure at $N = 39$ and (possibly defected) Ih structures at $N = 55$. Theoretical results are in reasonable agreement with these experimental findings. Different global-optimization results within semiempirical schemes (Doye and Wales, 1998b; Grygorian and Springborg, 2003) and tight-binding calculations (Lathiotakis *et al.*, 1996) predict fcc and Ih structures at $N = 38$ and 55 respectively. Moreover, capped Dh structures just above size 38 are found (Andriotis and Menon, 2004; Wetzel and DePristo, 1996). At larger sizes, the comparison of the different structural motifs by different semiempirical approaches (Cleveland and Landman, 1991; Mottet *et al.*, 2004) shows that the crossovers Ih $\rightarrow$ Dh and Dh $\rightarrow$ fcc take place at large sizes as in the case of Cu (see Table I).

## 4. General trends for the structural properties of noble and quasi-noble metal clusters

Here we sketch general trends among the six metals of the previous section concerning three items: formation of planar clusters, magnitude of crossover sizes among the motifs and preference for low-symmetry global minima at geometric magic sizes.

Concerning the preference to form planar structures, there is a clear indication of an increasing tendency going down from the 3d to the 5d series and from left to right in the periodic table. Thus Au has the strongest tendency, followed by Ag, Cu and Pt, all three being at the same level (however there is still some debate about planar Pt clusters); Cu and Ni have no preference at all for planar structures. Several groups have investigated the origin of this trend. Bravo-Pérez *et al.* (1999b) correlated the preference for planar structures in Au to the fact that non-additive many-body interactions are stronger than additive 2-body ones in this element. Bonacić-Koutecký *et al.* (2002) noticed that in planar Au clusters, d electrons contribute more to the bonding than in 3D structures; this would also qualitatively explain the weaker tendency to planar clusters for Ag, because in Ag the bonding is more of s type. Finally, Häkkinen *et al.* (2002) investigated $Au_7^-$, $Ag_7^-$ and $Cu_7^-$ by density-functional calculations and demonstrated that the propensity of Au clusters to favor planar structures is correlated with the strong hybridization of the atomic 5d and 6s orbitals due to relativistic effects.

The tendency to form strained structures like icosahedra and decahedra, leading to large crossover sizes, and the tendency to present low-symmetry structures at geometric magic numbers have been discussed, in the framework of the same well defined and quite reliable energetic model, by Baletto *et al.* (2002b) and Soler *et al.* (2000). What follows is a summary of these works. The energetic model is the Gupta (1981) or Rosato *et al.* (1989) potential, which predicts the correct surface reconstructions (Guillopé and Legrand, 1989) and reproduces quite accurately the diffusion barriers (Ala-Nissila *et al.*, 2002; Montalenti and Ferrando, 1999a,b) for these metals. In this framework, the potential energy $E$ of a cluster of $N$ atoms is $E = \sum_{i=1}^{N} E_i$, where the energy of atom $i$ is given by

$$E_i = A \sum_{j=1}^{n_v} \mathrm{e}^{-p\left(\frac{r_{ij}}{r_0}-1\right)} - \xi \sqrt{\sum_{j=1}^{n_v} \mathrm{e}^{-2q\left(\frac{r_{ij}}{r_0}-1\right)}}\,, \qquad (11)$$

where $n_v$ is the number of atoms within an appropriate cut-off distance (in the following we include only the first neighbors), and $A, \xi, p, q$ are parameters fitted on the bulk properties of the element. The first term in Eq. (11) is a repulsive Born-Mayer energy, while the second is the attractive band energy. Following Tománek *et al.* (1985), one can eliminate the parameters $A$ and $\xi$, in order to have a function of $(p, q)$ and of the cohesive energy per atom $E_{coh}$. This is achieved imposing that in the

bulk crystal at equilibrium $E_i = E_{coh}$ and $\partial E_i/\partial r = 0$ for $r = r_0$. The result is

$$E_i = \frac{|E_{coh}|}{12(p-q)} \left[ q \sum_{j=1}^{n_v} \mathrm{e}^{-p\left(\frac{r_{ij}}{r_0}-1\right)} - \sqrt{12}p \sqrt{\sum_{j=1}^{n_v} \mathrm{e}^{-2q\left(\frac{r_{ij}}{r_0}-1\right)}} \right]. \quad (12)$$

This explicitly shows that the properties of the potential depend only on the parameters $(p, q)$, $E_{coh}$ and $r_0$ playing the role of scale factors on energy and distance. Since atomic distances $r_{ij}$ in non-crystalline structures are not optimal one can expect that a metal which increases strongly its energy for a change in $r_{ij}$ (i.e. which has a sticky interatomic potential), would have small crossover sizes (Doye *et al.*, 1995). In the solid at equilibrium all 12 first neighbors are at $r_{ij} = r_0$; changing all $r_{ij}$ by a common factor $r_{ij} \to (1 + \varepsilon)r_{ij}$, developing the crystal energy per atom $E_i(\varepsilon)$ in Eq. (12) (with $n_v = 12$) to the second order and dividing it by the equilibrium value $|E_{coh}|$, one obtains (Baletto *et al.*, 2002b)

$$\rho(\varepsilon) = \frac{E_i(\varepsilon) - E_i(0)}{|E_i(0)|} = \frac{1}{2}\,\varepsilon^2 pq. \quad (13)$$

$\sigma_1 = \rho(\varepsilon)/\varepsilon^2 = pq/2$ is essentially the product of the bulk modulus and the atomic volume divided by the cohesive energy per atom of the bulk crystal. Thus, the larger is $pq$ the smaller are the crossover sizes from icosahedra to decahedra $N_{Ih\to Dh}$ and from decahedra to fcc crystallites $N_{Dh\to fcc}$ as can be seen in Table I.

Let us now discuss the tendency to form low-symmetry structures at geometric magic sizes (referred to as tendency to amorphization in the following). This tendency is due to a specific feature of the metallic bonding, which derives from its many-body character and relates the optimal distance of the bonding to the coordination of the atom (bond order - bond length correlation). This can be easily seen taking a number of neighbors $1 \le n_v \le 12$ in Eq. (12), all at the same distance $r$. Minimization with respect to $r$ leads to the optimum distance $r^*(n_v)$

$$\frac{r^*(n_v)}{r_0} = 1 + \frac{1}{2(p-q)} \log\left(\frac{n_v}{12}\right). \quad (14)$$

which is more and more *contracted* for decreasing $n_v$, and to the energy

$$E^*(n_v) = -|E_{coh}| \left(\frac{n_v}{12}\right)^{\frac{p-2q}{2(p-q)}}. \quad (15)$$

The atoms on the surface of the cluster try to contract in order to minimize their elastic energy (Soler *et al.*, 2001). In the case of highly coordinated structures as the icosahedra (which have intrashell expanded distances), the optimization of the bond lengths is made at the expense of the number of bonds. Therefore, one expects that amorphization is easy in the elements with high elastic energy (i.e. large $pq$), and strong contraction of the bonds with decreasing coordination, the latter leading to a weak dependence of $E^*$ on $n_v$. The contraction of the bonds and the dependence of $E^*$ on the coordination can be quantified by the following dimensionless parameters:

$$\begin{aligned} \sigma_2 &= \frac{n_v}{r_0}\frac{dr^*}{dn_v} = \frac{1}{2(p-q)} \\ \sigma_3 &= \frac{n_v}{E^*}\frac{dE^*}{dn_v} = \frac{p-2q}{2(p-q)}. \end{aligned} \quad (16)$$

As is evident from Table I, all parameters agree in indicating that Au has by far the strongest tendency to amorphization, having the largest $\sigma_1$ and $\sigma_2$ and the smallest $\sigma_3$, followed by Pt and Pd; Ag and especially Cu and Ni have the weakest tendency.

On the same line of reasoning, Soler *et al.* (2000) defined a parameter which is based solely on experimental quantities to extend the estimate of the tendency to amorphization to other systems. This parameter is $\sigma_A$ and is defined as the elastic energy $\delta E_{el}$ which is needed to form an ordered surface with contracted atomic distances, divided by the amorphization energy $\delta E_{am}$ which is required to form a scattered distribution of bond lengths. $\delta E_{el}$ is expressed by means of the (Voigt averaged) bulk and shear moduli $B$ and $G$. $\Delta E_{am}$ is approximated by the enthalpy of melting $\Delta H_{melt}$, which is an estimate of the energetic cost to form amorphous structures resembling those found in liquids. This leads to

$$\sigma_A = \frac{\delta E_{el}}{\Delta E_{am}} \simeq \frac{v(3B - 5G)^2}{320B\Delta H_{melt}}, \quad (17)$$

where $v$ is the atomic volume. Eq. (17) is valid for small clusters having almost all atoms are on their surface. Elements with large $\sigma_A$ are expected to have a stronger tendency to amorphization. As can be seen in Table I, also the inspection of $\sigma_A$ confirms the above trends, the only difference being the indication that Pt should have a stronger amorphization tendency than Pd, due essentially to the comparatively weaker enthalpy of melting of Pt (the ratio $\Delta H_{melt}/|E_{coh}|$ is much smaller in Pt than in Pd).

Finally, let us compare metals with LJ clusters, in order to sketch a qualitative picture of the effects of many-body forces. If one applies the criterion of Eq. (13) to LJ

clusters, one finds a value of $\sigma_1$ which is even larger than those for Au, Pt and Pd. This would suggest that LJ systems have a weaker tendency to form Ih clusters than these metals, but this is not the case, since crossover sizes Ih $\rightarrow$ Dh and Ih $\rightarrow$ fcc are much larger for LJ clusters than of Au, Pt an Pd. This happens because the bond order - bond length correlation of metallic elements tends to destabilize Ih structures. In fact, metals would prefer contracted interatomic distances for the low-coordination surface atoms, and bulk distances for the highly coordinated inner atoms. This is exactly the contrary of what happens in perfect Ih structures, which have contracted internal distances and expanded surface distances. Moreover, in some metals such as Pt, bond directionality effects (which are not included in the potentials considered in Table I can be important for transition metals (Fortunelli and Velasco, 2004)) favor the appearance of (111)-like hexagonal facets on the cluster surface (Aprà *et al.*, 2004), with a further destabilizing effect on Ih clusters.

## 5. Silicon clusters

Silicon nanoclusters are of great practical interest because of their intense photoluminescence at room temperature and the presence of quantum size effects. There is an ongoing debate about the size at which the most favorable clusters adopt the bulk-like diamond structure. Bachels and Schäfer (2000) produced neutral Si clusters in a laser vaporization source and measured their binding energy in samples having average sizes $\overline{N}$ from 65 up to 890 atoms. They showed that the binding energy per atom $E_b$ in this size range scales as $N^{1/3}$, this being characteristic of approximately spherical clusters (Kaxiras and Jackson, 1993a). At smaller sizes, different regimes in the behavior of $E_b$ with $N$ were found as can be seen from Fig. 15. There, Bachels and Schäfer (2000) plotted, besides their results at large sizes, $E_b$ for smaller clusters ($N \leq 7$) obtained from the results of other groups (Fuke *et al.*, 1994; Jarrold and Honea, 1991; Schmude *et al.*, 1995, 1993). Three regimes are clearly shown. For $N < 10$ the binding energy increases rapidly with the cluster sizes, and compact elementary units are built up. For $10 < N < 25$, $E_b$ is practically independent of $N$, as would happen for prolate structures (Kaxiras and Jackson, 1993a). This agrees with the previous observation of small prolate Si clusters by Jarrold and Constant (1991). Finally, for larger clusters the $N^{1/3}$ behavior is recovered. Bachels and Schäfer (2000) were able to produce also metastable prolate structures at sizes up to about 170 atoms. These structures were mostly present in the part of the molecular beam with short dwell times.

How do these results compare to calculations? And is the transition size to quasi-spherical structures the same as the transition size to bulk-like diamond structures? In the following we try to focus on these questions.

Theoretical results on the energetics of small silicon

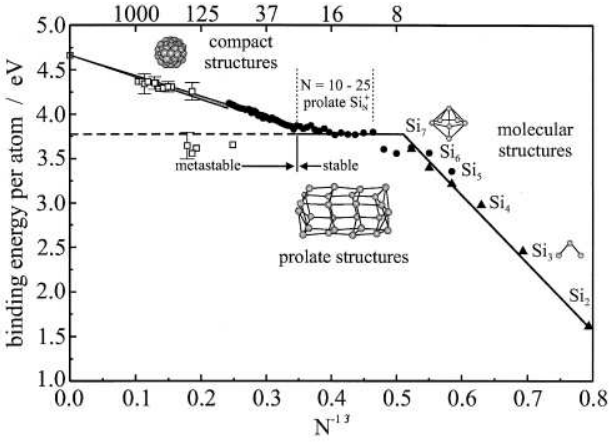


FIG. 15 Size dependence of the binding energies of neutral silicon clusters after Bachels and Schäfer (2000). The open squares indicate binding energies of the two groups of cluster isomers found by calorimetric measurements. The black circles are data for neutral silicon clusters obtained from the collision-induced dissociation experiments by Jarrold and Honea (1991) on the corresponding silicon cluster cations taking the experimentally determined photoionization potentials into account as from Fuke *et al.* (1994). The black triangles belong to the Knudsen mass spectrometric measurements of Schmude *et al.* (1995, 1993). The crossover from elongated to the spherical neutral silicon structures can be estimated from the binding energies to be located around $N = 25$. The structure for an elongated $Si_{26}$ cluster is taken from Grossman and Mitás (1995a).

clusters have been obtained by quantum MC, density-functional, and tight-binding calculations. The latter allowed also to apply global optimization methods such as simulated annealing (Yu *et al.*, 2002) and genetic algorithms (Ho *et al.*, 1998; Rata *et al.*, 2000; Wang *et al.*, 2001b).

For very small clusters, Raghavachari and Logovinsky (1985) found that the best clusters are planar only up to $N = 4$; several calculations (Fournier *et al.*, 1992; Li *et al.*, 1999; Yu *et al.*, 2002; Zickfeld *et al.*, 1999) found a generally good agreement with the above results. An important result at small sizes is that $Si_{10}$ is a very stable cluster (Grossman and Mitás, 1995b; Li *et al.*, 2000c; Raghavachari and McMichael-Rohlfing, 1988; Ramakrishna and Bahel, 1996) so that it can act as a subunit of larger ones (see Fig. 16). For example, quantum MC, density-functional (Mitás *et al.*, 2000) and tight-binding calculations (Yu *et al.*, 2002) give that the best structures at $N = 20$ are simply formed by linking two $Si_{10}$ subunits. Indeed, the most reliable explanation for the observation of prolate clusters is that they are built up by stacked subunits, whose structure is still under debate. Kaxiras and Jackson (1993a,b) proposed that the subunits are sixfold rings; Raghavachari and McMichael-Rohlfing (1988), Jarrold and Bower (1992), and Ho *et al.* (1998) were in favor of tricapped trigonal prisms of 9 atoms; Rata *et al.* (2000) found that $Si_{20}$ is made of six-

and eight-atom subunits. Rata *et al.* (2000) found also that the dissociation energies and inverse mobilities calculated from their global minima were in excellent agreement with the experiments (Hudgins *et al.*, 1999; Jarrold and Honea, 1991) up to $N = 18$, concluding that cluster formation is dominated by the energetics up to these sizes.

In summary, experiments and calculations agree in finding prolate structures of a few tens of atoms which are built up by small subunits in the range 6-10 atoms. This is also consistent with fragmentation experiments of clusters of about 150 atoms by Ehbrecht and Huisken (1999), yielding $Si_6^+$ - $Si_{11}^+$ products.

Clusters are quasi-spherical for about $N > 25$ (Hudgins *et al.*, 1999), even if they do not form crystalline structures at these sizes. Indeed, the experiments of Ehbrecht and Huisken (1999) could be interpreted assuming that compact shapes at $N \sim 150$ are built up by small subunits (the prolate metastable structures observed by Bachels and Schäfer (2000) being possibly unfolded versions of these clusters), and this agrees with the simulated annealing calculations by Yu *et al.* (2002). But this is not the only possibility, since Kaxiras and Jackson (1993a), Ho *et al.* (1998) and Mitás *et al.* (2000) have shown that quasi-spherical non-crystalline structures, which are not build up by stacking smaller subunits, become favorable at $N \geq 20$. These sizes are large enough to allow the formation of cages containing at least one Si atom inside (Mitás *et al.*, 2000). These results compare rather well with the experiments by Bachels and Schäfer (2000). However, the theoretical determination of the most stable structures in medium-size Si clusters is a very complex task: see for example the debate about the structure of $Si_{36}$ in Sun *et al.* (2003) and Bazterra *et al.* (2004).

Mélinon *et al.* (1998, 1997) demonstrated that the models based on quantum confinement in crystalline silicon clusters fail for films containing grains of less than 2 nm of diameter (say $N \simeq 200$). They were not able to observe any crystallization by transmission electron microscopy. On the other hand, if the grains are of 3 nm of diameter, there is evidence of crystalline ordering (Ehbrecht and Huisken, 1999; Ehbrecht *et al.*, 1997; Ledoux *et al.*, 2000). This would indicate that the transition to crystalline structures is around $N = 400$ atoms, as Yu *et al.* (2002) found by simulated annealing tight-binding calculations.

### 6. Clusters of fullerene molecules

The condensed-phase properties of $C_{60}$ molecules have been the subject of considerable interest because of the unusual character of molecular interactions. In fact, above room temperature, $C_{60}$ molecules can be considered as large spherical pseudoatoms which are free to rotate; the effective interaction between these pseudoatoms is extremely short-ranged relatively to the large equilibrium pair separation. This is at the origin of peculiar

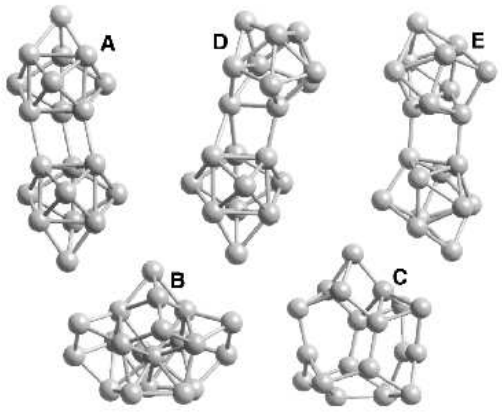


FIG. 16 The best isomers of $Si_{20}$ according to Mitás *et al.* (2000). Structure E is the lowest in energy according to quantum MC calculations.

properties; in fact, such sticky interactions (see Fig. 7) disfavor all strained configurations, as those occurring in icosahedra or in the liquid phase. Indeed, the existence of a liquid phase for bulk $C_{60}$ (Caccamo *et al.*, 1997; Ferreira *et al.*, 2000; Hagen *et al.*, 1993) is still debated. Therefore, clusters of $C_{60}$ molecules are on the opposite side with respect to clusters of alkali metals, and we expect non-crystalline structures to be the global minima only for aggregates of a small number $N$ of molecules.

This qualitative prediction has been confirmed by all existing calculations. We can classify these studies into two classes. The first one uses an all-atom potential, with each carbon atom interacting with atoms of other molecules by a LJ potential. This approach includes deviations from spherical symmetry, but presently allows the global optimization only for small $N$. The second one uses spherically averaged potentials, such as the Girifalco (1992) potential (Girifalco, 1992), where LJ centers are continuously and uniformly distributed on the surface of a sphere, or the potential developed by Pacheco and Prates-Ramalho (1997), which is derived by fitting density-functional calculations. The Girifalco (1992) potential is purely two-body, whereas the Pacheco and Prates-Ramalho (1997) potential includes two-body and three-body terms (the latter however being of rather small importance).

All these approaches agree in predicting that Ih structures are favorable only at very small $N$. All-atom potentials favor Ih structures up to $N = 16$ (Doye *et al.*, 1997; García-Rodeja *et al.*, 1997; Rey *et al.*, 1997), while calculations with the Girifalco (1992) potential, which is the stickiest, indicate that icosahedra are the lowest in energy only up to $N = 13$ (Doye and Wales, 1996b; Rey *et al.*, 1994; Wales, 1994a). Finally, the Pacheco and Prates-Ramalho (1997) potential favors Ih structures up to $N = 15$. Larger clusters are either based on Dh or on close-packed structures, as shown by Doye *et al.* (2001) who performed an exhaustive basin-hopping global optimization study up to $N = 105$ on the basis of

both Pacheco and Prates-Ramalho (1997) and Girifalco (1992) potentials. Close-packed structures become more frequent as the size increases. Both potentials indicate that the most stable isomers are found at $N = 38$ (TO), $N = 75$ ((2, 2, 2) Marks Dh) and 101 ((2, 3, 2) Marks Dh), and that $N = 55$ is not a magic number. At that size, the Ih is higher in energy than the best Dh structure by 0.3 and 2 eV according to the Pacheco and Prates-Ramalho (1997) and Girifalco (1992) potentials respectively.

These results completely disagree with the experimentally observed structures. In fact, Branz *et al.* (2002, 2000); Martin *et al.* (1993) found that clusters grown at low $T$ and annealed at ∼500 K (to let the less bound surface molecules to evaporate) present a mass spectrum with a clear sequence of Ih magic numbers up to very large sizes, well above $N = 100$ (see Fig. 17). The peak at $N = 55$ is very evident, and no peaks are found at $N = 38$ and 75. The mass spectra are qualitatively similar for neutral, positively and negatively charged clusters (Branz *et al.*, 2002). Recently, Rey *et al.* (2004) compared the neutral and singly-ionized cluster structures in a model including the Girifalco (1992) potential plus a point polarizable dipole electrostatic model. They found that the structure of ionized clusters are very similar to those of neutral clusters, thus confirming the observations. Branz *et al.* (2002) found Dh and close-packed structures only after further annealing at higher $T$. This result indicates the possible existence of kinetic trapping effects in the formation of the clusters of $C_{60}$ molecules (Baletto *et al.*, 2002a), as we discuss in Sec. V.B.5. Trapping effects are overcome only after a strong annealing.

The resulting high-$T$ experimental structures are however still not coinciding with those predicted by Pacheco and Prates-Ramalho (1997) and Girifalco (1992) potentials. In fact, there is a sequence of experimental magic numbers which can be attributed to the Leary tetrahedron at $N = 98$ and to its fragments down to $N = 48$, while the calculations do not attribute special stability to these structures. This discrepancy is probably due to the fact that even the Pacheco and Prates-Ramalho (1997) potential is too sticky; a slightly less sticky Morse potential gives the Leary tetrahedron as a magic structure (Doye *et al.*, 2001).

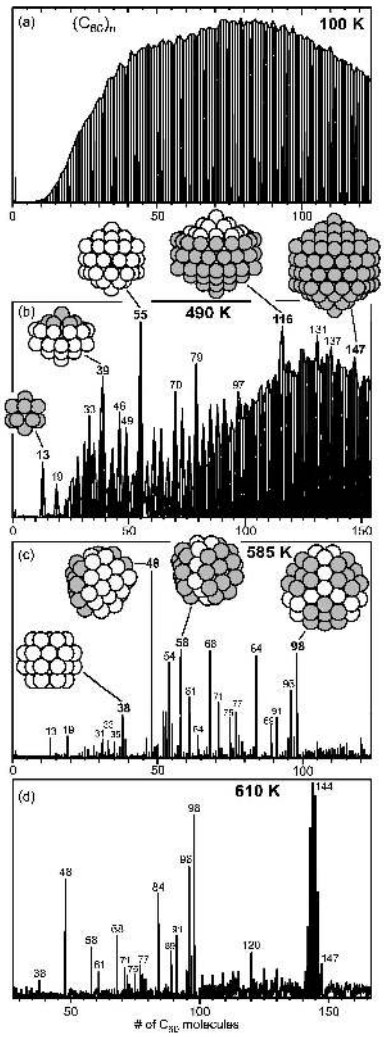


FIG. 17 Mass spectra of $C_{60}$ clusters. Clusters produced at low $T$ do not reveal any magic number (panel (a)). After mild annealing to evaporate the less bound molecules, a clear series of Ih magic numbers emerges (panel (b)). Dh and close packed magic numbers appear only after a high-$T$ annealing (panels (c) and (d)). After Branz *et al.* (2002).

## IV. THERMODYNAMICS OF FREE NANOCLUSTERS

In this Section, we analyze the effects of raising the temperature on the cluster structures. These effects may include solid-solid structural transitions, and the melting of the cluster if temperature is raised enough. Both solid-solid transitions and melting are nice cases for showing the peculiar thermodynamic behavior of small finite systems such as clusters. Indeed, the thermodynamics of finite systems is a very fascinating and complex field, where many subtleties are involved. Here we do not intend at all to be exhaustive, and suggest the readers who need more complete treatments to refer to existing monographs, from the classical book by Hill (1964) to the excellent book by Wales (2003). In the following we treat only those issues which have direct relationship with temperature-dependent changes in the cluster structures.

Generally speaking, two points must be kept in mind about cluster thermodynamics. First, *phase transitions in small systems are gradual, not sharp* (Hill, 1964). A consequence of this fact is that there are bands of temperature and pressure within which two or more cluster structures may coexist. This coexistence is dynamic, like that of chemical isomers coexisting [11]. Second, ther-

[11] See for example Honeycutt and Andersen (1987), Berry *et al.*

modynamic properties (like the melting point) can be strongly size-dependent, in analogy to what happens to the global-minimum structures. General trends on the temperature dependence of thermodynamic properties may be deduced on the basis of the following expression for the Gibbs free energy $G$ (Hill, 1964). In a bulk system, $G = Ng(p,T)$ where $g(p,T)$ is the specific Gibbs potential. For a small system, we have to consider also contributions coming from surfaces, edges etc. Thus, we write $G$ as:

$$G = Ng(p,T) + b(p,T)N^{2/3} + c(p,T)N^{1/3} + d(p,T), \quad (18)$$

the term in $N^{2/3}$ is a surface free energy, the term in $N^{1/3}$ is due to edge contributions, while the last term might be due, among other things, to the rotation of the cluster. In the limit $N \to \infty$, one has $G \to Ng$, the macroscopic relationship. But when the system is small all terms are important. The finite size of the clusters implies also that treatments in different thermodynamic ensembles (microcanonical and canonical) may give different behaviors for thermodynamic quantities such as the heat capacity (Bixon and Jortner, 1989; Jortner, 1992).

The thermodynamics of clusters has been studied by a variety of theoretical and simulation tools: MC and MD simulations, and analytical methods [12].

In Section IV.A we focus on the role of entropic contributions to the free energy at increasing temperature, which may cause solid-solid structural transitions when the structure corresponding to the global energy minimum ceases to be the most likely at high $T$, so that other structures prevail. In Section IV.B we deal with the melting transition. There, we first discuss what is intended for melting (and premelting) in clusters, briefly reviewing experimental and simulation methods. Then we focus on the size-dependence of the melting point, which may be very complex, as in the case shown in Fig. 18. We treat phenomenological theories for the (average) monotonic dependence of the melting point with size, and discuss the origin of its non-monotonic variations. Finally, in Section IV.C we focus on some systems of peculiar interest.

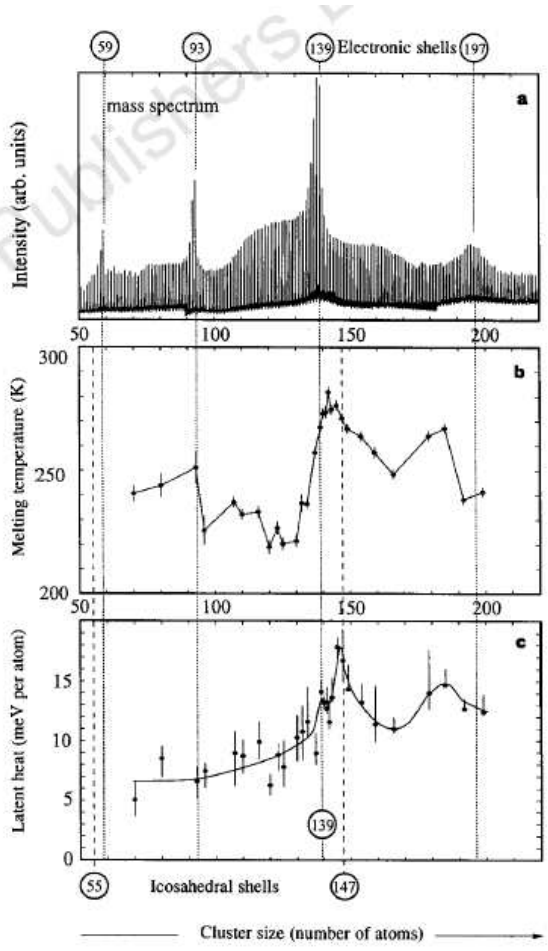


FIG. 18 Size-dependence of the measured melting temperatures and latent heat of melting for sodium clusters (after Schmidt *et al.* (1998)). These quantities are compared to the mass spectrum of the top panel which shows electronic magic numbers. The correlations between the electronic magic sizes and the peaks in the melting temperature are rather weak, indicating that the melting behavior of small sodium clusters cannot be explained by simple models. Reprinted with permission from Nature http://www.nature.com/

### A. Entropic effects and solid-solid transitions

Structural transitions can take place increasing the temperature for a given size because of entropic effects. When the minimum free-energy structure is different from the minimum energy structure, we can define a temperature $T_{ss}$ at which a solid-solid transformation occurs. In other words, for $T > T_{ss}$ the minimum energy structure (which is always the most likely for $T \to 0$) ceases to be the most probable to the advantage of some other structure which prevails because of entropic effects. Structural changes from fcc to Dh and Ih structures as $T$ increases has been predicted theoretically and seen in simulations of several systems (small LJ (Doye and Calvo, 2001), Au (Cleveland *et al.*, 1998, 1999), and Cu clusters (Baletto *et al.*, 2004)). Moreover, solid-solid entropy-driven structural transformations in LJ clusters of about 200 atoms and with different structures have been observed in MC simulations by Polak and Patrykiejew (2003). Recent experiments by Koga *et al.* (2004) support the existence of entropy-driven solid-solid

(1988), Labastie and Whetten (1990), Bartell (1992), Matsuoka *et al.* (1992), Cleveland and Landman (1994), Schmidt *et al.* (1998), Jellinek (1999)

[12] Early studies are found in Lee *et al.* (1973), Briant and Burton (1975), Imry (1980), Nautchil and Petsin (1980), Natanson *et al.* (1983), Berry *et al.* (1984), Quirke and Sheng (1984), Amar and Berry (1986), Davis *et al.* (1987), Luo *et al.* (1987), Beck and Berry (1988), Reiss *et al.* (1988), Bixon and Jortner (1989).

transitions. Here we follow the theoretical treatment by Doye and Calvo (2001, 2002), dealing first with the classical harmonic approximation, and then introducing anharmonic and quantum corrections.

### 1. Structural transitions in the harmonic approximation

Let $\mathcal{H}$ be the Hamiltonian of a cluster of size $N$:

$$\mathcal{H} = T(\{\mathbf{p}\}) + U(\{\mathbf{r}\}) \tag{19}$$

where $T(\{\mathbf{p}\}) = \sum_{i=1}^{N} p_i^2/2m$ is the kinetic energy and $U(\{\mathbf{r}\}) = U(\mathbf{r_1}, \ldots, \mathbf{r_N})$ is the potential energy. Assume now that the cluster has a (non-linear) structure, corresponding to a given minimum $s$ of energy $E_s^0$. If the coupling of rotational and vibrational motions can be neglected, $Z_s$ can be factored as follows

$$Z_s = Z_s^{tr} Z_s^{rot} Z_s^{vib}, \tag{20}$$

where $Z_s^{tr}$ and $Z_s^{rot}$ are related to the center-of-mass translation and to rigid rotational motions respectively, while $Z_s^{vib}$ is related to the vibrational motion around $s$. $Z_s^{vib}$ depends on the internal coordinates $\xi_{s,i}$ where $i$ ranges from 1 to $\kappa = 3N - 6$. For small oscillations, the vibrational motion can be treated within the harmonic approximation. In this case, it is convenient to choose the $\xi_{s,i}$ as the normal-mode coordinates, in order to write $U$ as

$$U = E_s^0 + \frac{1}{2}\sum_{i=1}^{\kappa} \omega_{s,i}^2 \xi_{s,i}^2, \tag{21}$$

where the $\omega_{s,i}$ are the normal-mode frequencies. The transformation to normal modes allows an easy evaluation of $Z_s^{vib}$, which, in the classical case, is given by

$$\begin{aligned} Z_s^{vib} &\simeq \frac{\mathrm{e}^{-\beta E_s^0}}{(2\pi\hbar)^\kappa} \prod_{i=i}^{\kappa} \int_{-\infty}^{\infty} d\xi_{s,i} d\dot{\xi}_{s,i} \mathrm{e}^{-\frac{\beta}{2}\left(\omega_{s,i}^2 \xi_{s,i}^2 + \dot{\xi}_{s,i}^2\right)} = \\ &= \mathrm{e}^{-\beta E_s^0} \prod_{i=i}^{\kappa} \left(\frac{k_B T}{\hbar \omega_{s,i}}\right) \end{aligned} \tag{22}$$

The classical expressions for $Z_s^{tr}$ and $Z_s^{rot}$ are

$$Z_s^{tr} = \mathcal{V}\left(\frac{M k_B T}{2\pi\hbar^2}\right)^{3/2} \qquad Z_s^{rot} = \left(\frac{2\pi k_B T \overline{I}_s}{\hbar^2}\right)^{3/2}, \tag{23}$$

where $\mathcal{V}$ is the volume of the box where the cluster is contained, $M$ is the cluster mass, and $\overline{I}_s$ is the average inertia moment in $s$ [$\overline{I}_s = (I_s^{xx} I_s^{yy} I_s^{zz})^{1/3}$, with $I_s^{xx}$, $I_s^{yy}$ and $I_s^{xx}$ principal inertia moments].

To estimate the temperature dependence of the probability of finding the cluster in $s$, we have to compute the total partition function $Z$. Before doing so, we note that each minimum $s$ has a number $n_s$ of equivalent permutational isomers, mamely of equivalent minima which are obtained by exchanging the coordinates of atoms of the same species. For homogeneous clusters $n_s = 2N!/h_s$, where $h_s$ is the order of the symmetry group of minimum $s$ (Wales, 2003). If, at a given $T$, there are $M_{min}$ minima with a non negligible probability of being occupied, the probability $p_s$ that the cluster is in the ensemble of the permutational isomers of minimum $s$ can be evaluated by the superposition approximation (Doye and Wales, 1995). Within this approximation, $Z$ is obtained by summing up the contributions from all significant minima. This gives

$$\begin{aligned} p_s &= \frac{n_s Z_s}{Z} \simeq \frac{n_s Z_s}{\sum_{\sigma=1}^{M_{min}} n_\sigma Z_\sigma} \simeq \\ &\simeq \frac{n_s \overline{I}_s^{3/2} \mathrm{e}^{-\beta E_s^0} \Omega_s^{-\kappa}}{\sum_{\sigma=1}^{M_{min}} n_\sigma \overline{I}_\sigma^{3/2} \mathrm{e}^{-\beta E_\sigma^0} \Omega_\sigma^{-\kappa}}. \end{aligned} \tag{24}$$

where $\Omega_s = \left(\prod_i^\kappa \omega_{i,s}\right)^{1/\kappa}$ is the geometric average of the vibrational frequencies of $s$.

Let us now consider the simplest case of a PES having two minima $s$ and $s'$ (with $E_s^0 < E_{s'}^0$), and calculate the ratio $p_s/p_{s'}$ between their occupation probabilities as a function of $T$. Assuming that $\overline{I}_s \simeq \overline{I}_{s'}$, one obtains

$$\frac{p_s}{p_{s'}} = \frac{Z_s n_s}{Z_{s'} n_{s'}} = e^{-\beta \Delta E^0} \left[\frac{n_s}{n_{s'}} \left(\frac{\Omega_{s'}}{\Omega_s}\right)^\kappa\right] \tag{25}$$

where $\Delta E^0 = E_s^0 - E_{s'}^0$. Since $\Delta E^0 > 0$ we have two

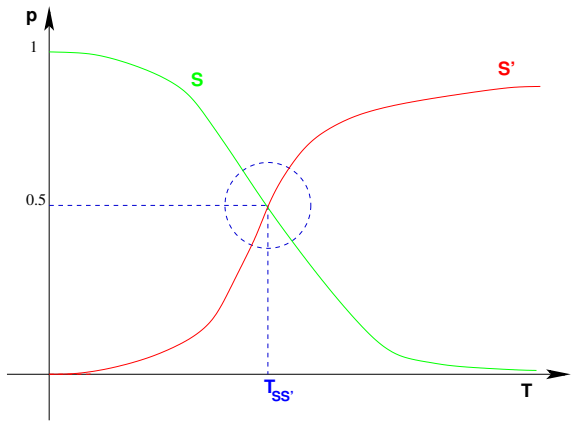


FIG. 19 Schematic representation of the probabilities $p_S$ and $p_{S'}$ of the local energy minima $S$ and $S'$, with $S'$ having higher energy than $S$ vs temperature. In the temperature range close to the transition temperature $T_{SS'}$ the two structures coexist being almost equally likely.

cases:
i) If $n_s/\Omega_s^\kappa > n_{s'}/\Omega_{s'}^\kappa$, $s$ is more favorable than $s'$ for all temperatures;
ii) If $n_s/\Omega_s^\kappa < n_{s'}/\Omega_{s'}^\kappa$, for $T > T_{ss}$, $s'$ becomes more favorable than $s$ and thus a solid-solid transition is possible, see Fig.19.
From the above equations, we estimate $T_{ss}$ as:

$$T_{ss} = \frac{\Delta E^0}{k_B\left[\ln(n_{s'}/n_s) + \kappa \ln(\Omega_s/\Omega_{s'})\right]}. \tag{26}$$

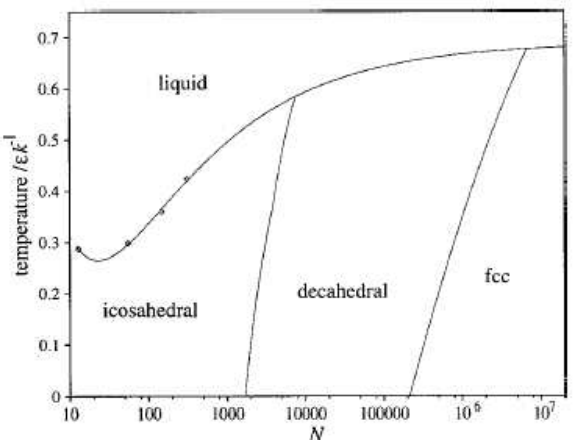


FIG. 20 Structural phase diagram in the $N, T$ plane for LJ clusters in the harmonic superposition approximation (from Doye and Calvo (2002)).

To find a solid-solid transition, not only case ii) must hold, but $T_{ss}$ must be below the melting range of the cluster.

How do entropic contributions behave in typical cases? Doye and Calvo (2002) analyzed thoroughly LJ clusters within the harmonic superposition approximation. They grouped together the minima pertaining to each motif (Ih, Dh and fcc), thus being able to estimate transition temperatures between structural motifs, and not simply between pairs of minima. They found that the entropic contributions shift upwards the Ih $\rightarrow$ Dh and Dh $\rightarrow$ fcc crossover sizes with increasing temperature, as can be seen in the (coarse grained) structural phase diagram of Fig. 20. This happens because Ih structures have on the average smaller vibrational frequencies than Dh ones, the latter having softer vibrations than fcc clusters (Doye and Calvo, 2002). Metals modelled by Sutton and Chen (1990) potentials behave in a qualitatively similar way (Doye and Calvo, 2001). A discussion of the observation of solid-solid transitions in experiments and simulations on specific systems is given in Section IV.C. Here we only remark that solid-solid transitions may be extremely slow in typical situations, so that their observation may require a substantial overheating of the initial structure (Koga *et al.*, 2004), to surmount the energy barriers leading to escape from the initial basin.

#### 2. Anharmonic and quantum corrections

The harmonic superposition approximation is often accurate for cluster thermodynamics up to temperatures close to the melting range, as shown for $Ag_{38}$ and $Cu_{38}$ in Baletto *et al.* (2004). However, there are cases in which this approximation is not sufficient, and anharmonic effects must be included (Doye and Wales, 1995). Solid-solid transitions can be close to the melting temperature; in this case anharmonic effects are not negligible. Moreover, the harmonic approximation may strongly overestimate the probability of minima which have low-barrier escape paths. An example of failure of the harmonic approximation is found in Wang *et al.* (2001a) and Doye and Calvo (2003).

One can introduce anharmonic effects via $T$-dependent frequencies, i.e. $\tilde{\Omega}_s(T) = \Omega_s(1 - \beta_s^0/\beta)$, where $\beta^0$ is a measure of the anharmonicity. This then gives for the transition temperature, neglecting the permutational contribution:

$$\beta_{ss}^{anHA} = \frac{\kappa}{\Delta E^0}\left[\ln(\Omega_s/\Omega_{s'}) + \ln\left(\frac{\beta - \beta_s^0}{\beta - \beta_{s'}^0}\right)\right], \quad (27)$$

where the second term represents the first order approximation to the anharmonic correction to $\beta_{ss}^{anHA} = 1/k_B T_{ss}^{anHA}$. To apply the previous equation is necessary to estimate $\beta_0$ but the available methods do not allow to treat large sizes.

Quantum corrections can be inserted both in $Z_s^{rot}$ and $Z_s^{vib}$. Since quantum corrections to $Z_s^{rot}$ should become important only at very low temperatures, we now consider only the corrections to $Z_s^{vib}$. These corrections are very easily introduced within the harmonic approximation. The quantum partition function of a set of oscillators is given by

$$Z_s^{vib} = e^{-\beta E_s^0}\prod_{i=1}^{\kappa}\left[2\sinh\left(\beta\hbar\omega_{i,s}/2\right)\right]^{-1}. \quad (28)$$

The classical limit is valid when it is possible to approximate the $\sinh(\beta\hbar\omega_{i,s}/2)$ with its argument and thus for high temperatures. The introduction of quantum oscillators modifies the expression of the ratio between the occupation probabilities of two minima $s$ and $s'$ in the following way:

$$\frac{p_s}{p_{s'}} = e^{-\beta\Delta E^0}\left[\frac{n_s}{n_{s'}}\frac{\prod_i^{\kappa}\sinh\left(\beta\hbar\omega_{i,s'}/2\right)}{\prod_i^{\kappa}\sinh\left(\beta\hbar\omega_{i,s}/2\right)}\right]. \quad (29)$$

In particular, we note that here the temperature dependence is also in the vibrational contribution and not only in the Boltzmann factor. To understand when quantum corrections are needed we may refer to the Debye temperature $\Theta_D$. If the temperature of the system is above $0.70\Theta_D$ the system can be treated as classical with good approximation, while at lower temperature we need to take into account also quantum effects (Ashcroft and Mermin, 1976). Calvo *et al.* (2003) satisfactorily explained the finite-temperature spectroscopic properties of $CaAr_N$ clusters including quantum and anharmonic corrections in their calculations.

### B. Melting of nanoclusters

The concepts of solid and liquid states, which are commonly employed in relation with extended systems, can be transferred to clusters. In fact, at low temperature,

the particles of a cluster spend the most part of the time by making small amplitude vibrations around the global minimum, in analogy to what happens in bulk solids. If temperature is increased, other minima begin to be populated, and this is associated with the onset of some diffusive motion. Finally, if temperature is high enough, the cluster explores the basins of a huge number of minima, with fast rearrangements, thus behaving as a liquid droplet. Within this description, cluster melting is seen as an isomerization transition, with the number of probable isomers increasing drastically after some threshold temperature. A nice example of this behavior for $Ag_6$ clusters is in Garzón *et al.* (1998a). However, there are several differences in the solid-liquid transition of clusters with respect to its bulk counterpart:

(i) The melting point is reduced (with a few known exceptions) with a complex dependence on size.

(ii) The latent heat is smaller; this can be understood for example noting that disordering the surface costs less than disordering inner atoms.

(iii) The transition is not taking place sharply at one definite temperature, but smoothly in a finite temperature range. There, solid and liquid phases may coexist dinamically in time (Berry *et al.*, 1988; Lynden-Bell and Wales, 1994). Observing the cluster for a long time interval, there will be subintervals in which the cluster appears as being solid and others in which the cluster is fully liquid.

(iv) The heat capacity can become negative in microcanonical environments (Schmidt *et al.*, 2001). This means that the microcanonical average kinetic energy may be a non-monotonically increasing function of the total energy in the range of the transition (Bixon and Jortner, 1989).

(v) The melting transition depends on cluster structure and chemical ordering (this being indeed a non-equilibrium effect)

Often the melting transition is preceded by premelting phenomena. To quote the words by Calvo and Spiegelman (2000) *premelting phenomena are characteristic of isomerizations taking place in a limited part of the configuration space*, for example isomerizations involving surface atoms only (in this case the term surface melting is used). Premelting phenomena are often singled out by additional peaks in the specific heat vs. temperature.

### 1. Experimental methods

Following Haberland (2002), experiments studying cluster melting can be divided into two classes :

(i) one studies the change of some physical property across the melting point (for example, changes in photon or X-ray diffraction patterns)

(ii) the caloric curve $E = E(T)$ is measured, that is the clusters internal energy $E$ as a function of $T$.

Takagi (1954) made the first observation of the melting point depression by transmission electron microscopy. This is a standard technique for studying the size-dependent melting point of small particles by monitoring the changes in the diffraction pattern associated with the disordering of the structure. Electron and X-ray diffraction, and nanocalorimetry techniques have been used to study melting in deposited clusters (Efremov *et al.*, 2000; Lai *et al.*, 1996; Peters *et al.*, 1998). At present these methods are, however, not applicable to free, mass selected clusters in vacuum for two reasons: first no method of temperature measurement is known in this case, and the density of mass selected clusters is so small that it is extremely difficult to collect a diffraction signal. In any case, as the size decreases, the diffraction techniques become increasingly inaccurate due to line broadening. Several experiments tried to measure the melting behavior of free cluster, mainly by methods belonging to class (i). Even *et al.* (1989) and Buck and Ettischer (1994) looked for some spectroscopic evidence. Electron diffraction from a (not mass selected) supersonic expansion gives Debye-Scherrer like diffraction rings, the intensity of them being a measure of cluster temperature. This method was pioneered by Farges *et al.* (1981) and later intensively studied by Hovick and Bartell (1997). Martin *et al.* (1994) were the first to publish a size dependence of the melting temperature of free clusters. They showed that the structure on mass spectra of large sodium clusters can depend sensitively on the temperature. The disappearance of the structure was interpreted as being due to melting. Another method has been proposed by Shvartsburg and Jarrold (2000) to measure the melting temperature $T_m$ for small tin clusters, with the surprising result that they melt higher than bulk tin. Here, cluster ions are injected into a helium gas atmosphere, and are pulled by an electric field through the gas. The collisions with the gas produce an effective friction force. Clusters having a small collision cross section experience a smaller friction force and arrive first. A new approach to study the melting processes in gallium nanoparticles embedded in a matrix has been recently developed by Parravicini *et al.* (2003a,b). This method is based on capacitance measurements through the derivative of the dielectric constant with respect to $T$.

Calorimetry experiments have been performed on deposited (for example Lai *et al.* (1996) considered tin clusters on a SiN substrate) and free clusters. Free-cluster calorimetry has been applied by Haberland's group (Kusche *et al.*, 1999; Schmidt *et al.*, 2001, 1998, 1997) to Na clusters and by Bachels *et al.* (2000) to Sn clusters. Haberland's method consists of two steps, the preparation of size-selected clusters of known temperature and the determination of their energy. A beam of cluster ions is produced and thermalized in a heat bath at temperature $T_1$; a mass spectrometer is used to select a single cluster size. Then the clusters are irradiated

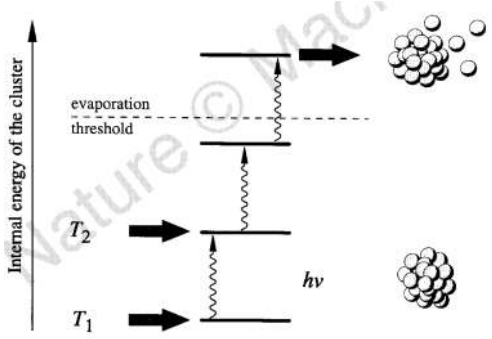


FIG. 21 Schematic representation of the experimental method for measuring $E(T)$ for free clusters (after Schmidt *et al.* (1998)). Reprinted with permission from Nature http://www.nature.com/

by a laser beam and absorb several photons. The basic idea of the experiment is to heat at temperature $T_1$ by absorbing photon of energy $\delta U = h\nu$. The photon energy quickly relaxes into vibrations and heats the cluster to a temperature $T_2$ where the clusters do not emit atoms on the time scale of the experiment (several microseconds). Only the adsorption of more photons from the laser pulse raises the temperature above $T_{evap}$, the temperature needed for evaporation of atoms from the cluster. The size distribution of the remaining cluster ions is measured, and this is a very sensitive measure of the cluster internal energy. The increased temperature of the cluster, $T_2$, is then identified by increasing the cluster source temperature until the thermally heated clusters show the same photofragmentation behavior as the laser-heated ones. A second mass spectrometer measures the distribution of the fragment ions produced. Different numbers of absorbed photons lead to clearly separated groups of fragments in the mass spectrum, with the distance between two groups corresponding to exactly one photon energy. This allows one to calibrate the mass scale in terms of energy. If the temperature of the heat bath is varied the internal energy of the selected clusters changes and thus also the number of evaporated atoms, see Fig. 21.

In the method by Bachels *et al.* (2000) Sn clusters are produced by a laser ablation source using a pulsed nozzle whose temperature is variable. Cluster temperatures should deviate from nozzle temperatures only by 10-20 K. Neutral clusters are studied, thus there is not mass selection; the width of the distribution of the cluster sizes can be of the order of 60% of the average size. Energy is measured by a sensitive pyroelectric foil where the clusters impinge causing a temperature increase which leads to a measurable voltage jump.

## 2. Computational methods

Here we first discuss the quantities that may be used to single out the melting transition, and then we briefly review the most common computational methods.

The most common method to study the melting transition is the calculation of the caloric curve, namely the total cluster energy $E$ as a function of $T$, in a simulation where the cluster is heated up from a low-$T$ solid configuration. $E(T)$ may show a smooth jump in the melting region (see Fig. 22), corresponding to a peak in the heat capacity $c(T) = \partial E/\partial T$, as in Fig. 23. However, the caloric curve is not always an efficient indicator because the jump may be small and difficult to find, or even absent. When properly calculated, peaks in the heat capacity can indicate the melting temperature $T_m$. However, when multiple peaks are present, the assignment of the melting point may become difficult. One may identify $T_m$ with the temperature of the highest peak, but sometimes this criterion fails (see the discussion in Frantz (2001)).

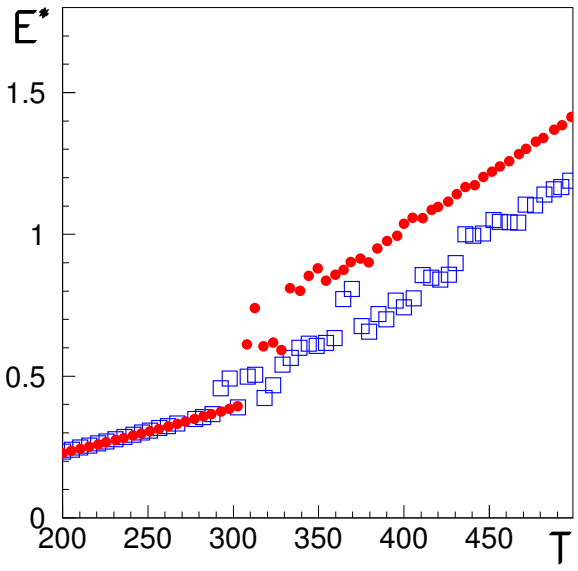


FIG. 22 Caloric curves from a MD melting simulation of $Ag_{38}$ (circles) and $Cu_{38}$ (squares) (courtesy of Christine Mottet). The heating rate is of 0.1 K/ns. The clusters are modelled by the Rosato *et al.* (1989) potential. $E^*$ is the average total energy $E$ of the cluster after the subtraction of the global-minimum energy and of the kinetic and harmonic contributions: $E^* = E - E_{GM} - 3(N-1)k_BT$. The jump in the caloric curve is clear for $Ag_{38}$, and less evident for $Cu_{38}$.

In general, criteria to distinguish solid-like and liquid-like phases, and sensitive indicators of the melting transition are needed.

Solid-like and liquid-like phases can be distinguished if an order parameter $Q$ can be found such that the Landau free energy $F_l(Q)$ is bistable for a range of temperatures. Then two distinct phases can be identified and can be said to coexist (Wales (2003) and references therein). The Landau free energy is defined as

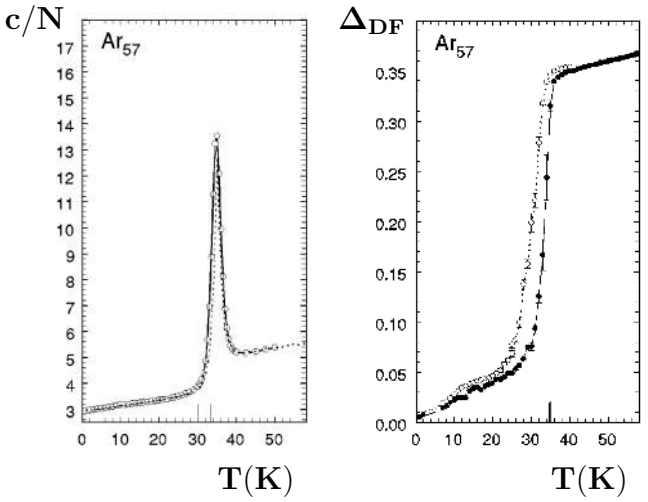


FIG. 23 Heat capacity and bond-length fluctuations in the $LJ_{57}$ cluster (after Frantz (2001)). Left panel: heat capacity curves. Open circles and solid line represent the results of parallel tempering simulations, while the dotted line and the thin solid line are the results of Metropolis MC runs of different length. Right panel: $\Delta_{DF}$ calculated in two MC simulations of different length (the longest one corresponds to the open circles). The temperature at which $\Delta_{DF}$ starts its strong increase corresponds well to the temperature of the heat capacity peak. The heat capacity $c$ and $\Delta_{DF}$ are given in reduced units (see Frantz (2001)).

$F_l(Q) = k_B T \ln P(Q) + \text{const}$, where $P(Q)$ is the probability of observing a value $Q$ of the order parameter for the transition in the simulation run. Thus, in an equivalent way, one can find that the probability distribution of the order parameter has two minima in the canonical ensemble. As $N \to \infty$, the free energy barrier between these minima is expected to increase and the phase transition tends to the first-order bulk phase transition.

The practical problem is now to find an adequate set of order parameters. A possible order parameter is the total potential energy $E_p$ or just the difference between the configurational energy and the global-minimum energy (Lynden-Bell and Wales, 1994; Shah *et al.*, 2003). Other parameters are related to the local ordering, such as the orientational bond order parameters $Q_L$ (Steinhardt *et al.*, 1983), or the common neighbor analysis (D. Faken and H. Jónsson, 1994) signatures [13]. The radial distribution function is also routinely monitored. This is useful also to single out surface disordering phenomena (Huang and Balbuena, 2002; Qi *et al.*, 2001).

Solid-like and liquid-like phases may be distinguished also from their different mobility. In bulk systems, the Lindemann criterion is commonly used. The atomic vibrational amplitude $\langle \Delta r^2 \rangle^{1/2}$ is defined as a disorder parameter $\Delta_L$; experiments and simulations show that its critical value is around 0.10-0.15 in units of the atomic spacing (Bilgram, 1987; Lowen, 1994). For irregular finite systems however the pure Lindemann criterion is not appropriate; a better idea is to introduce the distance-fluctuation (DF) measure $\Delta_{DF}$, as proposed by Etters and Kaelberer (1977) and Berry *et al.* (1988):

$$\Delta_{DF} = \frac{2}{N(N-1)} \sum_{i<j} \frac{\sqrt{\langle \Delta r_{ij}^2 \rangle}}{\langle r_{ij} \rangle} \qquad (30)$$

where $r_{ij}$ is the distance between atoms $i$ and $j$, $\langle \Delta r_{ij}^2 \rangle = \langle (r_{ij} - \langle r_{ij} \rangle)^2 \rangle$. The key difference between Lindemann and DF criteria is that the latter is based on the fluctuation of the distance between pairs of atoms while the former is based on the fluctuation of individual atoms relative to their average position. The critical value of $\Delta_{DF}$ for the solid-liquid transition has been suggested to be around 0.03-0.05 (Zhou *et al.*, 2002). Some caveats are necessary when using $\Delta_{DF}$. As pointed out by Frantz (1995, 2001), $\Delta_{DF}$ depends on the length of the simulation run. For very long simulations, a value $\Delta_{DF} \sim 0.1$ can be obtained even at low temperatures, at which the cluster is simply making isomerizations among permutational isomers in its solid form. However, computing $\Delta_{DF}$ can be a very sensitive method to monitor qualitatively the melting transition from below (Frantz, 2001).

In order to have quantitative information on the mobility of the cluster particles, but avoiding the shortcomings of $\Delta_{DF}$, one can consider quantities that do not depend on the simulation length. Rytkönen *et al.* (1998b) monitored the average rate of change in the nearest neighbors of the cluster atoms. Another possibility is to compute the number of distinct basins visited per unit time.

The melting of nanoclusters has been largely studied by standard simulation methods such as MD and MC (see for example Frenkel and Smit (1996)). Contrary to MC, which is based on a fictitious dynamics, MD closely mimicks the true dynamics of the system. This allows

[13] In the common neighbor analysis a signature is assigned to each pair of neighbors. This signature is a triplet of integers $(r, s, t)$, where $r$ is the number of common nearest neighbors of two atoms of the pair, $s$ is the number of nearest-neighbor bonds among the $r$ common neighbors, and $t$ is the length of the longest chain which can be formed with the $s$ bonds. We have found that the monitoring of the signatures $(r, s, t) = (5, 5, 5)$, $(4, 2, 1)$, $(4, 2, 2)$ is sufficient to distinguish Ih, Dh and fcc structures in wide size ranges (Baletto *et al.*, 2001a; Baletto, 2003) during growth simulations. The (5,5,5) signature singles pairs located along a (locally) fivefold symmetry axis. The (4,2,1) signature is associated to pairs with fcc neighborhood. The (4,2,2) signature is associated to pairs comprising an atom of a (locally) fivefold axis and an atom outside the axis. In perfect fcc clusters one expects a large percentage of (4,2,1) signatures and no (5,5,5) and (4,2,2) signatures. Comparing Ih and Dh clusters in the same size range, one finds that the percentage of (5,5,5) signatures is much larger in icosahedra, while the percentage of (4,2,1) signatures is larger in decahedra. Tables with the values of the percentages for these signatures are found in Baletto *et al.* (2001a); Baletto (2003).

the calculation of equilibrium time-dependent correlation functions, such as those related to the diffusion of the cluster particles. MD allows also the realistic simulation of melting and freezing processes, which take place on finite time scales and thus may include also kinetic effects. On the other hand, MC can be faster in sampling the configuration space, being thus more appropriate if one is interested in static quantities only.

In fact, a major problem when calculating thermodynamic properties by simulation is quasi-ergodicity, namely the incomplete sampling of the configurational space which may occur in the phase-change region. Quasi-ergodicity can lead to overestimated transition temperatures in MD caloric curves (Calvo and Guet, 2000) if the heating rate is too fast.

Various methods have been employed to reduce the systematic errors resulting from quasi-ergodicity, including histogram, jump-walking, smart-walking, and parallel tempering methods [14]. Many of these methods are based on the coupling of configurations obtained from ergodic higher-$T$ simulations to the quasi-ergodic lower-$T$ simulations. MC J-walking methods, for example, couple the usual small-scale Metropolis moves made by a lower-$T$ random walker, with occasional large-scale jumps that move the random walker out of confined regions of configurational space. These large scale jumps are to configurations that are obtained in higher-$T$ simulations. Neirotti *et al.* (2000) and Calvo *et al.* (2000) showed that parallel tempering is remarkably successful in overcoming quasi-ergodicity and in calculating accurate heat capacity curves. In parallel tempering, several simulations are run in parallel at different temperatures. Periodically, exchange moves between configurations pertaining to simulations at nearby temperatures are attempted, and accepted or rejected according to the Metropolis rule.

### 3. Size dependence of the melting point

The size dependence of the cluster melting point for a given material, presents usually an average monotonically decreasing trend with decreasing size, with irregular variations on a fine scale. Here we first deal with the justification of the monotonic trend, and then treat the fine-scale non-monotonic variations.

The average dependence of the melting point with size $N$ has been derived by means of a few phenomenological models. The classical calculation by Pawlow (1909) has been further extended and modified by several groups. A recent account of some of these developments is found in Chushak and Bartell (2001a). Here we derive Pawlow's formula following the approach of Buffat and Borel (1976). We consider a cluster of size $N$ and of spherical shape. At a given pressure $p$, its melting temperature is $T_m(N)$, which has to be compared with the bulk melting temperature $T_m(\infty)$. In analogy with bulk melting, one identifies the solid-liquid transition by equating the chemical potentials $\mu_s$ and $\mu_l$ of the solid and of the liquid, so that $T_m(N)$ at a given pressure $p$ follows from the solution of this equation:

$$\mu_s(p,T) = \mu_l(p,T). \tag{31}$$

This equation means that the chemical potential of a fully liquid and of a fully solid cluster are equal at melting. The chemical potential can be expanded around its value at the triple point; we retain first-order terms only

$$\mu(p,T) = \mu(p_0,T_0) + \frac{\partial\mu}{\partial T}(T-T_0) + \frac{\partial\mu}{\partial p}(p-p_0). \tag{32}$$

From the Gibbs-Duhem equation ($-Vdp+SdT+Nd\mu = 0$) follows that

$$\frac{\partial\mu}{\partial T} = -s \qquad\qquad \frac{\partial\mu}{\partial p} = \frac{1}{\rho}, \tag{33}$$

where $s = S/N$ is the entropy per particle and $\rho = V/N$ is the number density. From Eqs. (31-33), and taking into account that $\mu_s(p_0,T_0) = \mu_l(p_0,T_0)$, one obtains

$$-s_l(T-T_0)+\frac{1}{\rho_l}(p_l-p_0) = -s_s(T-T_0)+\frac{1}{\rho_s}(p_s-p_0) \tag{34}$$

Here, one must distinguish between the pressure $p_s$ of a solid cluster and the pressure $p_l$ of a liquid cluster. In fact, the pressure inside a small object of radius $r$ is larger than the external pressure because of the Laplace contribution $p_{Lap} = 2\gamma/r$ to the pressure where $\gamma$ is the interface tension of the cluster and $r$ is its radius. Since the liquid and the solid cluster of $N$ atoms can differ both in the interface tension ($\gamma_{lv}$ for the liquid-vapor interface, $\gamma_{sv}$ for the solid-vapor interface) and in the radius, they can have different Laplace pressure terms

$$p_l = p_{ext} + \frac{2\gamma_{lv}}{r_l} \qquad p_s = p_{ext} + \frac{2\gamma_{sv}}{r_s}. \tag{35}$$

For a cluster of $r \sim 10$ nm, typical interface tensions are of the order of $10^3$ erg/cm$^2$, so that the Laplace pressure is much larger than $p_{ext}$ in usual conditions. Thus $p_{ext}$ can be neglected in Eq. (35). Moreover, for spherical clusters,

$$\frac{r_s}{r_l} = \left(\frac{\rho_l}{\rho_s}\right)^{1/3}. \tag{36}$$

Substituting Eqs. (35,36) into Eq. (34), neglecting $p_{ext}$ and taking into account that $L = T_0(s_l - s_s)$ is the latent heat of melting per particle, one obtains:

$$1 - \frac{T_m(N)}{T_m(\infty)} = \frac{2}{\rho_s r_s L}\left[\gamma_{sv} - \gamma_{lv}\left(\frac{\rho_s}{\rho_l}\right)^{2/3}\right]. \tag{37}$$

[14] See for example Labastie and Whetten (1990), Frantz *et al.* (1990); Frantz (2001), Neirotti *et al.* (2000), Calvo *et al.* (2000), Ghayal and Curotto (2000), Fthenakis *et al.* (2003)

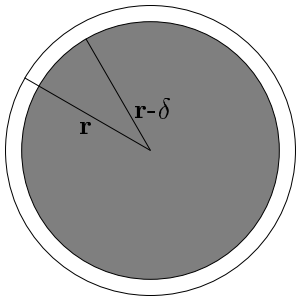


FIG. 24 A particle with a solid core of radius $r - \delta$ and a liquid shell of thickness $\delta$.

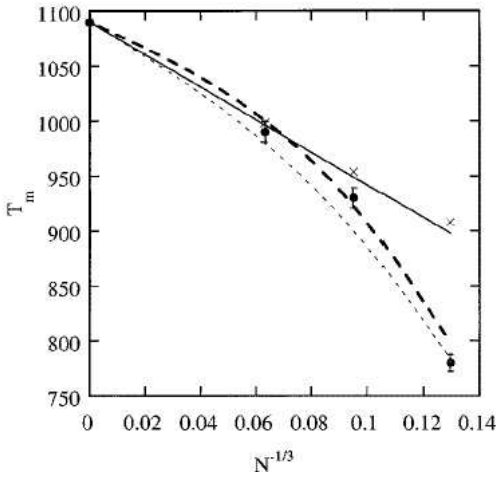


FIG. 25 Melting point of gold clusters from MD simulations (black dots), and comparison with different theoretical results. The solid line is Pawlow's theory; the crosses include second-order corrections from Buffat and Borel (1976); the thick dashed curves correspond to the liquid-shell model by Sambles (1971), namely to Eq. (42); the thin dashed curves includes second-order corrections to Sambles' formula. Reprinted with permission from Chushak and Bartell (2001a). Copyright 2001 American Chemical Society.

Since $r_l \propto N^{1/3}$, one finds that Eq. (37) can be rearranged to the form (Reiss *et al.*, 1988)

$$T_m(N) = T_m(\infty)\left[1 - \frac{\mathcal{C}}{N^{1/3}}\right], \qquad (38)$$

where $\mathcal{C}$ is a constant. This formula gives a very simple dependence for $T_m(N)$ which can be thus considerably lower than $T_m(\infty)$ (Buffat and Borel, 1976; Lewis *et al.*, 1997; Rytkönen *et al.*, 1998b). An expression for $\mathcal{C}$ easily follows from Eq. (37), but the quantities involved in that expression may not be easy to evaluate. Moreover, several (and rather crude) approximations are involved in Eq. (37), so that usually $\mathcal{C}$ is considered as a fitting parameter.

Several attempts have been made to improve Pawlow's

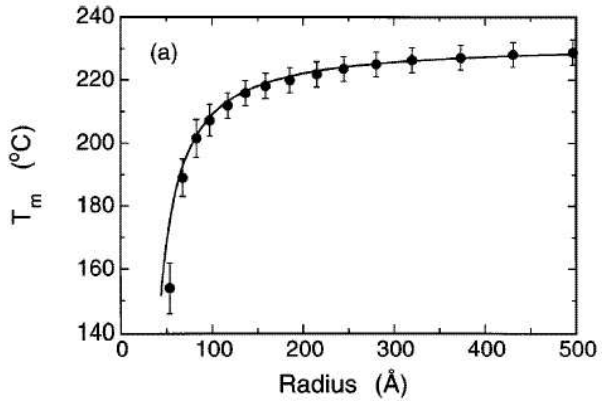


FIG. 26 Experimental melting point of supported tin clusters (black dots), and comparison with the fitting by means of Eq. (42). The figure is taken from Lai *et al.* (1996).

theory. Buffat and Borel (1976) included higher-order terms in Eq. (32), and solved numerically the resulting equation. Including higher-order terms is in principle more accurate, but these terms increase the number of unknown parameters to be evaluated. Reiss and Wilson (1948), Hanszen (1960) and finally Sambles (1971) refined Pawlow's model including the possibility of surface melting, that is of having clusters (of total radius $r$) made of an inner core of radius $r - \delta$ and an external liquid shell of thickness $\delta$. The melting temperature is found by imposing the equilibrium condition on this solid core -liquid shell particle. A derivation for the case of metallic particles was given by Kofman *et al.* (1994) and Vanfleet and Mochel (1995); here we briefly sketch their approach. The extension of this approach to molecular clusters (namely including Van der Waals forces) can be found in Levi and Mazzarello (2001).

Let us consider a particle as in Fig. 24, containing $N_l$ particles in the liquid shell. Its free energy $G$ is given by

$$\begin{aligned} G &= (N - N_l)\mu_s + N_l\mu_l + \\ &+ 4\pi r^2\left[\gamma_{sl}\left(\frac{r-\delta}{r}\right)^2 + \gamma_{lv} + S'\mathrm{e}^{-\delta/\zeta}\right], \end{aligned} \qquad (39)$$

where

$$S' = \gamma_{sv} - \left[\gamma_{lv} + \gamma_{sl}\left(\frac{r-\delta}{r}\right)^2\right]. \qquad (40)$$

$\zeta$ is the characteristic length of the interaction among atoms in liquid metals, and the term $S'\mathrm{e}^{\delta/\zeta}$ takes into account the effective interaction between the solid-liquid and liquid-vapor interfaces. This effective interaction is repulsive, and favors the formation of a liquid shell between the solid core and the vapor. For $T$ not too far from $T_m(\infty)$ one may approximate $N_l(\mu_l - \mu_s) \simeq V_l\rho L[T_m(\infty) - T]/T_m(\infty)$, where $V_l = 4\pi[r^3 - (r-\delta)^3]/3$ is the volume of the liquid layer, and the density difference between liquid and solid is neglected ($\rho_l = \rho_s = \rho$).

Minimizing $G$ with respect to $\delta$, one finds the following solution for $T_m(N)$

$$1-\frac{T_m(N)}{T_m(\infty)} = \frac{2\gamma_{sl}}{\rho L(r-\delta)}\left(1-\mathrm{e}^{-\delta/\zeta}\right)+\frac{S'r^2}{\rho L\zeta(r-\delta)^2}\mathrm{e}^{-\delta/\zeta}. \quad (41)$$

Pawlow's result of Eq. (37) is recovered in the limit $\zeta \to 0$, which means a sharp interface, or equivalently, no effective repulsive interaction between the solid-liquid and the liquid-vapor interfaces ($S' = 0$). For molecular clusters, this effective interaction is proportional to $1/\delta^2$, instead of $\mathrm{e}^{-\delta/\zeta}$ (Levi and Mazzarello, 2001).

Following a somewhat different line of reasoning Chushak and Bartell (2001a) derived a similar expression, which is close to those found by Hanszen (1960) and Sambles (1971):

$$1-\frac{T_m(N)}{T_m(\infty)} = \frac{2}{\rho_l L}\left\{\frac{\gamma_{sl}}{r-\delta}+\frac{\gamma_{lv}}{r}\left[1-\left(\frac{\rho_s}{\rho_l}\right)^{2/3}\right]\right\}, \quad (42)$$

If $\gamma_{sl}$ is evaluated as $\gamma_{sv}-\gamma_{lv}$ (namely the liquid shell perfectly wets the solid core), and $\delta = 0$, Eq. (42) reduces to Eq. (37).

Both Eqs. (41) and (42) are more accurate than Pawlow's result down to small sizes (see Fig. 25). Peters *et al.* (1998) found that the solid core - liquid shell model gives a better fit of the experimental melting temperatures of supported lead clusters. Chushak and Bartell (2001a) and Wang *et al.* (2003b) melted a series of selected fcc clusters of gold and copper respectively by MD simulations within an embedded atom energetic model. They found that Eq. (38) is accurate down to $N \sim 10^3$ and $5\,10^2$ for Au and Cu respectively. At smaller sizes, Eq. (42) is in better agreement with the simulation data in the case of Au. Other simulation results are found in Ercolessi *et al.* (1991); Lewis *et al.* (1997); Qi *et al.* (2001). Lai *et al.* (1996) obtained an excellent fit to their experimental data on the melting of tin clusters (see Fig. 26) by the formula of Hanszen (1960); the same data were successfully refitted by means of Eq. (41) (Bachels *et al.*, 2000).

When the size dependence of the melting point is examined on a fine scale, irregular variations are found, especially at small sizes, where the addition or the removal of a single atom can have dramatic effects. There is a good agreement among several simulation results in predicting that clusters of special stability, such as Ih clusters at magic sizes (55, 147 etc) melt higher than predicted by Eq. (38) (see for example the cases of LJ, Na and noble-metal clusters (Frantz, 2001; Rytkönen *et al.*, 1998b; Valkealahti and Manninen, 1993)). However, the situation can be more complicated.

Schmidt *et al.* (1998) measured the melting point of Na clusters up to 200 atoms. They found an irregular behavior of $T_m$, with few well-defined peaks, as shown in Fig. 18. Also $L$ showed the same kind of behavior. The peaks in $T_m(N)$ and $L$ were not well correlated with those in the mass spectrum, corresponding to the closing of electronic shells. These results showed that the most abundant clusters and the highest-melting point clusters do not always coincide. In a recent experiment, Schmidt *et al.* (2003) were able to measure the energy and the entropy change in the melting of Na clusters. They found that the peaks in $T_m(N)$ are driven by the energy difference between the liquid and the solid phases. The entropy difference is closely correlated to the energy difference and causes simply a damping of the energetic effects. This would show that the main indicator for a high $T_m$ is the energetic separation of the global minimum from higher isomers. However, it is not yet clear whether entropic differences are always correlated to energetic differences, or this is a specificity of Na clusters.

The irregular variations of the melting point in LJ clusters were studied by Frantz (2001), who analyzed thoroughly the range $26 \le N \le 60$ by the parallel tempering technique. Frantz (2001) found that the peaks in $T_m(N)$ were generally well correlated with those of other stability indicators, such as the energetic separation of the second isomer from the global minimum $E_{SM}(N) - E_{GM}(N)$, $\Delta_1(N)$, and $\Delta_2(N)$ (see Eq. (6)). An exception was $N = 58$, a magic size for the stability indicators, but not corresponding to a peak of $T_m(N)$.

Finally, even though the melting point in nanoclusters is usually depressed, some evidence in favor of exceptions to this rule is beginning to accumulate. The first experimental evidence of an exception is due to Shvartsburg and Jarrold (2000), who studied the melting of Sn clusters. Small Sn clusters have a rather elongated structure which should change to nearly spherical upon melting. No signature of this change was observed by Shvartsburg and Jarrold (2000), so they concluded that Sn cluster ions containing 10-30 atoms have a melting point which is at least 50 K above the bulk one. This behavior has been confirmed by Joshi *et al.* (2002) who performed *ab initio* MD simulations of the melting of $Sn_{10}$. They found that binding in such small cluster is indeed covalent, and that the specific heat of $Sn_{10}$ shows a shoulder around 500 K due to a permutational rearrangement of atoms that preserves the trigonal prism core of the ground state. Only at much higher temperatures $T \simeq 1500$ K this core distorts and breaks up, yielding a peak in the specific heat around 2300 K. Joshi *et al.* (2003) simulated also the melting of $Sn_{20}$, finding that it melts lower than $Sn_{10}$, but still much higher than bulk Sn. Chuang *et al.* (2004) have found by *ab initio* Langevin MD that also $Sn_6$, $Sn_7$ and $Sn_{13}$ melt higher than bulk Sn.

Small Sn cluster do not seem to be the only ones to melt higher than the bulk crystal. There is recent experimental and theoretical evidence for gallium clusters (Breaux *et al.*, 2003; Chacko *et al.*, 2004), whose high melting point is attributed to the fact that, contrary to bulk Ga, binding in small clusters is fully covalent. Finally, in their simulations, Akola and Manninen (2001) observed a bulk-like behavior of $Al_{13}^-$ above the Al bulk melting temperature.

As a final remark, we note that the results about the

thermodynamic effects on the structural stability and the melting of nanoclusters suggest a more general definition of the stability itself, including also the temperature effects (Baletto *et al.*, 2004).

### C. Studies of selected systems

#### 1. Lennard-Jones clusters

There are several computational studies about the melting of Lj clusters, especially at magic Ih sizes. Early MD studies on the melting of Ar clusters by Briant and Burton (1975) indicated a relatively sharp first-order-like transition at $T$ below the bulk melting temperature. This result has been confirmed later on. At $N = 55$ and $N = 147$ all simulations indicate relatively sharp jumps in the caloric curves at $T \simeq 35$ K and $T \simeq 42$ K, and the radial distributions confirm that the whole clusters melted during the transitions (Etters and Kaelberer, 1975; Honeycutt and Andersen, 1987; Matsuoka *et al.*, 1992). At $N = 13$ the cluster fluctuates back and forth between the two phases and a consistent determination of $T_m$ is very difficult. The broadness of the solid-liquid transition is revealed also for $Ar_{13}$ adsorbed on a surface (Blaisten-Barojas *et al.*, 1987) where the cluster changes from an Ih, solid-like structure at low $T$ to a set of liquid-like structures at high $T$. Clusters containing 309 or more atoms are observed to desorb atoms at temperatures where the core is still solid (Rytkönen *et al.*, 1997). Thus it is very complicated to define their melting point, if the heating rate is slow. Fast heating rates can however cause the superheating of the cluster. Rytkönen *et al.* (1998b) found a rather good agreement with Eq. (38), except that $T_m$ at small sizes and for Ih structures is higher than predicted analytically. To investigate how the melting takes place, Rytkönen *et al.* (1998b) calculated the radial distribution function finding that, at non-magic Ih sizes, there is a clear tendency to surface melting while the cores preserve an Ih morphology.

Frantz (1995, 2001) made a detailed systematic work on small LJ clusters by MC simulations. He found that the smallest clusters present an irregular dependence of their thermodynamic properties with size. For $N > 25$ some trends are better singled out. Icosahedral packing is dominant (with the exception of the TO at $N = 38$) and the heat capacity peak parameters form two overlapping sequences as a function of $N$, depending on the overlayer being either of Mackay or anti-Mackay stacking. In clusters with anti-Mackay overlayer the heat capacity peak shifts towards higher $T$ and becomes smaller at increasing $N$, while clusters with Mackay rearrangement have small, low-$T$ peaks that generally shift to higher $T$ and grow in size as $N$ increases. There is a sequence of magic numbers $N = 36, 39, 43, 46, 49, 55$ at which the heat capacity peak is stronger. As already discussed in Section IV.B.3, this sequence correlates well with the one extracted from the binding energy differences.

#### 2. Sodium clusters

Experiments by Martin *et al.* (1994) and Schmidt *et al.* (1998) have revealed a complex dependence of $T_m(N)$ for Na clusters. Its irregular small-size behavior has been already discussed in Section IV.B.3. Liu *et al.* (2002) performed a systematic simulation study of the melting of different morphologies in a wide size range. They found that the melting points for all sizes and structural types are in a narrow $T$ range (200-300 K) and all clusters present a liquid-gas transition around 1000 K.

Another interesting point about the melting of Na clusters (and of great general interest) is the presence of pre-melting effects. A detailed study on this topic at $8 \leq N \leq 147$ atoms has been performed by Calvo and Spiegelman (2000) by a MC thermodynamical analysis near to the solid-liquid transition, within a semiempirical modelling by Gupta (1981) potentials. Up to 147 atoms, the thermodynamics appears to be directly related to the lowest-energy structures and melting by steps is favored by the presence of surface defects. For $N < 75$ the $T_m$ presents a strong non-monotonic behavior with $N$, which is typical of geometric size effects. For larger sizes the transition becomes more and more similar to the bulk case. Calvo and Spiegelman (2000) find evidence of pre-melting phenomena at small sizes, with the caloric curves presenting multi-modal behavior with increasing $T$. Simple isomerization between a few structures, surface melting or competition between several funnels on the energy landscape may be the causes of this pre-melting. Pre-melting seems to be the rule for small Na clusters, the only exceptions being the very stable magic Ih structures. The secondary peaks in the heat capacity become less pronounced at $N > 100$, indicating that pre-melting becomes less important. Calculations by Gupta (1981) potentials and *ab initio* schemes (Reyes-Nava *et al.*, 2002; Rytkönen *et al.*, 1998a, 1999) are in some agreement with the experiments, but several aspects of the melting behavior of Na clusters are still to be understood. Calvo and Spiegelman (2004) have recently reexamined the melting behavior of Gupta Na clusters in the size range around 130 atoms, finding that the potential is somewhat inadequate because it predicts strong premelting effects that are not observed in the experiments. These premelting effects are related to the surface melting of the outer Ih shell.

Also in the case of the metallic clusters the literature is extensive, especially for Au clusters [15]. At first we remark that, although the melting point is depressed, its reduction is smaller than that of LJ clusters, and is strongly material dependent (Garzón and Jellinek, 1991; Jellinek *et al.*, 1986; Jellinek and Garzón, 1991). Usually melting is accompanied by a peak in the specific heat, and by a substantial rearrangement of the cluster. But there are exceptions. For example, the simulations by Westergren *et al.* (2003) revealed that $Pd_{34}$ melts without an accompanying peak in the heat capacity and the atoms become mobile without any significant change in geometric structure. At very small sizes, around 13 atoms, García-Rodeja *et al.* (1994) and Lee *et al.* (2001) studied several transition and noble metals, modelled by Gupta (1981) potentials. Their simulation results were in agreement with those obtained by Güvenc and Jellinek (1992). The salient results is that the behavior of Ni, Cu, Pd, Ag, and Pt is similar, the main difference being that $Pd_{13}$ presents a more complex anharmonic behavior than Ag (Westergren and Nordholm, 2003). The 13-atom clusters undergo a structural transition from a rigid, solid-like Ih structure to a non-rigid, liquid-like one via an intermediate temperature range in which both forms coexist. The caloric curves do not present any sharp transition and $T_m$ is found by monitoring $\Delta_{DF}$ (Eq. (30)) and looking for a maximum in the specific heat. The instability of some specific atom can play a key role in melting as in the case of the capped atoms at $N = 14$. The atom added to the 13-atom Ih can diffuse fast at $T$ below the melting region, and this causes a small peak in the specific heat (García-Rodeja *et al.*, 1994; Lee *et al.*, 2001) so that $T_m$ is smaller than for the 13-atom cluster. Similar behavior is found at $N = 20$ for the capped double Ih. On the contrary, when the double Ih is not the global minimum the heat capacity has an unexpected behavior; for example, $Pd_{19}$ shows a distinct abrupt change at $T \sim 400K$ and rounded-off broad peak at higher $T$ (Lee *et al.*, 2001).

Li *et al.* (2000b) made a thorough analysis at $N = 55$ for Au, Ag and Cu by means of MD simulations. $Ag_{55}$ and $Cu_{55}$ show abrupt changes during the melting-like transitions, while the transition of $Au_{55}$ seems to proceed for a relatively broader interval, with $\Delta_{DF}$ increasing gently from 300 up to 600K and with a small, ladder-like energy jump in the caloric curve. The degrees of reduction for $T_m$ is different among the three metals. Compared to Ag and Cu, Au exhibits the largest size-induced drop of $T_m$. This confirm the trends of Table I, since Cu gives the most stable Ih cluster also from the thermodynamic point of view.

[15] See Buffat and Borel (1976), Garzón and Jellinek (1993), Cleveland *et al.* (1997, 1998, 1999), Li *et al.* (2000b, 2002), Lee *et al.* (2001), and Koga *et al.* (2004).

At $N = 38$ Baletto *et al.* (2004) have found a complex melting behavior for Cu by MD simulations, with a solid-solid transition taking place: from the TO, which is the global minimum, the cluster rearranges itself into defected Dh structures before melting, in analogy with the behavior of $LJ_{38}$ (Doye *et al.*, 1998). On the other hand $Ag_{38}$, which has the same global-minimum structure as $Cu_{38}$, does not exhibit any solid-solid transition to defected Dh structures. Finally, at this size Au presents a coexistence phase region among different isomers already at $T \sim 250K$ (Garzón *et al.*, 1999).

Molecular-dynamics simulations of the melting transitions for crystalline nickel clusters above $N \sim 750$ show that $T_m(N)$ closely follows Eq.(38) (Qi *et al.*, 2001), while, for $N < 500$, Ih structures present higher $T_m$ and large latent heat. Similar results are found also for Cu (Wang *et al.*, 2003b). On the contrary, for smaller $N$, the Ih packing is more stable and presents higher melting points than those derived from Eq. (38) (Valkealahti and Manninen, 1993).

*a. Gold: pre-melting icosahedral precursors* Gold clusters have been studied intensively in the last decades, see Cleveland *et al.* (1998, 1999); Lee *et al.* (2001); Li *et al.* (2002). All these studies agree that a solid-solid structural transformations from the low-$T$ optimal structures to Ih structures takes place below the melting temperature. Detailed analysis of the atomic trajectories and of the structural evolution indicate that this solid-to-solid transition is essentially without diffusive motion, occurring fast and involving a high degree of cooperative (small) displacements of the atoms; the structural transformation is driven by the vibrational and configurational entropy at elevated $T$ (Ajayan and Marks, 1988; Luo *et al.*, 1987). A thorough MD simulation study was made by Liu *et al.* (2001). Different morphologies were compared up to $N \sim 25000$. At intermediate sizes, for all type of morphologies, Liu *et al.* (2001) found that the melting process occurs in three stages: a relatively long time of surface disordering and reordering, a relatively short time of surface melting, and finally a rapid overall melting. Concerning the differences among the structural motifs, star-like Dh are the hardest to melt, while Ih clusters are the easiest, regular decahedra being in between. Small CO, up to $N = 309$ at least, transform into icosahedra before melting, while large CO do not. Contrary to the other motifs, $T_m$ of icosahedra saturates at $N > 12000$. Liu *et al.* (2001) compared also different structures at identical sizes, finding that transition temperatures may differ even by 75 K. This non-equilibrium effect indicates the differences in kinetic stability of the different structures against heating.

Very recently Koga *et al.* (2004) were able to heat up metastable gold Ih produced in an inert gas aggregation source (see Section V.B.3). Upon heating to $T = 1273$ K, which is only 64 K below the bulk melting temperature of Au, they were able to produce a clearly domi-

nant fraction of Dh structures in the range 6-12 nm of diameter. A considerable fraction of fcc clusters was obtained only heating above the bulk melting temperature, and only for diameters above 10 nm. Since all calculated crossover sizes Dh → fcc at 0 K are much smaller (Baletto *et al.*, 2002b; Cleveland *et al.*, 1997), these experimental results give support to the hypothesis of an upward displacement of the crossover size with increasing temperature, in agreement with the predictions of the harmonic theory (Doye and Calvo, 2001), as can be seen in Fig. 20.

#### 4. Silicon clusters

Wang *et al.* (2001b) performed a systematic simulation study of structural transitions and thermodynamic properties of small Si clusters within a tight-binding MD scheme. They confirmed previous results about the thermodynamics of very small clusters found by means of empirical many-body potentials (Blaisten-Barojas and Levesque, 1986; Stillinger and Weber, 1985; Tchofo-Dinda *et al.*, 1995), and considered also larger sizes. Their canonical MC simulations revealed that the melting point of Si clusters changes dramatically when the global minimum structures changes from the prolate cage-like (for $N = 17$ in this study) to the atom-centered nearly spherical morphology. The nearly spherical clusters present a much broadened melting region, extending from 750 to 1300 K. This is due to the following fact. In the nearly-spherical structures, the cluster core is more tightly bonded than surface atoms, and a much higher temperature is needed for its disordering. In the range $650 < T < 1050$ K, the nearly-spherical clusters keep their structure although there is a noticeable surface diffusion. After that, melting can take place via two pathways. The first possibility is that, as $T$ increases, the clusters develop to the prolate morphology up to 1200 K, then break into subunits, which finally become less and less stable until the clusters disorder completely. The other possibility is that the clusters develop from quasi-spherical to prolate to molten oblate structures. Atoms in prolate cage-like structures are more stable than the surface atoms of the nearly spherical structures. The melting of cage-like structures often accompanies the overall deformation and fragmentation of the cage framework. Thus a much higher temperature is needed to break the cage, but the whole cluster melts at temperatures comparable with other nearly spherical structures.

## V. KINETIC EFFECTS IN THE FORMATION OF NANOCLUSTERS

From the results reported in the previous Sections, there is evidence of discrepancies between the results of energetic and/or thermodynamic calculations and the real outcome of the experiments, namely the structures which are actually observed in the production of free solid clusters. In some cases, the disagreement is of such a qualitative nature that one cannot expect that it is due to the failure of the energetic or of the thermodynamic modelling. To cite just the most striking cases, we mention the observation of small Dh and large Ih in the inert gas aggregation experiments on the production of Ag clusters (Reinhard *et al.*, 1997b), the production of large Ih clusters of $C_{60}$ molecules (Branz *et al.*, 2002, 2000; Martin *et al.*, 1993), the detection of octahedral Al clusters presenting only (111) facets (Martin *et al.*, 1992). Moreover, there is still quantitative disagreement between the theoretical estimates (based on the total energy optimization) and the experimental data about the crossover sizes for Ar clusters (Ikeshoji *et al.*, 2001). These results indicate that kinetic effects must be taken into account to explain the actual outcome of free cluster formation experiments. As discussed in Section II, the time scale of nanocluster formation in typical sources ranges from a fraction of a millisecond to a few milliseconds. On this time scale, clusters may not be able to reach the minimum free-energy structure, thus remaining trapped in some metastable configuration which can have very long lifetimes, especially when the clusters are further cooled down after their solidification.

In studying the formation process of solid clusters in contact with a thermal bath, such as the inert gas atmosphere in inert gas aggregation sources, we can think of two alternative models. In both models, clusters mainly grow by the addition of single atoms (de Heer, 1993).

In the first model (Section V.A), which is suited for high growth temperatures, the cluster solidifies after its growth is completed, namely at a further cooling stage taking place outside the growth chamber. In this case, the final cluster structure does not depend on the kinetics of the growth process, because the cluster remains a liquid droplet while growing, but on the kinetics of the cooling after growth, which may take place on time scales as those discussed in Section V.A, namely in the range of $1 - 10^{-2}$ K/ns. This model will be referred to as liquid state growth model, and is simulated by freezing a liquid droplet until it solidifies, namely by a procedure at constant $N$ and decreasing $T$, except for some cases. In fact, there are systems (such as the noble gases) in which evaporation of atoms is not negligible at temperatures close to the melting point, because melting and boiling temperatures are close to each other. Evaporating atoms can thus have an important role even in the cooling of solid clusters. On the contrary, metals present huge differences between melting and boiling points, so that evaporative cooling is negligible for solid metallic clusters.

In the second model (Section V.B), which is suited for relatively low growth temperatures, clusters solidify

while they are still growing [16]. This model will be referred to as solid state growth model. In this model, the final outcome is determined by the kinetics of the growth process itself. Solid state growth is simulated by adding single atoms on a small initial seed at constant temperature (Baletto *et al.*, 2000a,b), namely at constant $T$ and increasing $N$.

Finally (see Section V.C), there are cases in which the growth does not proceed only by the addition of single atoms, but also by the collision and coalescence of already formed clusters.

### A. Freezing of liquid nanodroplets

When simulating cluster freezing the relevant parameter is the rate $r_c$ at which the temperature $T$ is rescaled, in order to mimic a thermal contact with a cold atmosphere. For example, the cluster can be cooled down by small steps $\delta T$ at each time interval $\delta t$ so $r_c = \delta T/\delta t$. In an inert-gas atmosphere, one can estimate that a cluster of radius $R$ and area $A_{eff} = 4\pi R^2$ collides with gas atoms with a frequency $\phi^G_{exp}$ given by:

$$\phi^G_{exp} \sim \frac{P_G A_{eff}}{\sqrt{2\pi m_G k_B T_G}}, \tag{43}$$

where $P_G$ and $T_G$ are, respectively, the pressure and the temperature of the inert gas of mass $m_G$. In the harmonic approximation, the energy loss is given by:

$$\frac{\delta T}{\delta t} \sim \phi^G_{exp} \frac{\delta E}{3Nk_B}, \tag{44}$$

where $\delta E$ is the energy transfer at each collision, and since $A_{eff} \propto N^2$ and $N \propto R^3$ we obtain $\frac{\delta T}{\delta t} \propto \frac{1}{R}$. From Ref. (Westergren *et al.*, 1998), we can estimate that the loss for each collision (for example with a helium atom) $\delta E$ is of $1-10$ meV. Using typical parameters for the gas ($P_G \sim 1-100$ mbar, $T_G \sim 300$ K (Koga and Sugawara, 2003; Reinhard *et al.*, 1997b)) and considering $R \sim 1$ nm, we have $\frac{\delta T}{\delta t}$ in the range 0.01 - 1 K/ns.

#### 1. Lennard-Jones clusters

Ikeshoji *et al.* (2001) studied the freezing of LJ clusters by MD simulations. Contrary to what happens for metals, the melting and boiling points of LJ clusters are rather close in temperature, so that the evaporation of atoms is not negligible in the solidification process. Because of that, Ikeshoji *et al.* (2001) considered both ways of cooling clusters down, either by decreasing temperature in a canonical simulation or by letting the cluster evaporate atoms in a simulation at constant energy. They considered 380 clusters in the range $160 < N < 2200$, finding that there is a transition at increasing size from icosahedra to a mixture of structures (Dh, fcc, hcp, and Ih). The transition did not depend on the cooling method, either evaporation or thermostat, and took place for $N \simeq 450$. This is lower than the transition size (750 atoms) observed in experiments on argon clusters (Farges *et al.*, 1986), but it is closer than any other estimate based on total energy optimization, thus indicating the possible presence of kinetic trapping effects. Moreover, calculated and experimental diffraction patterns were in good agreement. Besides pure clusters, Ikeshoji *et al.* (2001) considered binary LJ systems, finding that the formation of large icosahedra is favored by the size mismatch. This finding may furnish a qualitative explanation of the experimental observation of large Ih clusters in binary (metallic) systems (Saha *et al.*, 1997, 1999).

#### 2. Silver clusters

Baletto *et al.* (2002c) studied the freezing of Ag liquid nanodroplets by MD simulations with realistic cooling rates $r_c$ in the range 0.1-5 K/ns. They made a systematic study of Ag freezing at $130 \leq N \leq 310$, and in addition considered the freezing at the Ih magic numbers 147, 309, 561 and 923. The latter simulations were made to investigate the possibility of obtaining large metastable Ag icosahedra by freezing liquid droplets, in order to ascertain whether the liquid state growth model could explain the experimental observation of metastable icosahedra by Reinhard *et al.* (1997b).

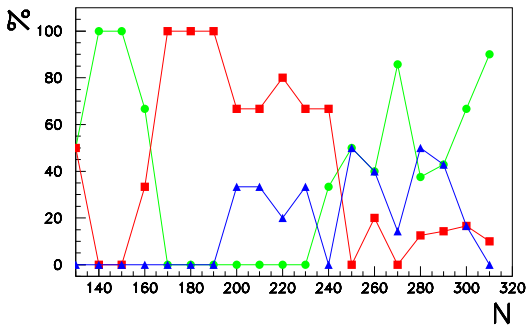


FIG. 27 Percentages of the different structures obtained in MD simulations of Ag cluster freezing at $r_c$=1 K/ns for $130 < N < 310$ (after Baletto *et al.* (2002c)). The circles are icosahedral structures, squares are decahedra and triangles are fcc clusters.

The results for $130 \leq N \leq 310$ are summarized in Fig. 27. On a coarse grained description, the energetic calculations by Baletto *et al.* (2002b) showed that Ih clusters are the best up to $N \simeq 170$; then the best structures are decahedral, except for the Ih magic number $N = 309$,

[16] Clusters may solidify during growth at constant temperature after reaching a critical size.

while fcc clusters become competitive with the Dh for $N > 600$. The freezing simulations in Baletto *et al.* (2002c) gave the following results. At $r_c = 1$ K/ns, particles solidified as icosahedra in the range $135 < N < 165$; around $N = 165$ there was a transition to Dh clusters, which were the most frequent for $170 < N < 245$. About 20% of the runs gave fcc structures in this range, and a few Ih clusters were formed. For $245 < N < 310$, the dominant structure at the end of the freezing were icosahedra, but also fcc clusters were common, especially in the range $N \sim$ 250-260 and $N \sim$ 280-300, in which they were more than 50%. At slower cooling rates $r_c = 0.12$ K/ns, the percentage of fcc and Ih particles in the range $170 < N < 245$ practically dropped to zero, indicating that Dh clusters are likely to be most favorable from the thermodynamic point of view in this size range. On the other hand, at faster cooling rates $r_c = 5$ K/ns, the percentage of fcc clusters in the range $245 < N < 310$ decreased to the advantage of Dh clusters, while the dominant proportion of icosahedra remained practically constant.

From the freezing results at the Ih magic numbers 147, 309, 561 and 923, it was possible to single out the following tendency (see Table II and Fig. 28). The percentage of Ih structures at the end of the freezing process decreased with cluster size for all cooling rates, passing from 100% at $N = 147$ to less than 20% at $N = 923$. There was no evidence of changes in the results when $r_c$ ranged within 1-20 K/ns, indicating probably that these rates are sufficient to mimic a freezing process which is taking place close to equilibrium.

TABLE II Numbers of Ih, Dh and fcc structures at magic icosahedral sizes. The results are obtained from five MD simulations for each cooling rate $r_c$ and for each size (after Baletto *et al.* (2002c)).

| $r_c$ $(K/ns)$ | $N$ | $N_{Ih}$ | $N_{Dh}$ | $N_{fcc}$ |
|---|---|---|---|---|
| 1. | 147 | 5 | - | - |
| | 309 | 4 | 1 | - |
| | 561 | 2 | 2 | 1 |
| | 923 | 1 | - | 4 |
| 5. | 147 | 5 | - | - |
| | 309 | 3 | - | 2 |
| | 561 | 2 | - | 3 |
| | 923 | - | 1 | 4 |
| 20. | 147 | 5 | - | - |
| | 309 | 2 | 1 | 2 |
| | 561 | 1 | 3 | 1 |
| | 923 | 1 | 3 | 1 |

In summary, the simulations showed that it is not possible to avoid the formation of a large percentage of small icosahedra (2-3 nm of diameter) if freezing takes place after the growth is completed. Moreover, the probability of forming large icosahedra by freezing liquid Ag droplets with realistic cooling rates is small. Both findings are in contrast with the experimental results by Reinhard *et al.* (1997b), who did not found strong evidence of small icosahedra, while they observed a dominant percentage of icosahedra at large sizes. Therefore, one can rule out the liquid state growth model to explain the outcome of this experiment.

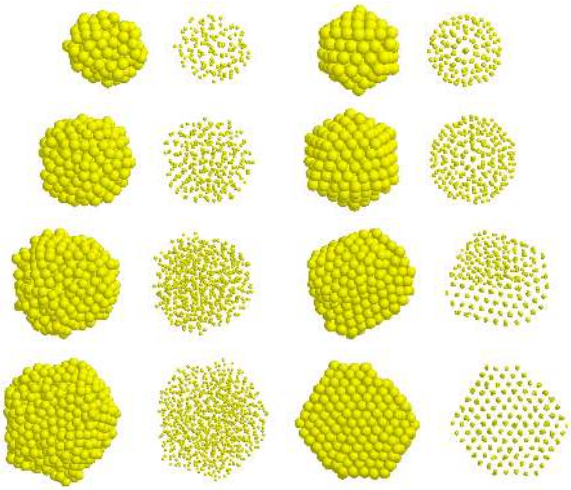

FIG. 28 MD simulation of silver cluster freezing. On the left, we report the initial configurations of Ag liquid nanodroplets at magic icosahedral numbers (147, 309, 561 and 923), while on the right, there are typical final structures obtained cooling at 1 K/ns: from top to bottom, icosahedra at 147 and 309, a decahedron at 561 (strongly asymmetric and with an island on hcp stacking above (Baletto and Ferrando, 2001)) and a fcc polyhedron at 923.

### 3. Gold clusters

Chushak and Bartell (2001a,b) studied the solidification of Au nanoclustersby MD simulations. However, their method is rather different from the one applied to Ag clusters by Baletto *et al.* (2002c). Chushak and Bartell (2001a,b) started from high $T$ liquid clusters of rather large sizes (459, 1157, and 3943 atoms). These clusters were then cooled down very fast with a rate $r_c = 5\,10^4$ K/ns down to a temperature of about 700 K, at which their most stable form is solid. At this temperature, production runs of 1 ns were performed. After that, clusters were further quenched down to 300 K, again with a fast rate (300 K/ns). As a result of this cooling procedure Chushak and Bartell (2001a,b) found that Ih clusters were preferentially produced, even though they should not be the lowest-energy structures at these sizes (see Baletto *et al.* (2002b)). In this case, Ih clusters were produced with high probability during freezing because of the width of the Ih funnel (Doye, 2004) with respect to the funnels leading to either close-packed or Dh structures. This is a kinetic trapping effect, which is stronger

at fast cooling rates. This tendency agrees with the results on Ag freezing by Baletto *et al.* (2002c).

Nam *et al.* (2002) have studied the mechanism of the formation of metastable gold Ih clusters in the freezing of nanodroplets by MD simulations within the embedded atom model. Their simulations start from a liquid droplet at 1500 K, which is cooled down at a quite fast rate of 100 K/ns. Again, the majority of clusters solidify in the Ih symmetry, with the solidification starting at the cluster surface, in such a way that a well ordered close-packed surface with fivefold symmetry points is formed, while the cluster is still amorphous inside. The formation of such a surface triggers the solidification process towards the formation of icosahedra: Nam *et al.* (2002) have noticed that when ordering starts at the surface, the final result is an Ih cluster; on the contrary, if the surface does not order first, the final cluster is either Dh or fcc.

#### 4. Entropic effects and kinetic trapping in $Pt_{55}$

As a paradigmatic example, showing a peculiar interplay between entropic and kinetic trapping effects, we report the MD study of the melting of $Pt_{55}$ (Baletto, 2003), modelled by the Rosato *et al.* (1989) potential. Within this model, $Pt_{55}$ presents the competing structures of Fig. 29: the Ih, the single-rosette (Sr) and the double-rosette (Dr), which are the minimum energy, the high-$T$ minimum free-energy structure and a structure frequently found in growth simulations (Baletto, 2003) respectively. Sr and Dr are obtained by modifying the external shell of the $Ih_{55}$. In the Sr, a single vertex atom is displaced to form a hexagonal ring (the *rosette*) together with its nearest-neighbor atoms on the surface. The Dr has two rosettes at nearby vertices, and has a close resemblance with the global minimum of $Au_{55}$ found by Garzón *et al.* (1998b) and shown in Fig. 13. In the melting simulations (see Fig. 30), the Sr becomes the most favorable structure for $600 < T < 700$ K. In this range, the cluster still oscillates among Ih, Sr and Dr structures. Finally, it melts above 750 $K$. This is due to entropic effects. In fact, calculations within the harmonic approximation (see Section IV.A.1) show that the probability of finding the Sr becomes considerable above 600 $K$, while the probability of the Dr remains always much smaller. Constant-$T$ simulations on long time scales (several $\mu$s) of the evolution of $Pt_{55}$ above 600 K confirm this scenario, showing also that the harmonic approximation is qualitatively right in predicting that the Sr is more probable than the Dr, but it is quantitatively poor because it underestimates both the probability of the Sr and of the Dr with respect to the probability of the Ih, see Fig.31. Another entropy-driven effect concerns Dh structures. Even though some Dh structures are lower in energy than the Sr and the Dr, we find that the entropic contribution favors Sr and Dr over Dh structures already at low temperatures.

The freezing simulations in Fig. 30 show an interplay of kinetic and entropic effects. The cluster starts to solidify at $T \simeq 700$ K, a temperature range in which the Sr is the most probable structure. Then the cluster is likely to remain kinetically trapped in this structure down to low temperatures.

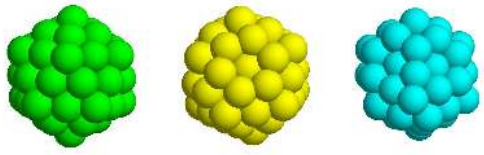


FIG. 29 Platinum cluster structures at $N = 55$. From left to right icosahedron (Ih), single rosette (Sr), and double rosette (Dr). The Ih is the lowest in energy, the Sr and the Dr are respectively 0.48 and 0.42 eV higher in energy.

#### 5. Copper, nickel and lead clusters

Valkealahti and Manninen (1997) performed a systematic MD study of the freezing of Cu nanodroplets within the Effective Medium model. They varied $r_c$ in the range 1000-10 K/ns, thus considering also rates which are rather close to the experimental ones, and analyzed

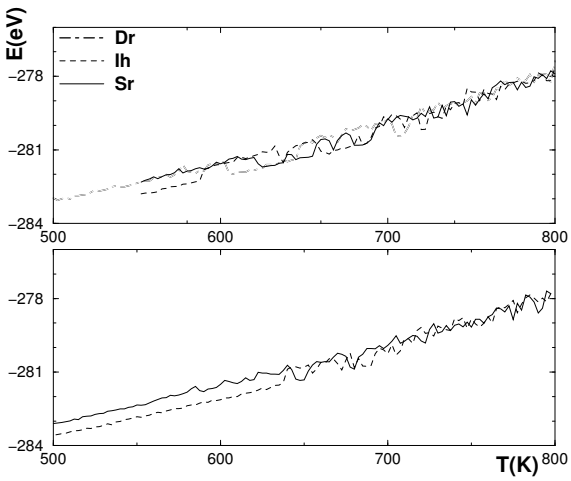


FIG. 30 Melting and freezing MD simulations of $Pt_{55}$ clusters. In the upper panel we report the melting caloric curves for for three structures: Ih (dashed line), Sr (solid line), and Dr (dash-dotted line). For $600 < T < 700$ K, all melting curves exhibit several oscillations among the three structures. In the lower panel we report two freezing curves. The dashed line ends with an Ih structure, while the solid line ends with a Sr structure. This is an example of interplay of entropic and kinetic effects. Due to entropic effects, the Sr structure is the most likely in the temperature range in which the cluster begins to solidify. Then this structure may be preserved down to low temperatures by a trapping effect.

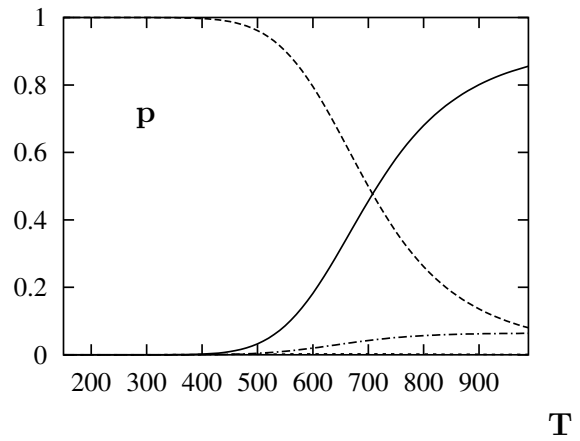


FIG. 31 Probabilities of the different structures of $Pt_{55}$ vs. $T$ in the harmonic superposition approximation. The full line is the probability of the Sr, the dashed line of the Ih, the dash-dotted line of the Dr and the dotted line (which coincides with the T axis on this scale) of the Dh structures. The latter have always a very small probability even if they are energetically favored with respect to the Sr, which is the best structure from the entropic point of view and becomes the most likely at high $T$.

a wide range of sizes up to about 4000 atoms. In their simulations, the clusters solidified as icosahedra at small Ih magic numbers (up to $N = 147$); small clusters with other sizes and large clusters can solidify as twinned fcc structures. No evidence of unfaulted TO or Dh clusters was found. The fact that Ih clusters are dominant at small sizes but not at larger ones is in agreement with the experimental findings of Reinhard *et al.* (1997a) who found however some evidence in favor of intermediate-size Dh clusters.

Qi *et al.* (2001) have studied the freezing of several Ni clusters at sizes from 336 to 8007 atoms by MD simulations within the embedded atom potential. In their simulations, they performed heating and cooling cycles at very fast rates (4000 K/ns): starting from a solid cluster they increase $T$ to melt the structure, and finally they cool down again. As a result, they found Ih clusters after freezing for $N < 500$, and fcc clusters for larger sizes. All these studies confirm the tendency to form icosahedral clusters only after freezing small liquid droplets, in agreement with the previous cases, whereas at larger sizes other structures are dominant.

The first study of the solidification of Pb clusters was made by Lim *et al.* (1994); they considered a single cluster of about 8000 atoms, obtaining an Ih after fast quenching, in disagreement with their own energetic calculations (Lim *et al.*, 1992), which gave that the CO is lower in energy than the Ih. This topic has been recently analyzed in a more systematic way by Hendy and Hall (2002), who quenched a large variety of liquid Pb droplets in the size range between 600 and 6000 atoms. In their simulations, the liquid droplet is quenched suddenly below the cluster melting point, and then equilibrated for 10 ns. Up to 4000 atoms, they found mostly icosahedra with a reconstructed surface, showing that they are lower in energy than any other known structure in the same size range. The freezing of clusters of about 6000 atoms produced faulted fcc structures. The production of Ih clusters agrees with the experimental observation of Ih particles of diameter between 3 and 6 nm by Hyslop *et al.* (2001) in inert gas aggregation experiments.

### B. Solid-state growth

Even though the liquid state growth model can be appropriate for the explanation of some kinetic effects in the growth of nanoclusters (see for instance the cases of lead and argon clusters treated in Section V.A), there are still several experimental results which cannot be explained in that way: the growth of large icosahedra in clusters of Ag and of $C_{60}$ molecules, and the growth of octahedra in Al clusters. For these systems, it turns out that the solid state growth model is much more appropriate.

In the following, we deal first with a very general mechanism for the solid-state growth of metastable icosahedra (Section V.B.1); then we treat (Section V.B.2) the MD simulation results for noble and quasi-noble metallic clusters at small sizes (Baletto *et al.*, 2001b): these simulations are run with very slow fluxes, in order to test the solid state growth model in comparison with the energetics and thermodynamics results. In Section V.B.3, results about the growth of Ag and Au clusters of intermediate and large size are reported. Finally Sections V.B.4 and V.B.5 are devoted to the growth of aluminum and $C_{60}$ clusters respectively.

#### 1. Universal mechanism of the solid-state growth of large icosahedra

Before focusing on specific systems, we treat a very general mechanism which we believe to be responsible for the observation of large metastable icosahedra in several systems (see Ag, Au and $C_{60}$ below). This mechanism consists of two steps. The first step is the solid-solid transformation of a Dh into an Ih, the second step is the shell by shell growth of the Ih to reach large sizes. This is a very peculiar example of structural transformation, because it has a clear kinetic origin, occurs only through solid states, and does not depend on the inter-particle potential, but is essentially due to geometric reasons. First of all, we note that this transformation is possible because a Dh is a fragment of a larger Ih, so that by proper addition of atoms, a Dh can grow towards an Ih. However, this is only a possibility, and a further ingredient is necessary to render this transformation kinetically favorable. This key ingredient is the fact that on the (111)-like facets of a Dh there is a larger number of stable adsorption sites of hcp stacking than of fcc stacking (Baletto

and Ferrando, 2001).

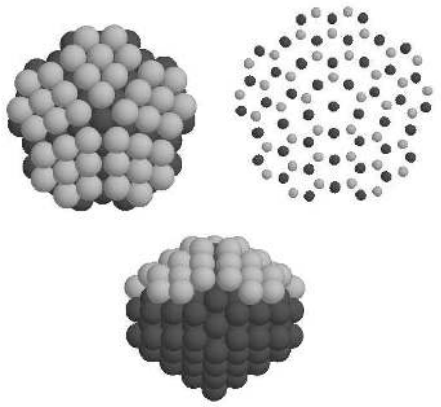

FIG. 32 A $Dh_{146}$ plus an hcp island above a cap. The black dots indicate fcc adsorption sites, the grey dots the hcp sites. The fcc sites on the edges between facets are not stable for single adatoms. Compared to adsorption on Ih clusters, the fcc and hcp sites correspond to Mackay and anti-Mackay sites respectively.

Islands of fcc stacking preserve the decahedral rearrangement in columns, around the fivefold symmetry axis, while hcp islands break the decahedral symmetry (see Fig. figsiti) and can lead to the transformation towards a larger Ih. A Dh plus a hcp island is a part of larger Ih. The displacement of a hcp island to the fcc stacking costs a considerable amount of energy, which increases with the stickiness of the potential. While the growth of islands of fcc stacking leads simply to a larger Dh (this is the umbrella growth model (Martin *et al.*, 1991b)), the nucleation of hcp islands can be the starting point for transforming a Dh into a larger Ih. The island can be either one- or two-layer thick, leading to transformations to icosahedra of different sizes, through different rearrangement pathways (Baletto *et al.*, 2001a). The size at which a solid-state Dh → Ih transformation can take place depends strongly on temperature. A larger starting Dh requires a higher temperature.

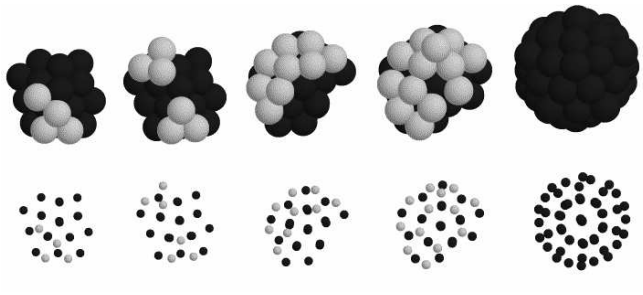

FIG. 33 The solid-state Dh → Ih transformation obtained in growth simulation of clusters of $C_{60}$ molecules (after Baletto (2003)). The same kind of transformation is found also in simulations of Ag cluster growth. Ag and $C_{60}$ present completely different interactions, soft and sticky respectively.

While a growing Dh can transform into an Ih, there is no natural growth sequence from Ih to Dh structures, because an Ih is not a fragment of a larger Dh. To transform a growing Ih into a Dh, a complete rearrangement of the cluster is necessary. This rearrangement becomes likely only at high temperatures, close to the melting point, as proved by the experiments of Koga *et al.* (2004). Therefore we can well understand that it is rather common to find wide temperature ranges in which kinetic trapping into Ih structures dominates the growth sequence. The solid-state Dh → Ih transformation thus allows to explain several experimental results: from small decahedra, larger icosahedra are grown, which can then grow further in a shell by shell mode preserving their symmetry.

The above considerations lead to a general observation about the possibility of building up non-crystalline (especially icosahedral) structures in nanoclusters. In fact, even though a sticky potential disfavors these structures, at the same time it enhances kinetic trapping effects, because diffusion barriers are high and rearrangements involving many particles become very difficult (Baletto *et al.*, 2003a; Wales, 1994b). These kinetic effects very likely lead to the growth of icosahedra.

### 2. Growth of small noble and transition metal clusters

Here we analyze the simulations of the growth of small Cu, Ag, Au, Ni, Pd and Pt clusters modelled by the Rosato *et al.* (1989) potential, in order to single out qualitative differences in the behavior of these elements. To this purpose, we report in Fig. 34 the quantity $\Delta$ (Eq. (5)) as a function of the cluster size for growth simulations at different temperatures, depending on the metals, with fixed $\tau_{dep} = 98$ ns. In this case, $\Delta$ is defined putting in Eq. (5) the temperature-dependent total energy $E$ of the cluster, averaged at each size over several snapshots, instead of the zero-temperature binding energy $E_b$. Stable structures are singled out by minima in $\Delta$. Finally we focus on the growth of Ag and Cu clusters at $N = 38$, to show that in this case kinetic trapping effects are overwhelming. In fact, the global-minimum structure, which is a TO according to this energetic model, is grown with a non-negligible probability only in a narrow temperature range for a given flux.

Growth sequences for Cu and Ni clusters are clearly dominated by icosahedral or polyicosahedral structures, as seen in Fig. 34. The magic sizes are 13, 19, 25, 40, 43, 46, 49 and 55, with 13, 19 and 55 being of special stability. The sequences are well reproducible in a wide range of growth temperatures. The main difference between Ni and Cu is that in Ni it is easier to obtain also the $TO_{38}$, even at relatively low temperatures (400 K). In this case, growth continues with the cluster trapped in non-Ih structures. Growth sequences for Ag show the same kind of structures, but they are reproducible in a narrower temperature range. On the contrary, the growth sequences of Au reveal complete different magic

sizes. Ih structures are completely unfavorable. The minima at $N = 13$ and 19 are absent, and substituted by peaks at $N = 16$ and 22. At $N = 30$ we find a decahedral minimum, which survives up to $T \sim 300$ K. At higher temperatures the clusters oscillate among different structures on a time scale shorter than $\tau_{dep}$ so that they can be considered either melted or quasi-melted. There is no evidence of entropic effects favoring the transition to Ih structures. Finally, Pt and Pd show an intermediate behavior between Cu, Ni and Ag on one side, and Au on the other. For Pd, there is a minimum at $N = 13$, but there is no evidence of any other magic size up to the $Ih_{55}$, which is likely to be grown. In Pt, minima are found at $N = 13$ (as in Cu) and 22 (as in Au). At high $T$, it is possible to grow the $TO_{38}$. Very interesting behavior takes place around for $Pt_{55}$, as anticipated in Section V.A.4, with the probable growth of rosette structures, either because of kinetic trapping in incomplete Ih structures formed at lower sizes, or because of the onset of entropic effects at high temperatures.

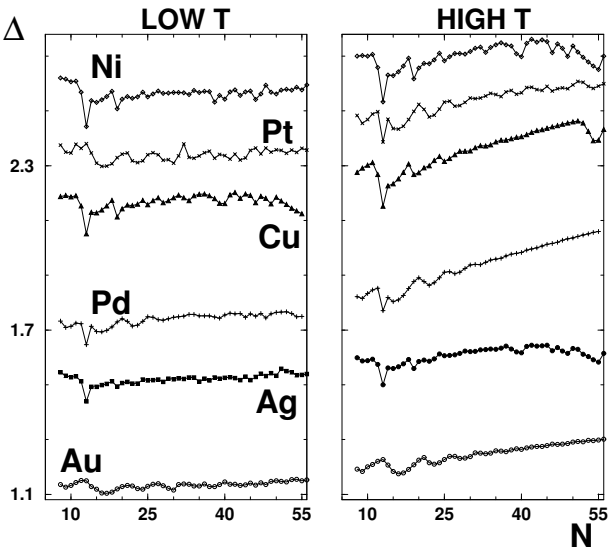


FIG. 34 Growth simulations of small metallic clusters. Δ as a function of cluster size at different temperatures: low temperatures (200 K for Au and Ag, 300 K for Ni and Pt, 400 K for Cu and Pd) on the left and high temperatures (400 K for Au and Ag, 600 K for Ni, 700 K for Pd, Pt, and Cu). Minima in Δ single out the most stable structures.

*a. Growth of $Ag_{38}$ and $Cu_{38}$* A complex interplay of thermodynamic and kinetic effects takes place in the growth simulations of $Ag_{38}$ and $Cu_{38}$ (Baletto *et al.*, 2004). At this size, the global minimum is a TO, which is in competition with a series of defected Dh structures (mostly based on there the Dh of 23 atoms covered by islands), and in the case of Ag, with a low-symmetry structure which is neither a defected Dh nor a close-packed cluster. In the case of copper, these Dh structures become more favorable than the TO at temperatures around 350 K, because of entropic effects. Moreover, for sizes just below $N = 38$, the global minima are defected decahedra in both Ag and Cu. For these reasons, the TO is not likely to be grown in the simulations. Performing several simulations at T = 200, 250, 300, 350 and 400 K, and observing the structures grown at $N = 38$, one obtains the results reported in Figs. 35 and 36. At 200 - 250 K, kinetic trapping into Dh structures is the fate of essentially all simulations, so that the magic structure never coincides with the global minimum, which is also the free-energy minimum in this temperature range. This kinetic trapping is due to the fact that the global minima in the range 30-37 atoms are decahedral (with the single exception of $Cu_{37}$). In the interval 300 - 350 K, kinetic trapping becomes less effective, even if it is still somewhat present. In this range, the TO structures are still quite likely at equilibrium, and they are indeed observed, together with Dh and low-symmetry structures (the latter in Ag only). Above 350 K, again Dh structures prevail in $Cu_{38}$, as at low temperature. However, this is not due to kinetic trapping, but to an entropic effect, because at these temperatures Dh structures are the most likely at equilibrium.

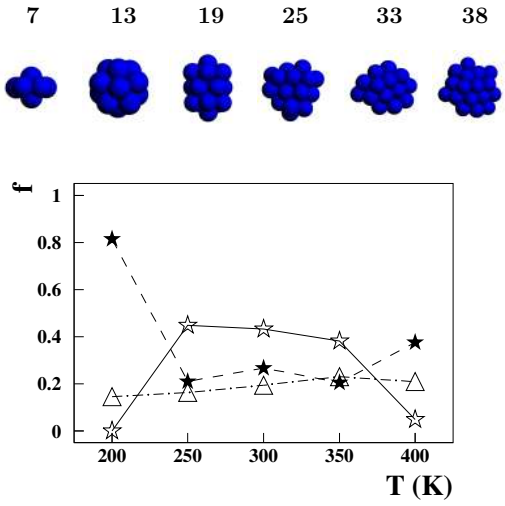


FIG. 35 $Ag_{38}$ growth simulation results. In the top row, snapshots from a simulation at $T = 200$ K are reported at different sizes. The structures of the snapshots pertain to the global minima up to $N = 33$; then growth is kinetically trapped into defected Dh structures, which are neither energetically nor entropically favorable. The graph reports the structural frequencies $f_{TO}, f_{Dh}, f_{LS}$ of the TO, Dh, and low-symmetry structures (open stars, full stars and triangles respectively), at $N = 38$ and at different growth temperatures. The lines are only guides to the eyes. At low temperatures, strong kinetic trapping into Dh structures occurs. This is followed by and intermediate temperature regime where the three structural motifs are essentially equally likely. At high temperatures, entropic effects favor Dh and low-symmetry structures at expense of the TO.

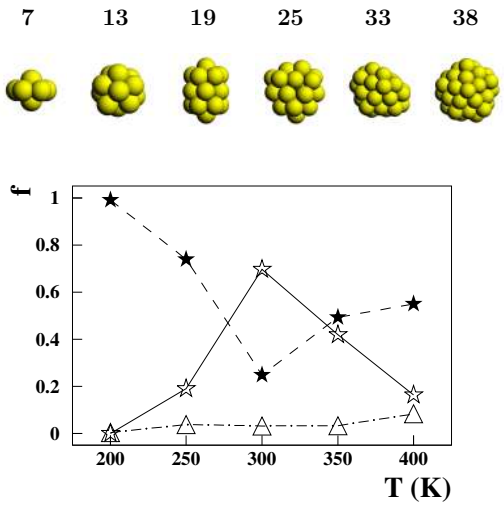


FIG. 36 $Cu_{38}$ growth simulation results. Symbols as in Fig. 35. In the top row, snapshots from a Cu simulation at $T = 400$ K are reported. Again, the snapshots reproduce the global minima up to $N = 33$. On the contrary, the growth structure at $N = 38$ is not the global minimum but a Dh, which is entropically favored at this temperature. Around 200 K, there is a strong kinetic trapping into Dh structures formed at smaller sizes. At intermediate temperatures the TO structure is preferentially grown; at high $T$, Dh structures again prevail due to entropic effects.

### 3. Growth of intermediate- and large-size Ag and Au clusters.

The experiments of production of Ag clusters in inert gas aggregation sources (Reinhard *et al.*, 1997b) show that the abundances of small clusters (2 nm of diameter) are not dominated by Ih structures, while icosahedra are the most abundant structures for much larger sizes. Here we discuss how these results can be explained in the framework of a solid-state growth model (Baletto *et al.*, 2000b, 2001a).

Let us consider first the sizes around 150 atoms, that is diameters of about 2 nm. In this range, the MD growth simulations show that a *reentrant morphology transition* takes place. This means that, at a give deposition flux, there is an intermediate temperature window (400 - 500 K for fluxes of experimental interest) in which Dh structures are preferentially grown, while at low and high temperatures icosahedra are obtained.

In fact, at intermediate temperatures, Ag clusters are able to optimize their shape up to $N \sim 100$ (the best structure is the (2,3,2) Dh at 101 atoms) and then remain trapped in Dh structures. This leads to the formation of a metastable Dh around $N = 150$ [the (3,2,2) Dh at 146 atoms is the best Dh cluster in this range] instead of the lower-energy Ih related to the $Ih_{147}$. At higher temperatures ($T > 550$ K), the clusters are liquid up to $N \simeq 130$, and the final outcome at $N \simeq 150$ are icosahedra. Finally, at low temperatures ($T < 450K$), the cluster has sufficient kinetic energy to optimize its shape only up to 75 atoms. Then it remains trapped in this structure and evolves towards the (6,1,1) Dh at $N = 100$. When the latter Dh is almost completed, the addition of further atoms causes the nucleation of hcp islands on the facets, and starts the formation of larger icosahedra. This is an example of solid-state Dh $\rightarrow$ Ih transformation (Baletto and Ferrando, 2001)). Typical simulation results are summarized by the snapshots reported in Fig. 37.

The metastable decahedra at $N \simeq 150$ can have very long lifetimes. Baletto *et al.* (2000b) calculated the lifetime $\tau_{Dh}$ of the (3,2,2) Dh in the range $550 \leq T \leq 650$ K, finding an activated behavior of the kind $\tau_{Dh} = \tau^0_{Dh} \exp[\Delta E/(k_B T)]$. After estimating the prefactor $\tau^0_{Dh}$ and the activation barrier $\Delta E$, they were able to extrapolate a lifetime of several milliseconds at 450 K. This should indicate that this structures is likely survive on the experimental time scale.

The reentrant morphology transition is due to kinetic trapping and not to entropic effects. In fact, on the basis of the considerations reported in Section IV.A, from Eq. (25) follows that, for $N = 147$, $p_{Dh}/p_{Ih}$ monotonically increases with $T$.

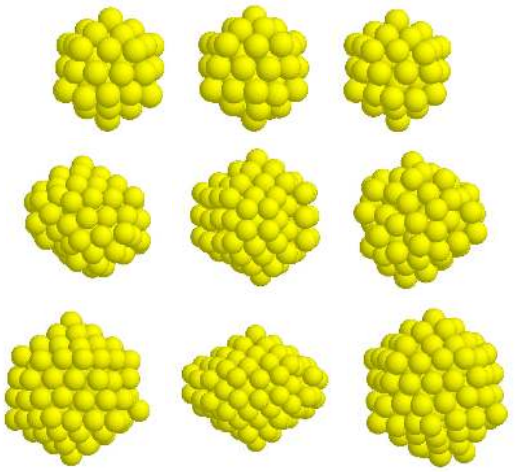

FIG. 37 Snapshots of silver cluster growth at $\tau_{dep} = 7$ ns from three simulations at three different temperatures: 400 K (left column), 500 K (middle column), 600 K (right column). In each column, the snapshots are taken at sizes of 55, 105 and 147 atoms from top to bottom. At 75 Dh are preferentially grown up to 500 K. $Ih_{147}$ structures are obtained in the simulations at 400 and 600 K and a Dh at 500 K. At 55 atoms, we obtain an Ih at 400 and 500 K (the structure at 600 K is rapidly fluctuating).

Let us now show a growth sequence leading to the formation of small decahedra and of large metastable icosahedra, in agreement with the results of the experiments by Reinhard *et al.* (1997b). This sequence is obtained for $400 < T < 500$ K and is essentially a solid-state Dh

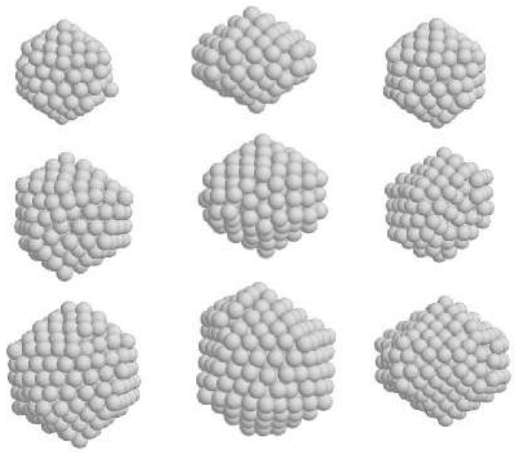

FIG. 38 Growth sequences of intermediate size Ag clusters at different $T$: from left to right, 400, 450 and 600 K. In the top row, $N \simeq 150$, in the middle row $N \simeq 200$ and in the bottom row $N \simeq 300$.

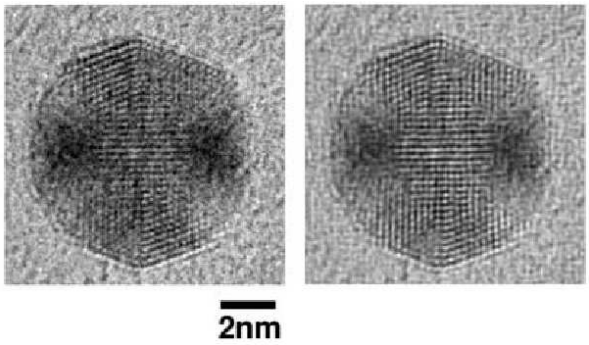


FIG. 39 High-resolution electron microscopy image of a large icosahedral Au cluster grown in an inert gas aggregation source and then deposited on a inert substrate (after Koga and Sugawara (2003)).

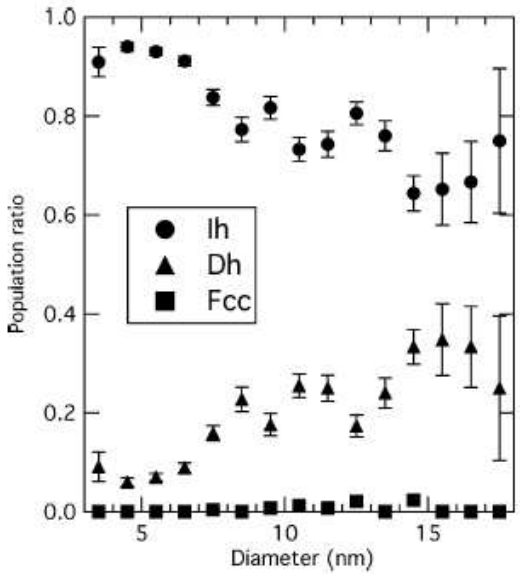


FIG. 40 Experimental population distributions of Ih, Dh and fcc Au clusters grown in a inert gas aggregation experiment (after Koga and Sugawara (2003)).

→ Ih transformation followed by a shell-by-shell trapping in Ih structures, as reported in Fig. 38. In fact, continuing the deposition on a metastable Dh of $\sim 150$ atoms, an island of hcp stacking is nucleated. This island can be either one or two layer thick, leading to the formation of the $Ih_{309}$ or the $Ih_{561}$ respectively (Baletto *et al.*, 2001a). For $T > 600$ K, Ih structures are never obtained for $N > 180$. The deposition of a few tens of atoms above the $Ih_{147}$ causes a sharp transition towards the $Dh_{192}$. This grows passing through different Dh structures, towards the $Dh_{318}$ by the nucleation of islands of fcc stacking. For $T > 650$ K, fcc structures are preferentially grown. This happens because around $N = 201$ and $N = 314$, Dh and fcc clusters are in close competition from the energetic point of view. Because of that, when temperature is high enough and the energy differences become less important, the growing cluster can pass through different faulted fcc and asymmetric Dh structures, growing finally as an fcc structure. At low temperatures, around 400 K, icosahedra are preferentially grown around $N = 150$, and these icosahedra continue growing by a shell-by-shell mode.

The growth of Au clusters has been investigated too, and there is evidence of kinetic trapping effects of the same kind as those found in Ag. In a recent experiment, Koga and Sugawara (2003) generated and analyzed a huge population of Au clusters in the range 3 - 18 nm of diameter. The clusters were produced in an inert gas aggregation source with carrier helium gas, then deposited on an amorphous carbon substrate and analyzed by high-resolution electron microscopy. Some of these clusters are reported in Figs. 2 and 39. The analysis of the cluster population revealed a striking feature: for all sizes, most of the clusters were Ih (see Fig. 40), with a proportion of about 90% at small sizes which slowly decreases to $60 - 70\%$ at large sizes. The remaining part of the clusters was mostly of Dh symmetry, while very few fcc clusters were observed. This result is in disagreement both with the energetic calculations (Baletto *et al.*, 2002b; Cleveland *et al.*, 1997) and with the experimental observation by Patil *et al.* (1993) indicating very low crossover sizes from the Ih to the other motifs. Patil *et al.* (1993) observed Au clusters after melting and very slow refreezing, and were thus very likely observing equilibrated clusters. Koga and Sugawara (2003) thus attributed the observation of large icosahedra to a kinetic trapping effect (Baletto *et al.*, 2000a, 2001a), caused by the shell by shell growth of small Ih clusters. At the moment, simulations on Au cluster growth are not available to rule out the possibility of a liquid state growth process, but the formation of such large Ih by the freezing of liquid droplets seems unlikely in the light of the results reported in Section V.A.2 and in Baletto *et al.* (2002c).

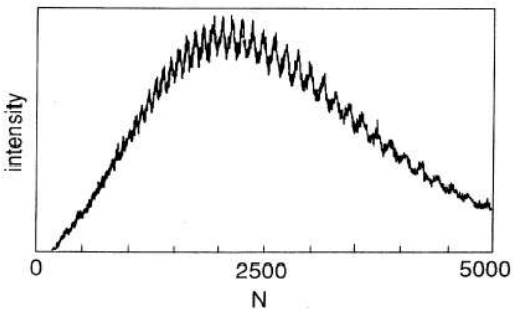


FIG. 41 Experimental mass spectrum of aluminum clusters (after Valkealahti *et al.* (1995)).

#### 4. Aluminum clusters

The formation of Al clusters was studied experimentally by different groups (Lermé *et al.*, 1992; Martin *et al.*, 1992). The mass spectra presented regular oscillations, whose maxima were equally spaced by a quantity $\delta N^{1/3}$ when the cluster abundance was plotted as a function of $N^{1/3}$ (see Fig. 41). The numerical value of the spacing turned out to be $\delta N^{1/3} \simeq 0.22$. Valkealahti *et al.* (1995) nicely explained these features as being of geometric origin within the octahedral growth model. In this model, each maximum corresponds to the addition of a single close-packed layer on one of the eight facets of the octahedron. Let us consider an octahedron with $n_1$ close-packed layers in the direction of one of its eight facets. This octahedron has $N_{oct}(n_1)$ atoms. Adding a further layer above one facet, the number of atoms becomes $N_{oct}(n_1+1)$. Valkealahti *et al.* (1995) demonstrated that

$$\delta N^{1/3} = [N_{oct}(n_1+1) - N_{oct}(n_1)]^{1/3} = \frac{1}{6}\left(\frac{3}{2}\right)^{2/3} \tag{45}$$

in very good agreement with the experiments.

In a subsequent MD study, Valkealahti and Manninen (1998) analyzed the possibility of growing octahedral clusters starting from truncated octahedra. As a first step to understanding the growth mechanism they calculated diffusion barriers for adatoms and dimers, finding very interesting mechanisms such as chain diffusion, which allows direct mass transport between two non-adjacent (111) facets through an intermediate (100) facet. Then, in their growth simulations, they took a $TO_{586}$ as starting seed, and deposited atoms one by one at constant temperature ($T = 400$ K) with a rather fast deposition rate ($\tau_{dep} = 0.5$ ns) up to a total of 201 deposited atoms. The results demonstrated the possibility of transforming a TO into an octahedron by the following mechanism. When depositing on the TO, atoms are very likely to fall on (111) facets, where they can diffuse fast. When an adatom reaches the border with a (100) facet, it can exchange easily with an edge atom, which is then trapped on the (100) facet. The reverse process (exchange from a (100) to a (111) facet) is very difficult because the adsorption energy is much more favorable on (100) than on (111) facets. The accumulation of atoms on (100) facets leads naturally to the formation of an octahedron exposing (111) facets only. This mechanism was confirmed later also in MD growth simulations of Ag and Au clusters (Baletto *et al.*, 2000a) that were performed starting from a $TO_{201}$ but with a much slower deposition rate. The growth simulations of TO clusters have revealed the formation of stacking faults (Baletto *et al.*, 2000a; Valkealahti and Manninen, 1998). Manninen *et al.* (2003); Manninen and Manninen (2002) showed that clusters with stacking faults are obtained also in the global optimization on an fcc lattice with all possible (111) stacking faults allowed, in the case of different model potentials.

#### 5. Clusters of $C_{60}$ molecules

In the case of $C_{60}$ clusters, growth takes place at the solid state. Baletto *et al.* (2002a) simulated their growth with $\tau_{dep}$ between 100-200 ns and $T < 600$ K, modelling the interactions by the Girifalco (1992) potential. Some results are shown in Fig. 42, where snapshots from typical growth simulations at different $T$ and $\tau_{dep} = 100$ ns are reported at some significant sizes. All the sequences $T < 525$ K develop along the same line and lead to the formation of a well ordered $Ih_{55}$. At $N = 13$ the structure is always icosahedral, in agreement with the global optimization results. Similarly, around $N$=25 the structure usually resembles the global minimum, although this is not necessarily the case in between these sizes. Only at very low $T$ ($< 300$ K) the structure remains trapped in the Ih shape after 13 molecules. The 25-molecule structure is decahedral but with an island on the bottom (111) faces of the cluster. This structure plays a key role, because growth is dominated by kinetic trapping effects beyond this size, since a complete solid-state Dh $\rightarrow$ Ih transformation takes place. Furthermore, the structure is a fragment of the $Ih_{55}$ and continued growth around the bottom apex of the Dh provides a pathway to this structure, with this apex ending up at the center of the resulting Ih (Baletto *et al.*, 2001a).

This growt pattern bears no resemblance to the sequence of global minima, which develops through either close-packed or Dh structures. In particular, the $(C_{60})_{38}$ global minimum is a TO, while the growth simulations always give structures with fivefold symmetries. The same happens at $N = 45$, and finally a Mackay Ih results at N=55. If the growth is continued for $N > 55$, a well-ordered anti-Mackay overlayer (Martin, 1996) develops on the surface of the Ih in agreement with the sequence of magic numbers observed experimentally for $55 < N < 100$ (Branz *et al.*, 2002, 2000). Decahedral and fcc structures are only obtained in a few cases at rather high growth temperatures (525-550 K) as found in Baletto *et al.* (2002a). If one uses the Pacheco and

Prates-Ramalho (1997) potential, the growth of non-icosahedral structures becomes more likely, but icosahedra are still obtained in most cases.

Let us discuss how these simulation results compare to the experiments by Branz *et al.* (2002, 2000) discussed in Section III.E.6. The experimental data concerning the formation of Ih clusters are easily explained by the outcome of the simulations in Baletto *et al.* (2002a): further annealing of the growth structures indicate that it is indeed quite easy to eliminate the less bound molecules from the surfaces of the clusters, thus leaving only Ih magic clusters.

On the other hand, the experimental results obtained after annealing at higher $T$ (close to 600 K) are more difficult to explain: in fact close-packed or Dh clusters were mostly observed in the experiments (Branz *et al.*, 2002, 2000). In principle, these clusters could be formed in two ways:

(i) the high-$T$ annealing allows some of the Ih clusters obtained at lower temperatures to rearrange in such a way that they are able to reach the structure with minimum free energy;

(ii) the high-$T$ annealing causes the evaporation of almost all Ih clusters, and only the few (already existing) non-icosahedral clusters, which are more stable, survive and are observed.

MD simulations of the annealing of Ih clusters of different sizes at high temperatures (650-750 K) have never produced a rearrangement of the cluster to either Dh or close-packed structures (Baletto *et al.*, 2002a). Instead, dissolution by desorption of molecules (with some local rearrangement within the structure) simply occurs. These results are consistent with mechanism (ii) but we cannot draw a firm conclusion. Some structural transformations from Ih to Dh structures have been observed in extremely long (0.1 ms) simulations by Branz *et al.* (2002); Branz (2001) at $T \sim 700$ K, where however, the number of atoms is forced to remain constant in a closed simulation box, and this forbids the cluster dissolution, which is, at this temperature, dominant. Unfortunately, at the moment it is not possible to simulate dissolution at 600 K, because the time scales involved are too long.

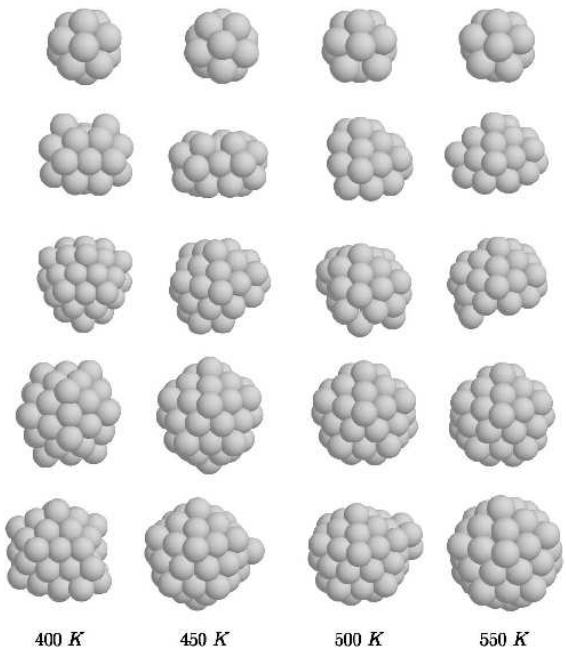


FIG. 42 Growth sequences of $C_{60}$ clusters for $\tau_{dep} = 100$ ns and different temperatures. From top to bottom snapshots at $N = 13$, 25, 38, 45 and 55 particles are shown. After Baletto *et al.* (2002a)

### C. Coalescence of nanoclusters

The coalescence of supported clusters is of great importance in the field of surface nanostructuring. This topic has been the subject of an excellent review paper by Jensen (1999). Here we intend to focus on the coalescence of free clusters intended as a mechanism which can be important for free cluster formation, especially in the late stages of the growth process, when already formed clusters can collide and join together. Some experimental evidence in favor of this mechanism may be inferred from the results by Patil *et al.* (1993), who found the formation of polycrystalline Au clusters in an inert gas aggregation source, and attributed them to the encounter and coalescence of different smaller units. However, we remark that polycrystalline clusters may result also as the outcome of the freezing of single liquid droplets (Valkealahti and Manninen, 1997).

Lewis *et al.* (1997) studied the coalescence of free Au clusters by MD simulations. They coupled the clusters to a thermostat, to keep temperature constant during the coalescence process, and therefore their results are probably better applied to supported clusters, that can exchange energy with the substrate at a fast rate. They considered the coalescence between two solid clusters, a liquid and a solid clusters and two liquid clusters. The coalescence of two liquid clusters takes place rapidly. A single spherical cluster is formed by the deformation of the two clusters in such a way as to optimize the contact surface, namely without interdiffusion. Later on, interdiffusion takes place, but the spherical shape is reached on much shorter time scales by a collective rearrangement phenomenon. The coalescence of a solid and a liquid cluster proceeds in two stages. At first the contact surface is maximized rapidly, on the same time scale as the coalescence of liquid clusters. At this stage the cluster is far from being spherical but has a faceted ovoidal shape. After that the spherical shape is reached by a slow process driven mainly by surface diffusion. The rapid changes seen at short times are due to elastic and plastic deformations; at long times the presence of facets slows down

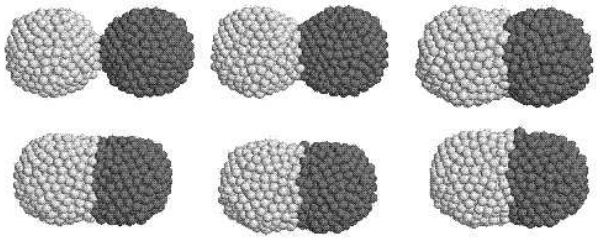

FIG. 43 MD simulation of the coalescence of two 565-atom lead icosahedra initially at 300 K. The sequence of snapshots at 3.75 ps intervals shows the early growth of the neck after the initial contact (after Hendy *et al.* (2003).

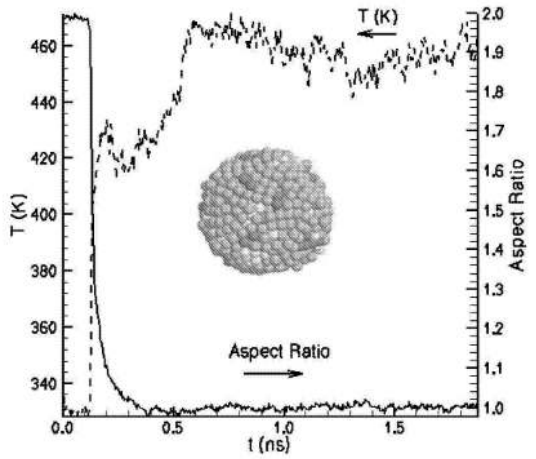


FIG. 44 Evolution of the temperature and of the aspect ratio during the MD simulation of the coalescence of two 565-atom lead icosahedra at the initial temperature of 300 K. At the point of the first contact between clusters (approximately 30 ps after the beginning of the simulation) the temperature rises sharply due to the release of surface energy. The inset shows the final cluster structure. The latter is almost spherical. The spherical shape is fastly reached, since the aspect ratio is very close to one after 1 ns. After Hendy *et al.* (2003).

the diffusion (Baletto and Ferrando, 2001), so that coalescence times are much longer (Mazzone, 2000) than predicted by the macroscopic theory of sintering (Jensen, 1999; Nichols and Mullins, 1965) via surface diffusion. Finally, the coalescence of two solid clusters (simulated also by Zhu (1996) for Cu clusters) is a complex phenomenon, which takes place on a slow time scale, and may involve either the formation of a single domain cluster or of complicated structures presenting grains. This depends on size and structure of the initial clusters, at variance with the previous cases. Moreover, the nucleation of a critical island on the surface can govern the rearrangement kinetics (Combe *et al.*, 2000).

Recently Hendy *et al.* (2003) simulated the coalescence of free lead clusters in the microcanonical ensemble, namely without coupling the clusters to a thermostat. This seems to be the most appropriate method when dealing with free clusters produced in inert gas aggregation sources. In fact, when two clusters come into contact, many new bonds form, causing a considerable release of surface energy. This can cause a noticeable temperature increase (more than 100 K for clusters of $N \simeq 500$). Since cooling rates are of less than 1 K/ns (see Eq. (44)), and the initial stage of coalescence develops in a few ns (see Fig. 43 and 44), the inert gas is not likely to affect strongly the process by taking energy away. The temperature increase makes the coalescence process much faster, by enhancing surface diffusion. Hendy *et al.* (2003) considered the coalescence of two solid surface-reconstructed Ih clusters (Hendy and Hall, 2001) of 565 atoms. They found that depending on the initial temperature and the size of the two clusters, the final aggregate may be either solid or liquid. When the final temperature $T_f$ of the resulting cluster of 1130 atoms is below $T_m$ of the $Ih_{565}$, the coalescence takes place through solid states. On the other hand, when $T_f$ is above $T_m$ of the resulting cluster of 1130 atoms, the final cluster is liquid. Finally, when $T_f$ is in between the two melting temperatures, the aggregate melt at first, and solidifies again at a later stage.

## VI. CONCLUSIONS AND PERSPECTIVES

In this review we have tried to present an overview of the physical properties of nanoclusters, with the aim of showing the interplay of energetic, thermodynamic and kinetic factors in building up the structures which are produced in the experiments or observed in the simulations. We hope that we have given a demonstration that the physics of nanoclusters can be understood only by taking into account all the three factors and relating them to the features inter-particle potential. Among these features, the potential range is always a guideline for understanding the qualitative features of structural properties and transformations. For example, we have seen that soft inter-particle interactions admit non-crystalline clusters as minimum-energy isomers. On the contrary, for sticky inter-particle potentials, crystalline structures are energetically favored but *at the same time* kinetic trapping phenomena are enhanced. The latter often cause the growth of non-crystalline structures in the actual experiments. In metallic systems, the bond order - bond length correlation plays a crucial role in destabilizing some clusters structures, such as the icosahedra, and favoring the formation of low-symmetry structures. Finally, bond directionality is crucial in semiconductor clusters and in some metals too.

Several examples have shown that the interplay of energetics, thermodynamics and kinetics is crucial, and that a satisfactory explanation of the experimental outcomes is very often impossible on the basis of energetic considerations alone. This can have deep consequences

on the very important issue of controlling the shapes of the produced nanoclusters, which is of relevant technological importance. Given that the interplay of the three factors is crucial, each one is extremely interesting by itself and poses stimulating theoretical challenges.

The development of reliable methods for modelling the energetics of nanoclusters is a rapidly developing field, both from the point of view of *ab initio* calculations, well suited for precise calculations on small systems, and from the point of view of semiempirical modelling, which is needed to treat larger systems, and to simulate long time scales. In cluster science, these approaches are complementary and are both necessary. Since the best structure of a cluster of given size and composition is generally unknown, the semiempirical modelling, which has a much lower computational cost, is the starting point for selecting the good candidates for subsequent *ab initio* local structural optimization. We have shown that there are already several examples in the literature showing that this approach is extremely fruitful, and now the challenge is to extend it to large sizes and complex systems (for example nanoalloys). The search for good structural candidates is performed by global optimization methods. The literature on these methods and their applications to clusters has exploded in the last few years; several different procedures have been proposed, with important progress towards the understanding of the requirements to build up efficient global optimization algorithms. The main point with this respect is that the most efficient algorithms work after transforming the original PES to a multidimensional staircase. Also in the field of global optimization, there is still the need to develop algorithms for complicated systems and large sizes. The latter task is however limited by the intrinsic NP-hard nature of the global optimization problem itself. Thus there is no hope in optimizing very large clusters, although good putative global minima are found by the present algorithms by exploring only a very small fraction of the incredibly huge number of local minima. The reason why these algorithms work lies in the features of the PES, which may present funnels in which optimization is fast, and in the favorable transformation of the thermodynamics of the system when working on the staircase PES.

The thermodynamics of nanoclusters is a very active research field, with several problems under debate. For example, the relation between the elementary interactions and the type of phase changes in clusters is still to be understood to a large extent for realistic model potentials. Moreover, the effect of chemical composition on melting and on structural transitions has been the subject of a very few studies. Finally, also the approach of the bulk limit is not yet well understood. Each of these problems poses complex theoretical and computational challenges.

The study of the growth kinetics of nanoclusters is a field which is just starting to develop. Here, a systematic study of small systems by the available methods is still to be performed. Moreover, new methods should be developed, first of all to extend the size of the simulated systems and the time scale of the simulations, and then to treat the formation of clusters in complex environments, such as formation in liquid solutions or on surfaces, interaction with passivating agents and adsorbed molecules, and so on.

In conclusion, we hope that our review article has given at least some ideas about the present development of the fascinating and lively subject of cluster science.

## Acknowledgments

The authors are grateful to Jonathan Doye, Alessandro Fortunelli, Ignacio Garzon, Hellmut Haberland, Roy Johnston, Andrea Levi, Christine Mottet, Arnaldo Rapallo and Giulia Rossi for their help and suggestions. The authors acknowledge financial support from the Italian MIUR under the project 2001021133.

## List of abbreviations

| | |
|---|---|
| Cuboctahedron, cuboctahedral | CO |
| Decahedron, decahedral | Dh |
| Double rosette | Dr |
| Face centered cubic | fcc |
| Hexagonal close packed | hcp |
| Icosahedron, icosahedral | Ih |
| Lennard-Jones | LJ |
| Molecular dynamics | MD |
| Monte Carlo | MC |
| Octahedron | Oh |
| Potential energy surface | PES |
| Single rosette | Sr |
| Tetrahedron, tetrahedral | $T_d$ |
| Truncated octahedron | TO |

## References

Ahlrichs, R., and S. D. Elliott, 1999, Phys. Chem. Chem. Phys. **1**, 13.

Ajayan, P. M., and L. D. Marks, 1988, Phys. Rev. Lett. **60**, 585.

Akola, J., and M. Manninen, 2001, Phys. Rev. B **63**, 193410.

Alameddin, G., J. Hunter, D. Cameron, and M. M. Kappes, 1992, Chem. Phys. Lett **192**, 122.

Ala-Nissila, T., R. Ferrando, and S. C. Ying, 2002, Adv. Phys. **51**, 949.

Alivisatos, A. P., K. P. Johnsson, X. G. Peng, T. E. Wilson, C. J. Loweth, M. P. Bruchez, and P. G. Schultz, 1996, Nature **382**, 609.

Alivisatos, A. P., 2001, Sci. Am. **285**, 66.

Alonso, J. A., 2000, Chem. Rev. **100**, 637.

Alvarez, M. M., J. T. Khoury, T. G. Schaaff, M. Shafigullin, I. Vezmar, and R. L. Whetten, 1997, Chem. Phys. Lett. **266**, 91.

Amara, P., D. Hsu, and J. E. Straub, 1993, J. Phys. Chem. **97**, 6715.

Amar, F. G., and R. S. Berry, 1986, J. Chem. Phys. **85**, 5943.

Anderson, J. B., and J. B. Fenn, 1985, Phys. Fluids **8**, 780.

Andriotis, A. N., and M. Menon, 2004, J. Chem. Phys. **120**, 230.

Aprà, E., F. Baletto, R. Ferrando, and A. Fortunelli, 2004, to be published.

Ascencio, J. A., C. Gutiérrez-Wing, M. E. Espinosa, M. Marín, S. Tehuacanero, C. Zorrilla, and M. José-Yacamán, 1998, Surf. Sci. **396**, 349.

Ascencio, J. A., M. Pérez, and M. José-Yacamán, 2000, Surf. Sci. **447**, 73.

Ashcroft, N. W., and N. D. Mermin, 1976, *Solid State Physics* (Saunders College, Orlando).

Aziz, R. A., F. R. W. McCourt, and C. C. K. Wong, 1987, Mol. Phys. **61**, 1487.

Bacelo, D. E., R. C. Binning, and Y. Ishikawa, 1999, J. Phys. Chem. A **103**, 4631.

Bachels, T., H. J. Güntherodt, and R. Schäfer, 2000, Phys. Rev. Lett. **85**, 1250.

Bachels, T., and R. Schäfer, 2000, Chem. Phys. Lett. **324**, 365.

Baguenard, B., M. Pellarin, J. Lermé, J. L. Vialle, and M. Broyer, 1994, J. Chem. Phys. **100**, 754.

Bailey, M. S., N. T. Wilson, C. Roberts, and R. L. Johnston, 2003, Eur. Phys. J. D **25**, 41.

Baletto, F., J. P. K. Doye, and R. Ferrando, 2002a, Phys. Rev. Lett. **88**, 075503.

Baletto, F., J. P. K. Doye, C. Mottet, and R. Ferrando, 2003a, Surf. Sci. .

Baletto, F., R. Ferrando, A. Fortunelli, F. Montalenti, and C. Mottet, 2002b, J. Chem. Phys. **116**, 3856.

Baletto, F., and R. Ferrando, 2001, Surf. Sci. **490**, 361.

Baletto, F., C. Mottet, and R. Ferrando, 2000a, Surf. Sci. **446**, 31.

Baletto, F., C. Mottet, and R. Ferrando, 2000b, Phys. Rev. Lett. **84**, 5544.

Baletto, F., C. Mottet, and R. Ferrando, 2001a, Phys. Rev. B **63**, 155408.

Baletto, F., C. Mottet, and R. Ferrando, 2001b, Eur. Phys. J. D **16**, 25.

Baletto, F., C. Mottet, and R. Ferrando, 2002c, Chem. Phys. Lett. **354**, 82.

Baletto, F., C. Mottet, and R. Ferrando, 2003b, Phys. Rev. Lett. **90**, 135504.

Baletto, F., A. Rapallo, G. Rossi, and R. Ferrando, 2004, phys. Rev. B, in press.

Baletto, F., 2003, *Energetics, Thermodynamics and Growth Kinetics of Nanoclusters*, Ph.D. thesis, Dip. di Fisica, Univ. di Genova.

Barranco, M., J. Navarro, and A. Poves, 1997, Phys. Rev. Lett. **78**, 4729.

Barreteau, C., M. C. Desjonquères, and D. Spanjaard, 2000a, Eur. Phys. J. D **11**, 395.

Barreteau, C., R. Guirado-López, D. Spanjaard, M. C. Desjonquères, and A. M. Oleś, 2000b, Phys. Rev. B **61**, 7781.

Bartell, L. S., 1992, J. Phys. Chem. **96**, 108.

Bauschlicher, C. W., S. R. Langhoff, and H. Partridge, 1989, J. Chem. Phys. **91**, 2412.

Bauschlicher, C. W., S. R. Langhoff, and H. Partridge, 1990, J. Chem. Phys. **93**, 8133.

Bauschlicher, C. W., S. R. Langhoff, and P. R. Taylor, 1988, J. Chem. Phys. **88**, 1041.

Bauschlicher, C. W., 1989, Chem. Phys. Lett. **156**, 91.

Bazterra, V. E., O. Oña, M. C. Caputo, M. B. Ferraro, P. Fuentealba, and J. C. Facelli, 2004, Phys. Rev. A **69**, 053202.

Becker, O. M., and M. Karplus, 1997, J. Chem. Phys. **106**, 1495.

Becke, A. D., 1988, Phys. Rev. A **38**, 3098.

Becke, A. D., 1996, J. Chem. Phys. **98**, 5648.

Beck, T. L., and R. S. Berry, 1988, J. Chem. Phys. **88**, 3910.

Berry, R. S., T. L. Beck, H. L. Davis, and J. Jellinek, 1988, in *Evolution of Size Effects in Chemical Dynamics* (John Wiley and Sons, New York), p. 75.

Berry, R. S., J. Jellinek, and G. Natanson, 1984, Phys. Rev. A **30**, 919.

Bilgram, J. H., 1987, Phys. Rep. **153**, 1.

Binns, C., 2001, Surf. Sci. Rep. **44**, 1.

Biswas, R., and D. R. Hamann, 1986, Phys. Rev. B **34**, 895.

Bixon, M., and J. Jortner, 1989, J. Chem. Phys. **91**, 1631.

Bjørnholm, S., J. Borggreen, O. Echt, K. Hansen, J. Pedersen, and H. D. Rasmussen, 1990, Phys. Rev. Lett. **65**, 1627.

Bjørnholm, S., J. Borggreen, O. Echt, K. Hansen, J. Pedersen, and H. D. Rasmussen, 1991, Z. Phys. D **19**, 47.

Blaisten-Barojas, E., I. L. Garzón, and M. Avalos-Borja, 1987, Phys. Rev. B **36**, 8447.

Blaisten-Barojas, E., and D. Levesque, 1986, Phys. Rev. B **34**, 3910.

Bobadova-Parvanova, P., K. A. Jackson, S. Srinivas, M. Horoi, C. Köhler, and G. Seifert, 2002, J. Chem. Phys. **116**, 3576.

Bonačić-Koutecký, V., J. Burda, R. Mitrić, M. Ge, G. Zampella, and P. Fantucci, 2002, J. Chem. Phys. **117**, 3120.

Bonačić-Koutecký, V., L. Cespiva, P. Fantucci, and J. Koutecký, 1993a, J. Chem. Phys. **98**, 7981.

Bonačić-Koutecký, V., L. Cespiva, P. Fantucci, J. Pittner, and J. Koutecký, 1994, J. Chem. Phys. **100**, 490.

Bonačić-Koutecký, V., P. Fantucci, C. Fuchs, C. Gatti, J. Pittner, and S. Polezzo, 1993b, Chem. Phys. Lett. **213**, 522.

Bonačić-Koutecký, V., P. Fantucci, and J. Koutecký, 1988, Phys. Rev. B **37**, 4369.

Bonačić-Koutecký, V., P. Fantucci, and J. Koutecký, 1991, Chem. Rev. **91**, 1035.

Borgia, I., B. Brunetti, I. Mariani, A. Sgamellotti, F. Cariati, P. Fermo, M. Mellini, C. Viti, and G. Padeletti, 2002, Appl. Surf. Sci. **185**, 206.

Boustani, I., W. Pewestorf, P. Fantucci, V. Bonačić-Koutecký, and J. Koutecký, 1987, Phys. Rev. B **35**, 9437.

Boyukata, M., Z. B. Güvenc, S. Ozcelik, P. Durmus, and J. Jellinek, 2001, Int. J. Quantum Chem. **84**, 208.

Brack, M., 1993, Rev. Mod. Phys. **65**, 677.

Branz, W., N. Malinowski, A. Enders, and T. P. Martin, 2002, Phys. Rev. B **66**, 094107.

Branz, W., N. Malinowski, H. Schaber, and T. P. Martin, 2000, Chem. Phys. Lett. **328**, 245.

Branz, W., 2001, Ph.D. thesis, University of Stuttgart.

Bravo-Pérez, G., I. L. Garzón, and O. Novaro, 1999a, J. Mol. Struc. (THEOCHEM) **493**, 225.

Bravo-Pérez, G., I. L. Garzón, and O. Novaro, 1999b, Chem. Phys. Lett. **313**, 655.

Breaux, G. A., R. C. Benirschke, T. Sugai, B. S. Kinnear, and M. F. Jarrold, 2003, Phys. Rev. Lett. **91**, 215508.

Briant, C. L., and J. J. Burton, 1975, J. Chem. Phys. **63**, 2045.

Brühl, R., R. Guardiola, A. Kalinin, O. Kornilov, J. Navarro,

T. Savas, and J. P. Toennies, 2004, Phys. Rev. Lett. **92**, 185301.
Buck, U., and I. Ettischer, 1994, J. Chem. Phys. **100**, 6974.
Buffat, P.-A., M. Flueli, R. Spycher, P. Stadelmann, and J.-P. Borel, 1991, Faraday Discuss. **92**, 173.
Buffat, P., and J.-P. Borel, 1976, Phys. Rev. A **13**, 2287.
Caccamo, C., D. Costa, and A. Fucile, 1997, J. Chem. Phys. **106**, 255.
Callegari, C., K. K. Lehmann, R. Schmied, and G. Scoles, 2001, J. Chem. Phys. **115**, 10090.
Calvo, F., and C. Guet, 2000, J. Chem. Phys. **113**, 1315.
Calvo, F., J. P. Neirotti, D. L. Freeman, and J. D. Doll, 2000, J. Chem. Phys. **112**, 10350.
Calvo, F., F. Spiegelman, and M.-C. Heitz, 2003, J. Chem. Phys. **118**, 8739.
Calvo, F., and F. Spiegelman, 2000, J. Chem. Phys. **112**, 2888.
Calvo, F., and F. Spiegelman, 2004, J. Chem. Phys. **120**, 9684.
Car, R., and M. Parrinello, 1985, Phys. Rev. Lett. **55**, 2471.
Castleman, A. W., and K. H. Bowen, 1996, J. Phys. Chem. **100**, 12911.
Ceperley, D. M., 1994, Rev. Mod. Phys. **67**, 279.
Chacko, S., K. Joshi, D. G. Kanhere, and S. A. Blundell, 2004, Phys. Rev. Lett. **92**, 135506.
Cheng, H.-P., R. N. Barnett, and U. Landman, 1993, Phys. Rev. B **48**, 1820.
Cheng, L., W. Cai, and X. Shao, 2004, Chem. Phys. Lett **389**, 309.
Chin, S. A., and E. Krotscheck, 1992, Phys. Rev. B **45**, 852.
Chin, S. A., and E. Krotscheck, 1995, Phys. Rev. B **52**, 10405.
Christensen, O. B., and M. L. Cohen, 1993, Phys. Rev. B **47**, 13643.
Chuang, F.-C., C. Z. Wang, S. Ögüt, J. R. Chelikowsky, and K. M. Ho, 2004, Phys. Rev. B **69**, 165408.
Chushak, Y. G., and L. S. Bartell, 2001a, J. Phys. Chem. B **105**, 11605.
Chushak, Y., and L. S. Bartell, 2001b, Eur. Phys. J. D **16**, 43.
Clemenger, K., 1985, Phys. Rev. B **32**, 1359.
Cleveland, C. L., U. Landman, T. G. Schaaff, M. N. Shafigullin, P. W. Stephens, and R. L. Whetten, 1997, Phys. Rev. Lett. **79**, 1873.
Cleveland, C. L., and U. Landman, 1991, J. Chem. Phys. **94**, 7376.
Cleveland, C. L., and U. Landman, 1994, J. Phys. Chem. **98**, 6272.
Cleveland, C. L., W. D. Luedtke, and U. Landman, 1998, Phys. Rev. Lett. **81**, 2036.
Cleveland, C. L., W. D. Luedtke, and U. Landman, 1999, Phys. Rev. B **60**, 5065.
Coleman, T., and D. Shalloway, 1994, J. Global Optim. **4**, 171.
Combe, N., P. Jensen, and A. Pimpinelli, 2000, Phys. Rev. Lett. **85**, 110.
Cottancin, E., J. Lermé, M. Gaudry, M. Pellarin, J.-L. Vialle, M. Broyer, B. Prével, M. Treilleux, and P. Mélinon, 2000, Phys. Rev. B **62**, 5179.
Cox, H., R. L. Johnston, and J. N. Murrell, 1999, , J. Solid State Chem. **145**, 517.
Dai, D., and K. Balasubramanian, 1995, J. Chem. Phys. **103**, 648.
Darby, S., T. V. Mortimer-Jones, R. L. Johnston, and C. Roberts, 2002, J. Chem. Phys. **116**, 1536.
Davis, H. L., J. Jellinek, and R. S. Berry, 1987, J. Chem. Phys. **86**, 6456.
Daw, M. S., and M. I. Baskes, 1984, Phys. Rev. B **29**, 6443.
Deaven, D. M., and K. M. Ho, 1995, Phys. Rev. Lett. **75**, 288.
Deaven, D. M., M. Tit, J. R. Morris, and K. M. Ho, 1996, Chem. Phys. Lett. **256**, 195.
Desjonqueres, M. C., and D. Spanjaard, 1998, *Concepts in Surface Physics* (Springer Verlag, Berlin).
Dietz, T. G., M. A. Duncan, D. E. Powers, and R. E. Smalley, 1981, J. Chem. Phys. **74**, 6511.
Doye, J. P. K., and F. Calvo, 2001, Phys. Rev. Lett. **86**, 3570.
Doye, J. P. K., and F. Calvo, 2002, J. Chem. Phys. **116**, 8307.
Doye, J. P. K., and F. Calvo, 2003, J. Chem. Phys. **119**, 12680.
Doye, J. P. K., A. Dullweber, and D. J. Wales, 1997, Chem. Phys. Lett. **269**, 408.
Doye, J. P. K., and S. C. Hendy, 2003, Eur. Phys. J. D **22**, 99.
Doye, J. P. K., D. J. Wales, and R. S. Berry, 1995, J. Chem. Phys. **103**, 4234.
Doye, J. P. K., D. J. Wales, W. Branz, and F. Calvo, 2001, Phys. Rev. B **64**, 235409.
Doye, J. P. K., D. J. Wales, and M. A. Miller, 1998, J. Chem. Phys. **109**, 8143.
Doye, J. P. K., and D. J. Wales, 1995, J. Chem. Phys. **112**, 9659.
Doye, J. P. K., and D. J. Wales, 1996a, Science **271**, 484.
Doye, J. P. K., and D. J. Wales, 1996b, Chem. Phys. Lett. **262**, 167.
Doye, J. P. K., and D. J. Wales, 1998a, Phys. Rev. Lett. **80**, 1357.
Doye, J. P. K., and D. J. Wales, 1998b, New J. Chem. **22**, 733.
Doye, J. P. K., and D. J. Wales, 2001, Phys. Rev. Lett. **86**, 5719.
Doye, J. P. K., 2003, J. Chem. Phys. **119**, 1136.
Doye, J. P. K., 2004, in *Global Optimization-Selected Case Studies*, edited by J. D. Pinter (Kluwer Academic Press, Dordrecht, The Netherlands).
D. Faken and H. Jónsson, 1994, Comput. Mater. Sci. **2**, 279.
Efremenko, I., and M. Sheintuck, 2000, J. Mol. Cat. A **160**, 445.
Efremenko, I., 2001, J. Mol. Cat. A **173**, 19.
Efremov, M. Y., F. Schiettekatte, M. Zhang, E. A. Olson, A. T. Kwan, R. S. Berry, and L. H. Allen, 2000, Phys. Rev. Lett. **85**, 3560.
Ehbrecht, M., and F. Huisken, 1999, Phys. Rev. B **59**, 2975.
Ehbrecht, M., B. Kohn, F. Huisken, M. A. Laguna, and V. Paillard, 1997, Phys. Rev. B **56**, 6958.
Ercolessi, F., W. Andreoni, and E. Tosatti, 1991, Phys. Rev. Lett. **66**, 911.
Ercolessi, F., M. Parrinello, and E. Tosatti, 1988, Phil. Mag. A **58**, 213.
Erkoç, S., and T. Yilmaz, 1999, Physica E **5**, 1.
Ervin, K. M., J. Ho, and W. C. Lineberger, 1988, J. Chem. Phys. **89**, 4514.
Etters, R. D., and J. Kaelberer, 1975, Phys. Rev. A **11**, 1068.
Etters, R. D., and J. Kaelberer, 1977, J. Chem. Phys. **66**, 5112.
Even, U., N. Ben-Horin, and J. Jortner, 1989, Phys. Rev. Lett. **62**, 140.
Farges, J., M.-F. de Feraudy, B. Raoult, and G. Torchet, 1981, Surf. Sci. **106**, 95.
Farges, J., M. F. de Feraudy, B. Raoult, and G. Torchet, 1983,

J. Chem. Phys. **78**, 881.
Farges, J., M. F. de Feraudy, B. Raoult, and G. Torchet, 1985, Surf. Sci. **156**, 370.
Farges, J., M. F. de Feraudy, B. Raoult, and G. Torchet, 1986, J. Chem. Phys. **84**, 3491.
Farges, J., M.-F. de Feraudy, B. Raoult, and G. Torchet, 1988, Adv. Chem. Phys. **70**, 45.
Ferreira, A. L. C., J. M. Pacheco, and J. P. Prates-Ramalho, 2000, J. Chem. Phys. **113**, 738.
Finnila, A. B., M. A. Gomez, C. Sebenik, C. Stenson, and J. D. Doll, 1994, Chem. Phys. Lett. **219**, 343.
Finnis, M. W., and J. E. Sinclair, 1984, Philos. Mag. **50**, 45.
Fortunelli, A., and E. Aprà, 2003, J. Phys. Chem. **107**, 2934.
Fortunelli, A., and A. M. Velasco, 2004, int. J. Quantum Chem., in press.
Fortunelli, A., 1999, J. Mol. Struc. (TEOCHEM) **493**, 233.
Fournier, R., S. B. Sinnott, and A. E. DePristo, 1992, J. Chem. Phys. **97**, 4149.
Fournier, R., 2001, J. Chem. Phys **115**, 2165.
Frantz, D. D., D. L. Freeman, and J. D. Doll, 1990, J. Chem. Phys. **93**.
Frantz, D. D., 1995, J. Chem. Phys. **102**.
Frantz, D. D., 2001, J. Chem. Phys. **115**.
Freeman, D. L., and J. D. Doll, 1985, J. Chem. Phys. **82**, 462.
Freeman, D. L., and J. D. Doll, 1996, Annu. Rev. Phys. Chem. **47**, 43.
Frenkel, D., and B. Smit, 1996, *Understanding Molecular Simulations* (Academic Press, San Diego).
Fthenakis, Z., A. N. Andriotis, and M. Menon, 2003, J. Chem. Phys. **119**, 10911.
Fujima, N., and T. Yamaguchi, 1989, J. Phys. Soc. Jpn. **58**, 1334.
Fuke, K., K. Tsukamoto, F. Misaizu, and M. Sanekata, 1994, J. Chem. Phys. **99**, 7807.
Ganteför, G., and W. Eberhardt, 1996, Phys. Rev. Lett. **76**, 4975.
Ganteför, G., M. Gauss, K. H. Meiwes-Broer, and H. . Lutz, 1990, J. Chem. Soc. Faraday T. **86**, 2483.
García-Rodeja, J., C. Rey, and L. J. Gallego, 1994, Phys. Rev. B **49**, 8495.
García-Rodeja, J., C. Rey, and L. J. Gallego, 1997, Phys. Rev. B **56**, 6466.
Garzón, I. L., M. R. Beltrán, G. Gonzalez, I. Gutierrez-Gonzalez, K. Michaelian, J. A. Reyes-Nava, and J. I. Rodriguez-Hernandez, 2003, Eur. Phys. J. D **24**, 105.
Garzón, I. L., and J. Jellinek, 1991, Z. Phys. D **20**, 235.
Garzón, I. L., and J. Jellinek, 1993, Z. Phys. D **26**, 316.
Garzón, I. L., I. G. Kaplan, R. Santamaria, and O. Novaro, 1998a, J. Chem. Phys. **109**, 2176.
Garzón, I. L., K. Michaelian, M. R. Beltrán, A. Posada-Amarillas, P. Ordejón, E. Artacho, D. Sánchez-Portal, and J. M. Soler, 1998b, Phys. Rev. Lett. **81**, 1600.
Garzón, I. L., K. Michaelian, M. R. Beltrán, A. Posada-Amarillas, P. Ordejón, E. Artacho, D. Sánchez-Portal, and J. M. Soler, 1999, Eur. Phys. J. D **9**, 211.
Garzón, I. L., and A. Posada-Amarillas, 1996, Phys. Rev. B **54**, 11796.
Garzón, I. L., J. A. Reyes-Nava, J. J. Rodriguez-Hernandez, I. Sigal, M. R. Beltrán, and K. Michaelian, 2002, Phys. Rev. B **66**, 073403.
Ghayal, M. R., and E. Curotto, 2000, J. Chem. Phys. **113**, 4298.
Gilb, S., P. Weis, F. Furche, R. Ahlrichs, and M. M. Kappes, 2002, J. Chem. Phys. **116**, 4094.
Girifalco, L. A., and V. G. Weizer, 1959, Phys. Rev. **687**, 114.
Girifalco, L. A., 1992, J. Phys. Chem. **96**, 858.
Grisenti, R. E., W. Schöllkopf, J. P. Toennies, G. C. Hegerfeldt, T. Köhler, and M. Stoll, 2000, Phys. Rev. Lett. **85**, 2284.
Grönbeck, H., and W. Andreoni, 2000, Chem. Phys. **262**, 1.
Grossman, J. C., and L. Mitás, 1995a, Phys. Rev. B **52**, 16735.
Grossman, J. C., and L. Mitás, 1995b, Phys. Rev. Lett. **74**, 1323.
Grygorian, V. G., and M. Springborg, 2003, Chem. Phys. Lett. **375**, 219.
Guardiola, R., and J. Navarro, 2000, Phys. Rev. Lett. **84**, 1144.
Guardiola, R., and J. Navarro, 2002, Phys. Rev. Lett. **89**, 193401.
Guardiola, R., 2000, Phys. Rev. B **62**, 3416.
Guillopé, M., and B. Legrand, 1989, Surf. Sci. **215**, 577.
Guirado-López, R., M. C. Desjonquères, and D. Spanjaard, 2000, Phys. Rev. B **62**, 13188.
Gupta, R. P., 1981, Phys. Rev. B **23**, 6265.
Güvenc, Z. B., and J. Jellinek, 1992, in *Physics and Chemistry of Finite Systems: From Clusters to Crystals*, edited by P. Jena, S. N. Khanna, and B. K. Rao (Kluwer Academic Publ., Dordrecht).
Haberland, H., 1994, in *Clusters of Atoms and Molecules*, edited by H. Haberland (Springer Verlag, Berlin), p. 374.
Haberland, H., 2002, in *Atomic Clusters and Nanoparticles: Les Houches Session LXXIII 2-28 July 2000* (Springer Verlag, Berlin).
Häberlen, O. D., S.-C. Chung, M. Stener, and N. Rösch, 1996, J. Chem. Phys. **106**, 5189.
Hagen, M. H. J., E. J. Meijer, G. C. A. M. Mooij, D. Frenkel, and H. N. W. Lekkerkerker, 1993, Nature **365**, 425.
Häkkinen, H., and U. Landman, 2000, Phys. Rev. B **62**, R2287.
Häkkinen, H., M. Moseler, and U. Landman, 2002, Phys. Rev. Lett. **89**, 033401.
Hall, B. D., M. Flüeli, R. Monot, and J.-P. Borel, 1991, Phys. Rev. B **43**, 3906.
Hanszen, K. J., 1960, Z. Phys. **157**, 523.
Harris, I. A., R. S. Kidwell, and J. A. Northby, 1984, Phys. Rev. Lett. **53**, 2390.
Hartke, B., 1993, J. Phys. Chem. **97**, 9973.
Hartke, B., 1999, J. Comput. Chem. **20**, 1752.
Hartke, B., 2000, Z. Phys. Chem. **214**, 1251.
Hartke, B., 2002, Angew. Chem. Int. Ed. **41**, 1468.
Hartke, B., 2003, Phys. Chem. Chem. Phys. **5**, 275.
de Heer, W. A., 1993, Rev. Mod. Phys. **65**, 611.
Hendy, S. C., and B. D. Hall, 2001, Phys. Rev. B **64**, 85425.
Hendy, S. C., and B. D. Hall, 2002, Phys. Rev. B **64**, 085425.
Hendy, S., S. A. Brown, and B. D. Hall, 2003, Phys. Rev. B **68**, 241403.
Henry, C. R., 1998, Surf. Sci. Rep. **31**, 235.
Hill, T. L., 1964, *Thermodyanmics of small systems*, volume parts I and II (W. A. Benjamin, INC., Amsterdam).
Hoare, M. R., and J. McInnes, 1976, J. Chem. Soc. Faraday Discuss. **61**, 12.
Hoare, M. R., and P. Pal, 1975, Adv. Phys. **24**, 645.
Hohenberg, P., and W. Kohn, 1964, Phys. Rev. **136**, B864.
Honeycutt, J. D., and H. C. Andersen, 1987, J. Phys, Chem. **91**, 4950.
Hovick, J. W., and L. S. Bartell, 1997, J. Mol. Struc. **413**, 615.

Ho, J., K. M. Ervin, and W. C. Lineberger, 1990, J. Chem. Phys. **93**, 6987.
Ho, J., K. M. Ervin, M. L. Polak, M. K. Gilles, and W. C. Lineberger, 1991, J. Chem. Phys. **95**, 4845.
Ho, K. M., A. A. Shvartsburg, B. G. Pan, Z. Y. Lu, C. Z. Wang, J. G. Wacker, J. L. Fye, and M. F. Jarrold, 1998, Nature **392**, 582.
Huang, S. P., and P. B. Balbuena, 2002, J. Phys. Chem. B **106**, 7225.
Hudgins, R. R., M. Imai, M. F. Jarrold, and P. Dugourd, 1999, J. Chem. Phys. **111**, 7865.
Hyslop, M., A. Wurl, S. A. Brown, B. D. Hall, and R. Monot, 2001, Eur. Phys. J. D **16**, 233.
Ikeshoji, T., B. Hafskjold, Y. Hashi, and Y. Kawazoe, 1996, Phys. Rev. Lett. **76**, 1792.
Ikeshoji, T., G. Torchet, M.-F. de Feraudy, and K. Koga, 2001, Phys. Rev. E **63**, 031101.
Imry, Y., 1980, Phys. Rev. B **21**, 2042.
Ino, S., 1969, J. Phys. Soc. Jpn. **27**, 941.
Ishikawa, Y., Y. Sugita, T. Nishikawa, and Y. Okamoto, 2001, Phys. Lett. A **333**, 199.
Jackschath, C., I. Rabin, and W. Schulze, 1992, Z. Phys. D **22**, 517.
Jacobsen, K. W., J. K. Nørskov, and M. J. Puska, 1987, Phys. Rev. B **35**, 7423.
Jarrold, M. F., and J. E. Bower, 1992, J. Chem. Phys. **96**, 9180.
Jarrold, M. F., and V. A. Constant, 1991, Phys. Rev. Lett. **67**, 2994.
Jarrold, M. F., and E. C. Honea, 1991, J. Phys. Chem. **95**, 9181.
Jellinek, J., T. L. Beck, and R. S. Berry, 1986, J. Chem. Phys. **84**, 2783.
Jellinek, J., V. Bonacić-Koutecký, P. Fantucci, and M. Wiechert, 1994, J. Chem. Phys. **101**, 10092.
Jellinek, J., and I. L. Garzón, 1991, Z. Phys. D **20**, 239.
Jellinek, J., 1999, *Theory of Atomic and Molecular Clusters* (Springer Verlag, Berlin).
Jennison, D. R., P. A. Schultz, and M. P. Sears, 1997, J. Chem. Phys. **106**, 1856.
Jensen, P., 1999, Rev. Mod. Phys. **71**, 1695.
Johnston, R. L., 2002, *Atomic and Molecular Clusters* (Taylor and Francis, London).
Johnston, R. L., 2003, Dalton Trans. , 4193.
Jones, R. O., and G. Seifert, 1992, J. Chem. Phys. **96**, 7564.
Jones, R. O., 1991, Phys. Rev. Lett. **67**, 224.
Jones, R. O., 1993, J. Chem. Phys. **99**, 1194.
Jortner, J., 1992, Z. Phys. D **24**, 247.
Jortner, J., 2003, J. Chem. Phys. **119**, 11335.
José-Yacamán, M., J. A. Ascencio, H. B. Liu, and J. Gardea-Torresdey, 2001a, J. Vac. Sci. Tech. B **19**, 1091.
José-Yacamán, M., M. Marín-Almazo, and J. A. Ascencio, 2001b, J. Mol. Cat. A **173**, 61.
Joshi, K., D. G. Kanhere, and S. A. Blundell, 2002, Phys. Rev. B **66**, 155329.
Joshi, K., D. G. Kanhere, and S. A. Blundell, 2003, Phys. Rev. B **67**, 235413.
Jug, K., B. Zimmermann, P. Calaminici, and A. M. Köster, 2002a, J. Chem. Phys. **116**, 4497.
Jug, K., B. Zimmermann, and A. M. Köster, 2002b, Int. J. Quantum Chemistry **90**, 594.
Kallinteris, G. C., N. I. Papanicolaou, G. A. Evangelakis, and D. A. Papaconstantopoulos, 1997, Phys. Rev. B **55**, 2150.
Kaxiras, E., and K. Jackson, 1993a, Phys. Rev. Lett. **71**, 727.
Kaxiras, E., and K. Jackson, 1993b, Z. Phys. D **26**, 346.
Kirkpatrick, S., C. D. Gelatt, and M. P. Vecchi, 1983, Science **220**, 671.
Knight, W. D., K. Clemenger, W. A. de Heer, W. A. Saunders, M. Y. Chou, and M. L. Cohen, 1984, Phys. Rev. Lett. **52**, 2141.
Kofman, R., P. Cheyssac, A. Aouaj, Y. Lereah, G. Deutscher, T. Ben-David, J. M. Penisson, and A. Bourret, 1994, Surf. Sci. **303**, 231.
Koga, K., T. Ikeshoji, and K. Sugawara, 2004, Phys. Rev. Lett. **92**, 115507.
Koga, K., and K. Sugawara, 2003, Surf. Sci. **529**, 23.
Kohn, W., and L. J. Sham, 1965, Phys. Rev. **140**, A1133.
Krivov, S. V., 2002, Phys. Rev. E **66**, 025701.
Krüger, S., S. Vent, F. Nörtemann, M. Staufer, and N. Rösch, 2001, J. Chem. Phys. **115**, 2082.
Kumar, V., and R. Car, 1991, Phys. Rev. B **44**, 8243.
Kumar, V., and Y. Kawazoe, 2002, Phys. Rev. B **66**, 144413.
Kusche, R., T. Hippler, M. Schmidt, B. von Issendorff, and H. Haberland, 1999, Eur. Phys. J. D **9**, 1.
Labastie, P., and R. L. Whetten, 1990, Phys. Rev. Lett. **65**, 1567.
Lai, S. K., P. J. Hsu, K. L. Wu, W. K. Liu, and M. Iwamatsu, 2002, J. Chem. Phys **117**, 10715.
Lai, S. L., J. Y. Guo, V. Petrova, G. Ramanath, and L. H. Allen, 1996, Phys. Rev. Lett. **77**, 99.
Lathiotakis, N. N., A. N. Andriotis, M. Menon, and J. Connolly, 1996, J. Chem. Phys. **104**, 992.
Leary, R. H., and J. P. K. Doye, 1999, Phys. Rev. E **60**, R6320.
Ledoux, G., O. Guillois, D. Porterat, C. Reynaud, F. Huisken, B. Kohn, and V. Paillard, 2000, Phys. Rev. B **62**, 15942.
Lee, J. K., J. A. Barker, and F. F. Abraham, 1973, J. Chem. Phys. **58**, 3166.
Lee, J., I.-H. Lee, and J. Lee, 2003, Phys. Rev. Lett **91**, 080201.
Lee, Y. H., and B. J. Berne, 2000, J. Phys. Chem. A **104**, 86.
Lee, Y. J., R. M. Nieminen, E.-K. Lee, and S. Kim, 2001, Comput. Phys. Commun. **142**, 201.
Lermé, J., M. Pellarin, J. L. Vialle, B. Baguenard, and M. Broyer, 1992, Phys. Rev. Lett. **68**, 2818.
Levi, A. C., and R. Mazzarello, 2001, J. Low Temp. Phys. **122**, 75.
Lewerenz, M., 1996, J. Chem. Phys. **106**, 4596.
Lewis, L. J., P. Jensen, and J.-L. Barrat, 1997, Phys. Rev. B **56**, 2248.
Lim, H. S., C. K. Ong, and F. Ercolessi, 1992, Surf. Sci. **270**, 1109.
Lim, H. S., C. K. Ong, and F. Ercolessi, 1994, Comput. Mater. Sci. **2**, 495.
Liu, H. B., J. A. Ascencio, M. Pérez-Alvarez, and M. José-Yacamán, 2001, Surf. Sci. **491**, 88.
Liu, H. B., R. Perez, G. Canizal, and J. A. Ascencio, 2002, Surf. Sci. **518**, 14.
Liu, P., and B. J. Berne, 2003, J. Chem. Phys. **118**, 2999.
Li, B. X., P. L. Cao, and M. Jiang, 2000a, Phys. Status Solidi B **218**, 399.
Li, B. X., M. Qiu, and P. L. Cao, 1999, Phys. Lett. A **256**, 386.
Li, J., X. Li, H.-J. Zhai, and L.-S. Wang, 2003, Science **299**, 864.
Li, T. X., Y. J. Ji, S. W. Yu, and G. H. Wang, 2000b, Solid St. Comm. **116**, 547.
Li, T. X., S. M. Lee, S. J. Han, and G. H. Wang, 2002, Phys.

Lett. A **300**, 86.
Li, T. X., S. Y. Yin, Y. L. Ji, B. L. Wang, G. H. Wang, and J. J. Zhao, 2000c, Phys. Lett. A **267**, 403.
Li, Y., E. Blaisten-Barojas, and D. A. Papaconstantopoulos, 1998, Phys. Rev. B **57**, 15519.
Li, Z., and H. A. Scheraga, 1987, P. Natl. Acad. Sci. **84**, 6611.
Lloyd, L. D., R. L. Johnston, S. Sahli, and N. T. Wilson, 2004, J. Mater. Chem. , 1691.
Locatelli, M., and F. Schoen, 2003, Comput. Optim. Appl. **26**, 173.
López, M. J., and J. Jellinek, 1999, J. Chem. Phys. **110**, 8899.
Lowen, H., 1994, Phys. Rep. **237**, 249.
Luo, F., G. C. McBane, G. Kim, G. F. Giese, and W. R. Gentry, 1993, J. Chem. Phys. **98**, 3564.
Luo, J., U. Landman, and J. Jortner, 1987, in *Physics and Chemical of Small Clusters*, edited by Plenum (P. Jena and B. K. Rao and S. N. Khanna, New York), p. 201.
Lynden-Bell, R. M., and D. J. Wales, 1994, J. Chem. Phys. **101**, 1460.
Mackay, A. L., 1962, Acta Crystallogr. **15**, 916.
Manninen, K., J. Akola, and M. Manninen, 2003, Phys. Rev. B **68**, 235412.
Manninen, K., and M. Manninen, 2002, Eur. Phys. J. D **20**, 243.
Maranas, C. D., and C. A. Floudas, 1992, J. Chem. Phys. **97**, 7667.
Marks, L. D., 1984, Philos. Mag. A **49**, 81.
Marks, L. D., 1994, Rep. Prog. Phys. **57**, 603.
Martin, T. P., T. Bergmann, H. Gohlich, and T. Lange, 1991a, Z. Phys. D **19**, 25.
Martin, T. P., T. Bergmann, H. Gohlich, and T. Lange, 1991b, J. Phys. Chem. **95**, 6421.
Martin, T. P., U. Näher, H. Schaber, and U. Zimmermann, 1993, Phys. Rev. Lett. **70**, 3079.
Martin, T. P., U. Näher, H. Schaber, and U. Zimmermann, 1994, J. Chem. Phys. **100**, 2322.
Martin, T. P., U. Näher, and H. Schaber, 1992, Chem. Phys. Lett. **199**, 470.
Martin, T. P., 1996, Phys. Rep. **273**, 199.
Martin, T. P., 2000, Solid State Ionics **131**, 3.
Massen, C., T. V. Mortimer-Jones, and R. L. Johnston, 2002, J. Chem. Soc. Dalton **23**, 4375.
Massobrio, C., A. Pasquarello, and R. Car, 1995, Chem. Phys. Lett. **238**, 215.
Matsuoka, H., T. Hirokawa, M. Matsui, and M. Doyama, 1992, Phys. Rev. Lett. **69**, 297.
Matulis, V. E., O. A. Ivashkevich, and V. S. Gurin, 2003, J. Mol. Struc. (THEOCHEM) **664-665**, 291.
Matveentsev, A., A. Lyalin, I. A. Solov'yov, A. V. Solov'yov, and W. Greiner, 2003, Int. J. Mod. Phys. E **12**, 81.
Mazzone, A. M., 2000, Philos. Mag. B **80**, 95.
Ma, J. P., and J. E. Straub, 1994, J. Chem. Phys. **101**, 533.
Mélinon, P., P. Keghelian, B. Prével, V. Dupuis, A. Perez, B. Champagnon, Y. Guyot, M. Pellarin, J. Lermé, M. Broyer, J. L. Rousset, and P. Délichere, 1998, J. Chem. Phys. **108**, 4607.
Mélinon, P., P. Keghelian, B. Prével, A. Perez, G. Guiraud, J. LeBrusq, J. Lermé, M. Pellarin, and M. Broyer, 1997, J. Chem. Phys. **107**, 10278.
Meunier, I., 2001, *PhD Thesis* (University of Aix-Marseille II).
Michaelian, K., N. Rendón, and I. L. Garzón, 1999, Phys. Rev. B **60**, 2000.
Michaelian, K., 1998, Chem. Phys. Lett. **293**, 202.
Milani, P., and S. Iannotta, 1999, *Cluster Beam Synthesis of Nanostructured Materials* (Springer Verlag, Berlin).
Mirkin, C. A., R. L. Letsinger, R. C. Mucic, and J. J. Storhoff, 1996, Nature **382**, 607.
Mitás, L., J. C. Grossman, I. Stich, and J. Tobik, 2000, Phys. Rev. Lett. **84**, 1479.
Montalenti, F., and R. Ferrando, 1999a, Phys. Rev. B **59**, 5881.
Montalenti, F., and R. Ferrando, 1999b, Phys. Rev. Lett **82**, 1498.
Morse, P. M., 1929, Phys. Rev. **34**, 57.
Moseler, M., H. Häkkinen, R. N. Barnett, and U. Landman, 2001, Phys. Rev. Lett. **86**, 2545.
Mottet, C., J. Goniakowski, F. Baletto, R. Ferrando, and G. Tréglia, 2004, Phase Transit. **77**, 101.
Mottet, C., G. Tréglia, and B. Legrand, 1997, Surf. Sci. **383**, L719.
Nalwa, H. S. (ed.), 2004, *Encyclopedia of Nanoscience and Nanotechnology* (American Scientific Publishers, New York).
Nam, H.-S., N. M. Hwang, B. D. Yu, and J.-K. Yoon, 2002, Phys. Rev. Lett. **89**, 275502.
Natanson, G., F. Amar, and R. S. Berry, 1983, J. Chem. Phys. **78**, 399.
Nautchil, V. V., and A. J. Petsin, 1980, Mol. Phys. **40**, 1341.
Nava, P., M. Sierka, and R. Ahlrichs, 2003, Phys. Chem. Chem. Phys. **5**, 3372.
Nayak, S. K., B. Reddy, B. K. Rao, S. N. Khanna, and P. Jena, 1996, Chem. Phys. Lett. **253**, 390.
Neirotti, J. P., F. Calvo, D. L. Freeman, and J. D. Doll, 2000, J. Chem. Phys. **112**, 10340.
Nelson, D. R., and F. Spaepen, 1989, Solid State Phys. **42**, 1.
Nichols, F. A., and W. W. Mullins, 1965, J. Appl. Phys. **36**, 1826.
Nishioka, H., K. Hansen, and B. R. Mottelson, 1990, Phys. Rev. B **42**, 9377.
Northby, J. A., J. Xie, D. L. Freeman, and J. D. Doll, 1989, Z. Phys. D **12**, 69.
Northby, J. A., 1987, J. Chem. Phys. **87**, 6166.
Northby, J. A., 2001, J. Chem. Phys. **115**, 10065.
Nygren, M. A., P. E. M. Siegbahn, U. Wahlgren, and H. Akeby, 1992, J. Phys. Chem. **96**, 3633.
Oviedo, J., and R. E. Palmer, 2002, J. Chem. Phys. **117**, 9548.
Pacheco, J. M., and J. P. Prates-Ramalho, 1997, Phys. Rev. Lett. **79**, 3873.
Padeletti, G., and P. Fermo, 2003, Appl. Phys. A **76**, 515.
Parks, E. K., K. P. Kerns, and S. J. Riley, 1998, J. Chem. Phys. **109**, 10207.
Parks, E. K., G. C. Nieman, K. P. Kerns, and S. J. Riley, 1997, J. Chem. Phys. **107**, 1861.
Parks, E. K., L. Zhu, J. Ho, and S. J. Riley, 1994, J. Chem. Phys. **100**, 7206.
Parks, E. K., L. Zhu, J. Ho, and S. J. Riley, 1995, J. Chem. Phys. **102**, 7377.
Parravicini, G. B., A. Stella, P. Tognini, P. G. Merli, A. Migliori, P. Cheyssac, and R. Kofman, 2003a, Appl. Phys. Lett. **82**, 1461.
Parravicini, G. B., A. Stella, M. C. Ungureanu, P. G. Merli, A. Migliori, and R. Kofman, 2003b, Phys. Status Sol. B **237**, 374.
Patil, A. N., D. Y. Paithankar, N. Otsuka, and R. P. Andres, 1993, Z. Phys. D **26**, 135.
Pawlow, P., 1909, Z. Phys. Chem. **65**, 1.

Perdew, J. P., K. Burke, and Y. Wang, 1996, Phys. Rev. B **54**, 16533.
Perdew, J. P., J. A. Chevary, S. H. Vosko, K. A. Jackson, M. R. Pederson, D. J. Singh, and C. Fiolhais, 1992, Phys. Rev. B **46**, 6671.
Perdew, J. P., and Y. Wang, 1986, Phys. Rev. B **33**, 8800.
Peters, K. F., J. B. Cohen, and Y.-W. Chung, 1998, Phys. Rev. B **57**, 13430.
Pillardy, J., and L. Piela, 1995, J. Phys. Chem. **99**, 11805.
Pimpinelli, A., and J. Villain, 1998, *Physics of Crystal Growth* (Cambridge University Press, Cambridge).
Polak, W., and A. Patrykiejew, 2003, Phys. Rev. B **67**, 115402.
Poteau, R., and F. Spiegelmann, 1993, J. Chem. Phys. **98**, 6540.
Qi, Y., T. Cagin, W. L. Johnson, and W. A. Goddard III, 2001, J. Chem. Phys. **115**, 385.
Quirke, N., and P. Sheng, 1984, Chem. Phys. Lett. **110**, 63.
Raghavachari, K., and V. Logovinsky, 1985, Phys. Rev. Lett. **55**, 2853.
Raghavachari, K., and C. McMichael-Rohlfing, 1988, J. Chem. Phys. **89**, 2219.
Ramakrishna, M. V., and A. Bahel, 1996, J. Chem. Phys. **104**, 9833.
Raoult, B., J. Farges, M. F. de Feraudy, and G. Torchet, 1989a, Philos. Mag. B **60**, 5067.
Raoult, B., J. Farges, M. F. de Feraudy, and G. Torchet, 1989b, Z. Phys. D **12**, 85.
Raoult, B., and J. Farges, 1973, Rev. Sci. Instrum. **44**, 430.
Rata, I., A. A. Shvartsburg, M. Horoi, T. Frauenheim, K. W. M. Siu, and K. A. Jackson, 2000, Phys. Rev. Lett. **85**, 546.
Reddy, B. V., S. N. Khanna, and B. I. Dunlap, 1993, Phys. Rev. Lett. **70**, 3323.
Reinhard, D., B. D. Hall, P. Berthoud, S. Valkealahti, and R. Monot, 1997a, Phys. Rev. Lett. **79**, 1459.
Reinhard, D., B. D. Hall, P. Berthoud, S. Valkealahti, and R. Monot, 1998, Phys. Rev. B **58**, 4917.
Reinhard, D., B. D. Hall, D. Ugarte, and R. Monot, 1997b, Phys. Rev. B **55**, 7868.
Reiss, H., P. Mirabel, and R. L. Whetten, 1988, J. Phys. Chem. **92**, 7241.
Reiss, H., and I. B. Wilson, 1948, J. Colloid Sci. **3**, 551.
Reuse, F. A., S. N. Khanna, and S. Bernel, 1995, Phys. Rev. B **52**, R11650.
Reuse, F. A., and S. N. Khanna, 1995, Chem. Phys. Lett. **234**, 77.
Reyes-Nava, J. A., I. L. Garzón, M. R. Beltrán, and K. Michaelian, 2002, Rev. Mex. Fis. **48**, 450.
Rey, C., L. J. Gallego, and J. A. Alonso, 1994, Phys. Rev. B **49**, 8491.
Rey, C., G. García-Rodeja, and L. J. Gallego, 2004, Phys. Rev. B **69**, 073404.
Rey, C., J. García-Rodeja, and L. J. Gallego, 1997, Z. Phys. D **40**, 395.
Romero, G., C. Barrón, and S. Gómez, 1999, Comp. Phys. Comm. **123**, 87.
Roques, J., C. Lacaze-Dufaure, and C. Mijoule, 2001, Surf. Sci. **479**, 231.
Rosato, V., M. Guillopé, and B. Legrand, 1989, Philos. Mag. A **59**, 321.
Rossi, G., A. Rapallo, C. Mottet, A. Fortunelli, F. Baletto, and R. Ferrando, 2004.
Röthlisberger, U., W. Andreoni, and P. Giannozzi, 1992, J. Chem. Phys. **96**, 1248.
Röthlisberger, U., and W. Andreoni, 1991, J. Chem. Phys. **94**, 8129.
Rousset, J. L., A. M. Cadrot, F. S. Aires, A. Renouprez, P. Melinon, A. Pérez, M. Pellarin, J. L. Vialle, and M. Broyer, 1996, Surf. Rev. Lett. **3**, 1171.
Rytkönen, A., H. Häkkinen, and M. Manninen, 1998a, Phys. Rev. Lett. **80**, 3940.
Rytkönen, A., H. Häkkinen, and M. Manninen, 1999, Eur. Phys. J. D **9**, 451.
Rytkönen, A., S. Valkealahti, and M. Manninen, 1997, J. Chem. Phys. **106**, 1888.
Rytkönen, A., S. Valkealahti, and M. Manninen, 1998b, J. Chem. Phys. **108**, 5826.
Sachdev, A., R. I. Masel, and J. B. Adams, 1992, Catal. Lett. **15**, 57.
Saha, D. K., K. Koga, and H. Takeo, 1997, Nanostruct. Mater. **8**, 1139.
Saha, D. K., K. Koga, and H. Takeo, 1999, Eur. Phys. J. D **9**, 539.
Sambles, J. R., 1971, Proc. R. Soc. London A **324**, 339.
Santamaria, R., I. G. Kaplan, and O. Novaro, 1994, Chem. Phys. Lett. **218**, 395.
Sattler, K., J. Mühlback, and E. Recknagel, 1980, Phys. Rev. Lett. **45**, 821.
Schaaff, T. G., and R. L. Whetten, 2000, J. Phys. Chem. B **104**, 2630.
Schmidt, M., J. Donges, T. Hippler, and H. Haberland, 2003, Phys. Rev. Lett. **90**, 103401.
Schmidt, M., R. Kusche, T. Hippler, J. Donges, W. Kronmüller, B. von Issendorff, and H. Haberland, 2001, Phys. Rev. Lett. **86**, 1191.
Schmidt, M., R. Kusche, B. von Issendorff, and H. Haberland, 1998, Nature **393**, 238.
Schmidt, M., R. Kusche, W. Kronmüller, B. von Issendorff, and H. Haberland, 1997, Phys. Rev. Lett. **79**, 99.
Schmude, R. W., Q. Ran, K. A. Gingerich, and J. E. Kingcade, 1995, J. Chem. Phys. **102**, 2574.
Schmude, R. W., Q. Ran, and K. A. Gingerich, 1993, J. Chem. Phys. **99**, 7998.
Scoles, G., and K. K. Lehmann, 2000, Science **287**, 2429.
Sebetci, A., and Z. B. Güvenc, 2003, Surf. Sci. **525**, 66.
Shah, P., S. Roy, and C. Chakravarty, 2003, J. Chem. Phys. **118**, 10671.
Shao, X., H. Jiang, and W. Cai, 2004, J. Chem. Inf. Comput. Sci. **44**, 193.
Shvartsburg, A. A., and M. F. Jarrold, 2000, Phys. Rev. Lett. **85**, 2530.
Soler, J. M., M. R. Beltrán, K. Michaelian, I. L. Garzón, P. Ordejón, D. Sánchez-Portal, and E. Artacho, 2000, Phys. Rev. B **61**, 5771.
Soler, J. M., I. L. Garzón, and J. D. Joannopoulos, 2001, Solid State Comm. **117**, 621.
Solov'yov, I. A., A. V. Solov'yov, W. Greiner, A. Koshelev, and A. Shutovich, 2003a, Phys. Rev. Lett. **90**, 053401.
Solov'yov, I. A., A. V. Solov'yov, and W. Greiner, 2002, Phys. Rev. A **65**, 053203.
Solov'yov, I. A., A. V. Solov'yov, and W. Greiner, 2003b, eprint hep-physics/0306185.
Spiegelman, F., R. Poteau, B. Montag, and P.-G. Reinhard, 1998, Phys. Lett. A **242**, 163.
Stave, M. S., and A. E. DePristo, 1992, J. Chem. Phys. **97**, 3386.
Steinhardt, P. J., D. R. Nelson, and M. Ronchetti, 1983, Phys.

Rev. B **28**, 784.
Stillinger, F. H., and T. A. Weber, 1982, Phys. Rev. A **25**, 978.
Stillinger, F. H., and T. A. Weber, 1985, Phys. Rev. B **31**, 5262.
Sung, M.-W., R. Kawai, and J. H. Weare, 1994, Phys. Rev. Lett. **73**, 3552.
Sun, Q., Q. Wang, P. Jena, S. Waterman, and Y. Kawazoe, 2003, Phys. Rev. A **67**, 063201.
Sutton, A. P., and J. Chen, 1990, Phil. Mag. Lett. **61**, 139.
Swendsen, R. H., and J.-S. Wang, 1986, Phys. Rev. Lett. **57**, 2607.
Takagi, M., 1954, J. Phys. Soc. Jpn. **9**, 359.
Tchofo-Dinda, P., G. Vlastou-Tsinganos, N. Flyzanis, and A. D. Mistriotis, 1995, Phys. Rev. B **51**, 13697.
Tekin, A., and B. Hartke, 2004, Phys. Chem. Chem. Phys. **6**, 503.
Toennies, J. P., and A. F. Vilesov, 1998, Annu. Rev. Phys. Chem. **49**, 1.
Tománek, D., A. A. Aligia, and C. A. Balseiro, 1985, Phys. Rev. B **32**, 5051.
Tsai, C. J., and K. D. Jordan, 1993, J. Phys. Chem. **97**, 11227.
Turner, G. W., R. L. Johnston, and N. T. Wilson, 2000, J. Chem. Phys. **112**, 4773.
Uppenbrink, J., and D. J. Wales, 1992, J. Chem. Phys. **96**, 8520.
Valerio, G., and H. Toulhoat, 1996, J. Phys. Chem. **100**, 10827.
Valerio, G., and H. Toulhoat, 1997, J. Phys. Chem. A **101**, 1969.
Valkealahti, S., and M. Manninen, 1993, Z. Phys. D **26**, 255.
Valkealahti, S., and M. Manninen, 1997, J. Phys. CM **9**, 4041.
Valkealahti, S., and M. Manninen, 1998, Phys. Rev. B **57**, 15533.
Valkealahti, S., U. Näher, and M. Manninen, 1995, Phys. Rev. B **51**, 11039.
Vanfleet, R. R., and J. M. Mochel, 1995, Surf. Sci. **341**, 40.
Vlachos, D. G., L. D. Schmidt, and R. Aris, 1992, J. Chem. Phys. **96**, 6880.
Voter, A. F., 1993, Los Alamos Unclassified Technical Report **LA-UR 93**, 3901.
van de Waal, B. W., G. Torchet, and M.-F. de Feraudy, 2000, Chem. Phys. Lett. **331**, 57.
van de Waal, B. W., 1989, J. Chem. Phys. **90**, 3407.
van de Waal, B. W., 1996, Phys. Rev. Lett. **76**, 1083.
Wales, D. J., J. P. K. Doye, M. A. Miller, P. N. Mortenson, and T. R. Walsh, 2000, Adv. Chem. Phys. **111**, 1.
Wales, D. J., and J. P. K. Doye, 1997, J. Phys. Chem. A **101**, 5111.
Wales, D. J., and M. P. Hodges, 1998, Chem. Phys. Lett. **286**, 65.
Wales, D. J., 1994a, J. Chem. Soc. Faraday T. **90**, 1061.
Wales, D. J., 1994b, J. Chem. Phys. **101**, 3750.
Wales, D. J., 2003, *Energy Landscapes with Applications to Clusters, Biomolecules and Glasses* (Cambridge University Press, Cambridge).
Wang, G. M., E. Blastein-Barojas, A. E. Roitberg, and T. P. Martin, 2001a, J. Chem. Phys. **115**, 3640.
Wang, J. L., G. H. Wang, F. Ding, H. Lee, W. F. Shen, and J. J. Zhao, 2001b, Chem. Phys. Lett. **341**, 529.
Wang, J. L., G. H. Wang, and J. J. Zhao, 2002, Phys. Rev. B **66**, 035418.
Wang, J., G. Wang, and J. Zhao, 2003a, Chem. Phys. Lett **380**, 716.
Wang, L., Y. Zhang, X. Bian, and Y. Chen, 2003b, Phys. Lett. A **310**, 197.
Watari, N., and S. Ohnishi, 1998, Phys. Rev. B **58**, 1665.
Westergren, J., H. Grönbeck, A. Rosen, and S. Nordholm, 1998, J. Chem. Phys. **109**, 9848.
Westergren, J., S. Nordholm, and A. Rosen, 2003, Phys. Chem. Chem. Phys. **5**, 136.
Westergren, J., and S. Nordholm, 2003, Chem. Phys. **290**, 189.
Wetzel, T. L., and A. E. DePristo, 1996, J. Chem. Phys. **105**, 572.
Whaley, K. B., 1994, Int. Rev. Phys. Chem. **13**, 41.
Whetten, R. L., J. T. Khoury, M. M. Alvarez, S. Murthy, I. Vezmar, Z. L. Wang, P. W. Stephens, C. L. Cleveland, W. D. Luedtke, and U. Landman, 1996, Adv. Mater. **5**, 428.
Wille, L. T., and J. Vennik, 1985, J. Phys. A **18**, L419.
Wille, L. T., 1987, Chem. Phys. Lett. **133**, 405.
Wilson, N. T., and R. L. Johnston, 2000, Eur. Phys. J. D **12**, 161.
Xiao, Y., and D. E. Williams, 1993, Chem. Phys. Lett. **215**, 17.
Xie, J., J. A. Northby, D. L. Freeman, and J. D. Doll, 1989a, J. Chem. Phys. **91**, 612.
Xie, J., J. A. Northby, D. L. Freeman, and J. D. Doll, 1989b, J. Chem. Phys. **91**, 612.
Xue, G. L., 1994, J. of Global Optimization **4**, 425.
Yang, S. H., D. A. Drabold, J. B. Adams, P. Ordejón, and K. Glassford, 1997, J. Phys. CM **9**, L39.
Yu, D. K., R. Q. Zhang, and S. T. Lee, 2002, Phys. Rev. B **65**, 245417.
Zacarias, A. G., M. Castro, J. M. Tour, and J. M. Seminario, 1999, J. Phys. Chem. A **103**, 7692.
Zanchet, D., B. D. Hall, and D. Ugarte, 2000, J. Phys. Chem. B **104**, 11013.
Zeiri, Y., 1995, Phys. Rev. E **51**, R2769.
Zhang, W., Q. Ge, and L. Wang, 2003, J. Chem. Phys. **118**, 5793.
Zhao, J., Y. Luo, and G. Wang, 2001, Eur. Phys. J. D **14**, 309.
Zhao, J., J. L. Yang, and J. G. Hou, 2003, Phys. Rev. B **67**, 085404.
Zhou, Y., M. Karplus, K. D. Ball, and R. S. Berry, 2002, J. Chem. Phys. **116**, 2323.
Zhu, H., 1996, Philos. Mag. Lett. **73**, 27.
Zickfeld, K., M. E. García, and K. H. Bennemann, 1999, Phys. Rev. B **59**, 13422.